STUDY OF INDICIAL LOAD EFFECTS ON MULTI-STAGE SPACE VEHICLE SYSTEMS

FINAL REPORT
22 April 1965 - 31 March 1967

Contract No. NAS8-20075
Control No. DCN 1-6-75-00034 (IF)

MRI Project No. 2867-P

FACILITY FORM 602

N67-26325 (ACCESSION NUMBER)
(THRU)
128 (PAGES)
None (CODE)
CR-84060 (NASA CR OR TMX OR AD NUMBER)
31 (CATEGORY)

For

National Aeronautics and Space Administration
George C. Marshall Space Flight Center
Huntsville, Alabama 35812

MRI

MIDWEST RESEARCH INSTITUTE
425 VOLKER BOULEVARD/KANSAS CITY, MISSOURI 64110/AC 816 LO 1-0202

DISTRIBUTION LIST

Contract No. NAS8-20075, MRI Project No. 2867-P

No. of Copies	Recipient
13 + Reproducible	National Aeronautics and Space Administration George C. Marshall Space Flight Center Huntsville, Alabama 35812 Attn: R. S. Ryan, R-AERO-DD
1	National Aeronautics and Space Administration George C. Marshall Space Flight Center Huntsville, Alabama 35812 Attn: PR-SC
2	National Aeronautics and Space Administration George C. Marshall Space Flight Center Huntsville, Alabama 35812 Attn: MS-IPL
1	National Aeronautics and Space Administration George C. Marshall Space Flight Center Huntsville, Alabama 35812 Attn: MS-T
1	National Aeronautics and Space Administration George C. Marshall Space Flight Center Huntsville, Alabama 35812 Attn: R-AERO-R
2	National Aeronautics and Space Administration George C. Marshall Space Flight Center Huntsville, Alabama 35812 Attn: MS-I

STUDY OF INDICIAL LOAD EFFECTS ON MULTI-STAGE SPACE VEHICLE SYSTEMS

by

Robert R. Blackburn

FINAL REPORT
22 April 1965 - 31 March 1967

Contract No. NAS8-20075
Control No. DCN 1-6-75-00034 (IF)

MRI Project No. 2867-P

For

National Aeronautics and Space Administration
George C. Marshall Space Flight Center
Huntsville, Alabama 35812

MIDWEST RESEARCH INSTITUTE
425 VOLKER BOULEVARD/KANSAS CITY, MISSOURI 64110/AC 816 LO 1-0202

PREFACE

This report was prepared by Midwest Research Institute under Contract No. NAS8-20075. The work was performed under the technical direction of the Aero-Astrodynamics Laboratory, George C. Marshall Space Flight Center, with Mr. Robert S. Ryan acting as project manager.

This report covers work on the contract during the contract period 22 April 1965 to 31 March 1967.

Mr. Robert R. Blackburn was the project leader and principal investigator. Among members of the staff who contributed to the preparation of the numerical results were Mrs. Geraldine Coombs and Mr. Donald R. Kobett. Special acknowledgements are given to Mr. A. D. St. John and Dr. William D. Glauz for their timely suggestions and technical assistance.

Approved for:

MIDWEST RESEARCH INSTITUTE

Sheldon L. Levy, Director
Mathematics and Physics Division

10 April 1967

ABSTRACT

The investigation reported is divided into two main phases. Phase I is a study to determine the effects and importance of penetration and lift growth on vehicle responses. The objective of this phase is to make wind-induced response comparisons for the Saturn V when the effects of (1) fins and engine shrouds and (2) third and fourth bending are incorporated into the analysis. Phase II of the investigation is a study to determine the relative merits of two types of control systems on load alleviation when gust penetration effects are considered. The two methods of control considered are: (1) angle of attack and (2) attitude control. The bending moment responses are the main basis of comparison in phase II. The Sinusoidal Gust and Imbedded Gust Criterias are used as the wind environments in phases I and II, respectively.

The inclusion of third and fourth bending and the effects of fins and engine shrouds into the analysis produced significant differences (in an engineering sense) between responses computed with and without penetration effects. This is opposite from the results obtained in an earlier study wherein penetration effects were found to be insignificant when third and fourth bending and empennage effects were neglected.

Smaller maximum bending moment responses result from an attitude control system than from an angle of attack control system.

TABLE OF CONTENTS

	Page No.
Notation	viii
Summary	1
I. Introduction	3
II. Basic Goal of the Investigation	3
III. Description of the Investigation	4
A. Saturn V Model	4
B. Indicial and Impulsive Aerodynamic Forces	5
C. Method of Solution for Indicial and Impulsive Responses of Saturn V Configuration with Fins and Engine Shrouds	14
D. Wind-Induced Responses	32
IV. Results and Discussion of Response Investigation	52
A. Phase I	52
B. Phase II	71
V. Supplementary Discussion of Bending Moment Computation	80
VI. Conclusions and Recommendations	81
A. Phase I - Response to Sinusoidal Gust Criteria	81
B. Phase II - Response to Imbedded Gust Criteria	82
Bibliography	84
Appendix I - Equations of Motion and Control for Saturn V	85
Appendix II - Aerodynamic Force Expressions Resulting From Unit Step and Impulse Wind Profile	93
Appendix III - Formulation of Bending Moment Expressions Resulting From a Unit Impulse and Arbitrary Wind Profile	103
Appendix IV - Sinusoidal and Imbedded Gust Criteria	115

TABLE OF CONTENTS (Continued)

List of Figures

Figure No.	Title	Page No.
1	Indicial Normal Force Growth Functions for 70-sec. Flight Time	8
2	Indicial Rotational Moment Growth Functions for 70-sec. Flight Time	8
3	Indicial First Bending Moment Growth Functions for 70-sec. Flight Time	9
4	Indicial Second Bending Moment Growth Functions for 70-sec. Flight Time	9
5	Indicial Third Bending Moment Growth Functions for 70-sec. Flight Time	10
6	Indicial Fourth Bending Moment Growth Functions for 70-sec. Flight Time	10
7	Impulsive Normal Force Growth Functions for 70-sec. Flight Time	11
8	Impulsive Rotational Moment Growth Functions for 70-sec. Flight Time	11
9	Impulsive First Bending Moment Growth Functions for 70-sec. Flight Time	12
10	Impulsive Second Bending Moment Growth Functions for 70-sec. Flight Time	12
11	Impulsive Third Bending Moment Growth Functions for 70-sec. Flight Time	13
12	Impulsive Fourth Bending Moment Growth Functions for 70-sec. Flight Time	13
13 - 27	Impulsive Responses of Several Generalized Coordinates Considering Three Aerodynamic Representations - Angle of Attack Control, 70-sec. Flight Time	17 - 31

TABLE OF CONTENTS (Continued)

List of Figures (Concluded)

Figures No.	Title	Page No.
28	Sinusoidal Gust Profile, A = 8.6 m/sec, λ = 190. 2 m .	36
29 - 43	Sinusoidal Wind-Induced Responses of Several Generalized Coordinates Considering Three Aerodynamic Representations - Angle of Attack Control, 70-sec. Flight Time	37 - 51
44	Imbedded Gust Profile	53
45 - 56	Bending Moment Responses at Three Vehicle Station Locations Considering Two Aerodynamic Representations - Angle of Attack and Attitude Control, 70-sec. Flight Time	54 - 65
57	Saturn V Coordinate System	86
58	Saturn V Body Geometry	95
59	Sinusoidal and Imbedded Gust Criteria	116

List of Tables

Table No.	Title	Page No.
I	- Wind-Induced Forcing Functions	6
II	- Ratios of Observed Maximum Responses to Sinusoidal Gust Criteria	68
III	- Maximum Penetration With Lift Growth Wind-Induced Response Values Resulting From Sinusoidal Gust Criteria	69
IV	- Maximum Pure Penetration Wind-Induced Responses Resulting From Imbedded Gust Criteria	72
V	- Ratios (II/PP) of Observed Maximum Responses to Imbedded Gust Criteria	73

TABLE OF CONTENTS (Concluded)

List of Tables (Concluded)

Table No.	Title	Page No.
VI	- Pure Penetration Maximum Reduced Bending Moment Responses and Ratios (II/PP) of Maximum Reduced Bending Moment at Three Station Locations	77
VII	- Values of the Ratio, R	78
VIII	- Definition of Saturn V Body Geometry	96
IX	- Equivalent Cone Angles for Simulated Fins and Engine Shrouds	98
X	- Coefficients Used in Evaluating Indicial and Impulsive Aerodynamic Forcing Functions	102

NOTATION

a_o = gain value of attitude control channel

a_1 = gain value of control damping

b_o = gain value of flow direction channel

D_o = base diameter of vehicle

F = thrust

g_{Bm} = structural damping coefficient of mth bending mode

g_g = longitudinal vehicle acceleration

g_{S1} = damping coefficient associated with first sloshing mode

g_{S2} = damping coefficient associated with second sloshing mode

II = instantaneous immersion

I_{cg} = mass moment of inertia of vehicle about its c.g.

$I(\tau)$ = Heaviside step function

L = length of vehicle

$M_i(\tau)$ = aerodynamic moment growth function due to a unit impulse wind

$M_s(\tau)$ = aerodynamic moment growth function due to a unit step wind

$M_{B_M}(x_k,\tau)$ = mode displacement bending moment expression (see III-34)

$M_{B_R}(x_k,\tau)$ = reduced bending moment expression (see III-28)

$M_{B_T}(x_k,\tau)$ = total bending moment expression (see III-14)

M = Mach number

m = total mass of vehicle

m_{S1} = sloshing mass associated with first sloshing mode

m_{S2} = sloshing mass associated with second sloshing mode

$N_i(\tau)$ = aerodynamic normal force growth function due to a unit impulse wind

$N_s(\tau)$ = aerodynamic normal force growth function due to a unit step wind

PP = pure penetration

PWLG = penetration with lift growth

Q = $\frac{\pi}{2} D_o^2 q$

$Q_{\eta_m}(\tau)_i$ = aerodynamic bending moment growth function associated with the mth bending mode and due to a unit impulse wind

$Q_{\eta_m}(\tau)_s$ = aerodynamic bending moment growth function associated with the mth bending mode and due to a unit step wind

q = $\frac{1}{2} \rho U^2$, dynamic pressure

R = radius of vehicle

$S(x)$ = missile cross-sectional area

T_m = generalized mass associated with m^{th} bending mode

t = time

U = vehicle free stream velocity

$v_y(x,t)$ = horizontal wind velocity

x_g = coordinate of vehicle c.g.

x_k = vehicle station location

x_E = coordinate of gimbal point

x_{S1} = coordinate of sloshing mass associated with first sloshing mode

x_{S2} = coordinate of sloshing mass associated with second sloshing mode

x_T = coordinate of top of vehicle

Y_m = m^{th} bending mode deflection curve (normalized to one at the gimbal point)

y_o = lateral translation of rigid mode

Aerodynamic Integrals

$$A_{mi} = -\int_{-L/2}^{L/2} Y_m(x)\left[2\lambda(x)\lambda'(x)Y_i'(x) + \lambda^2(x)Y_i''(x)\right]dx \qquad (m,i = 1,2,3,4)$$

$$B_{mi} = -2\int_{-L/2}^{L/2} Y_m(x)\left[\lambda(x)\lambda'(x)Y_i(x) + \lambda^2(x)Y_i'(x)\right]dx \qquad (m,i = 1,2,3,4)$$

$$C_{mi} = \int_{-L/2}^{L/2} \lambda^2(x)Y_m(x)Y_i(x)dx \qquad (m,i = 1,2,3,4)$$

$$D_m = \int_{-L/2}^{L/2} \lambda(x)\lambda'(x)Y_m(x)dx \qquad (m = 1,2,3,4)$$

$$\overline{D}_m = \int_{-L/2}^{L/2} \lambda(x)\lambda'(x)(x-x_g)Y_m(x)dx \qquad (m = 1,2,3,4)$$

$$E_m = \int_{-L/2}^{L/2} \left[2\lambda(x)\lambda'(x)Y_m' + \lambda^2(x)Y_m''(x)\right]dx \qquad (m = 1,2,3,4)$$

$$\overline{E}_m = -\int_{-L/2}^{L/2} \left[2\lambda(x)\lambda'(x)Y_m'(x) + \lambda^2(x)Y_m''(x)\right](x-x_g)dx \qquad (m = 1,2,3,4)$$

$$F_k = \int_{-L/2}^{L/2} \lambda(x)\lambda'(x)(x-x_g)^k dx \qquad (k = 0,1,2)$$

$$G_m = \int_{-L/2}^{L/2} \lambda^2(x)Y_m(x)dx \qquad (m = 1,2,3,4)$$

$$\bar{G}_m = \int_{-L/2}^{L/2} \lambda^2(x)(x-x_g)Y_m(x)dx \qquad (m = 1,2,3,4)$$

$$H_m = \int_{-L/2}^{L/2} \lambda^2(x)Y_m'(x)dx \qquad (m = 1,2,3,4)$$

$$\bar{H}_m = \int_{-L/2}^{L/2} \lambda^2(x)(x-x_g)Y_m'(x)dx \qquad (m = 1,2,3,4)$$

$$J_k = \int_{-L/2}^{L/2} \lambda^2(x)(x-x_g)^k dx \qquad (k = 0,1,2)$$

Greek Symbols

α_i = indicated angle of attack

α_L = local angle of attack

β_C = control deflection

β_E = actual swivel engine deflection ($= \beta_C$)

η_m = amplitude of the mth bending mode at gimbal point

$\lambda(x) = \dfrac{2R(x)}{D_o}$

ρ = air density

τ = time

ξ_1 = amplitude of first sloshing mass relative to tank wall

ξ_2 = amplitude of second sloshing mass relative to tank wall

ϕ = pitch angle

ϕ_i = indicated attitude angle

ω_{Bm} = natural frequency of mth bending mode

ω_{S1} = natural frequency of first sloshing mode

ω_{S2} = natural frequency of second sloshing mode

Subscripts

i,m,n = integers

(') = denotes differentiation with respect to x

($\dot{}$) = denotes differentiation with respect to time

SUMMARY

The investigation reported herein is divided into two main phases. Phase I is a study to determine the effects and importance of penetration and lift growth on vehicle responses. The objective of this phase is to make response comparisons when the effects of (1) fins and engine shrouds and (2) third and fourth bending are incorporated into the analysis. Phase II of the investigation is a study to determine the relative merits of two types of control systems on load alleviation when gust penetration effects are considered. The two methods of control considered are: (1) angle of attack and (2) attitude control. The bending moment responses at three vehicle station locations are the main basis of comparison in phase II.

The wind-induced responses of a Saturn V configuration with fins and engine shrouds are computed and compared in both phases for the peak dynamic pressure region (70 and 80-sec. flight time conditions). The Sinusoidal Gust and Imbedded Gust Criterias are used as the wind environments in phases I and II, respectively.

The analytical model of the Saturn V includes the following degrees of freedom: translation, rotation, first four bending modes, two sloshing modes, and control deflection. Frozen coefficients are used, with each set of coefficients applicable to a 10-sec. flight time interval. The bending moment response comparisons are made using a "reduced bending moment expression." This expression is developed from a summation of moments technique.

The maximum responses of the bending modes and control deflection to the Sinusoidal Gust Criteria are most notably affected by the inclusion of penetration and lift growth effects. Instantaneous immersion (the conventional aerodynamic representation) results are generally conservative (large) for the first three bending modes and unconservative for the fourth bending and control deflection. The amount of conservativeness and unconservativeness of instantaneous immersion depends on the driving frequency of the sinusoidal gust.

Smaller maximum bending moment responses result from an attitude control system than from an angle of attack control system. The maximum bending moment responses computed with instantaneous immersion are conservative (large) compared to those obtained with penetration effects. The amount of conservativeness is largest near the top of the vehicle where bending mode dynamics are a significant part of the total load.

The inclusion of third and fourth bending and the effects of fins and shrouds into the analysis produced significant differences (in an

engineering sense) between responses computed with and without penetration considerations. This is opposite from the results obtained in [1] wherein penetration effects were found to be insignificant when third and fourth bending and empennage effects were neglected.

I. INTRODUCTION

In a previous program [1], the wind-induced responses of a Saturn V configuration (without fins and engine shrouds) were calculated and compared for three aerodynamic theories or representations. The most accurate representation accounted for the time delays of penetration and used unsteady aerodynamics so that growth of lift smoothing and delays were included. The second representation, referred to as pure penetration, used pseudo-steady aerodynamics but included penetration delays. The third representation used pseudo-steady aerodynamics and assumed that the cross wind at the tip of the vehicle acted instantaneously over the entire vehicle length. This latter representation was referred to as instantaneous immersion.

The responses in [1], which included two bending modes, were affected by penetration to a detectable but insignificant degree. The addition of growth of lift caused a very small change. The conventional, instantaneous immersion, responses were found to be slightly conservative (large) for the cases computed.

The calculations in [1] did not provide an example of significant response changes due to penetration and lift growth. The lack of significance was believed to result from the simplified mathematical model of the Saturn V used.

It was therefore recommended that the model be expanded to include four bending modes and simulated fins and engine shrouds. Also investigated are the effects of various control systems on vehicle response when penetration aerodynamics are considered. Bending moment responses were computed in conjunction with the control study.

The investigation reported was conducted to supplement the response studies in [2,3 and 4].

II. BASIC GOAL OF THE INVESTIGATION

The basic goal of the work presented in this report is divided into two main phases. Phase I of the contract is an investigation to determine the effects and importance of penetration and growth of lift on vehicle responses. The objective of this phase is to make response comparisons when the effects of (1) fins and engine shrouds and (2) third and fourth bending modes are incorporated into the analysis. Phase I is a direct extension of the response study reported in [1].

Phase II of the investigation is a study to determine the relative merits of two types of control systems on load alleviation when gust penetration effects are considered. The two methods of control considered are: (1) angle of attack and (2) attitude.* To augment the load alleviation analysis, the vehicle's bending moment responses are computed at three station locations. The effects of fins and engine shrouds and the higher bending modes were included also in the phase II study.

To accomplish this basic goal, the investigation proceeded in the following manner.

1. The indicial** and impulsive*** responses of the vehicle were computed in the peak dynamic pressure region using three aerodynamic considerations: (1) penetration with lift growth effects, (2) pure penetration, and (3) instantaneous immersion. Slender-body theory was used throughout the investigation.

2. The wind-induced responses of the vehicle were computed from the impulsive responses using the Duhamel superposition integral. In Phase I, the wind-induced responses of the generalized coordinates were evaluated for the three aerodynamic considerations. NASA's Sinusoidal Gust Criteria was used as the atmospheric wind environment. In Phase II, the wind-induced responses of both the generalized coordinates and bending moments were computed for two aerodynamic considerations: (1) pure penetration and (2) instantaneous immersion. In this phase, NASA's Imbedded Gust Criteria was used as the wind environment.

III. DESCRIPTION OF THE INVESTIGATION

A. Saturn V Model

The Saturn V configuration with fins and engine shrouds was used in the response investigation of both phases I and II. The equations of

---

* The angle of attack control system utilizes both an attitude reference control (position and rate gyro sensors) and a flow direction indicator (angle of attack sensor). The attitude control system contains only the position and rate gyro sensors. The mathematical descriptions of both control systems are given in Appendix I.

** Response to a unit step.

*** Response to a unit impulse.

motion and the control equations of the vehicle system are presented in Appendix I. Nine generalized coordinates were considered in the response calculations: lateral translation, y_o ; rotation, ϕ ; the first four bending coordinates, η_1, η_2, η_3 and η_4; two sloshing coordinates, ξ_1 and ξ_2 ;* and control deflection, β_C .** The angle of attack control system was used in the phase I study. Both this control system and the attitude control system were utilized in the phase II investigation.

The equations are valid for a swivel engine controlled vehicle where the swiveled engines account for four-fifths of the total thrust force. The vehicle and atmospheric parameters appearing in the equations are considered constant (frozen) in predetermined flight time intervals.

The fins and engine shrouds located on the aft end of the vehicle were simulated by two adjacent conic sections (see Appendix II). The equivalent conic sections were designed to provide the same normal force in the steady-state condition as the actual empennages. Experimental data for the normal force coefficients of the fins and engines shrouds were used in the approximation. These data are taken from wind tunnel test [5] and account for the fin-shroud-body interference effect.

B. Indicial and Impulsive Aerodynamic Forces

A detailed development of the transient and quasi-steady indicial and impulsive generalized aerodynamic forces is presented in [1] for a Saturn V configuration without fins and engine shrouds. Since the aerodynamic configuration considered in this report includes fins and engine shrouds, it was necessary to extend the force expressions in [1] to include the aerodynamic effects of these empennages. A brief summary of the development in [1] is presented in Appendix II along with the aerodynamic influence of simulated fins and engine shrouds. This formulation of the generalized aerodynamic forcing functions is based on slender-body theory.

Three types of wind-induced forcing functions are compared in this report. The three types are termed instantaneous immersion (II), pure penetration (PP), and penetration with lift growth (PWLG). Each one is assembled using combinations of geometric and aerodynamic representations as shown in Table I.

---

* The two sloshing coordinates considered are associated with the fundamental fluid motion in the LOX and fuel tanks located in the booster stage of the vehicle.

** The actual engine deflection, β_E , and the control deflection, β_C , are considered to be equal.

TABLE I

WIND-INDUCED FORCING FUNCTIONS

Type	Representation: Geometric	Representation: Aerodynamic
II	Uniform Cross Flow	Quasi-Steady
PP	Wind-Induced Cross Flow* A Function of Vehicle Station Location	Quasi-Steady
PWLG	Wind-Induced Cross Flow A Function of Vehicle Station Location	Transient

* The cross flows induced by the vehicle motions are in all cases treated with quasi-steady aerodynamics. These cross flows are small in comparison to the wind-induced cross flows and appear in the left hand side of the equations of motion (see Appendix I).

The air forces described by quasi-steady aerodynamics, are those which would exist at any vehicle station if the local cross flow persisted unchanged for an extended time. The transient aerodynamic representation is based on the theory of unsteady motion of slender bodies of revolution and includes the growth of lift with time.

The simplest type of forcing function is instantaneous immersion; while the most accurate is penetration with lift growth. Both instantaneous immersion and pure penetration forcing functions can be obtained as special cases of the penetration with lift growth expressions (see [1] and Appendix II).

The extension of the aerodynamic force expressions in [1] to include the effects of the fins and engine shrouds is presented in Appendix II. The aerodynamic contributions of the fins and engine shrouds are approximated by an equivalent body of revolution - in this case, two adjacent conic sections. The conic sections are designed to produce the same steady-state slope of the normal force coefficient as the actual fin and engine shroud region. The upstream position of one frustum is located at the beginning of the engine shrouds, while the other frustum starts at the beginning of the fins. The cone angle, α_4 , of the upstream frustum is selected to provide a steady-state normal force equal to the force due to

the shrouds alone. The second cone angle, α_5 , is chosen so that the second frustum and the exposed fraction of the first cone provide the steady normal force due to the fin-shroud combination.

The ability to approximate the fin and engine shrouds by an equivalent body of revolution permitted the use of the general indicial and impulsive force expressions given in [1]. The aerodynamic addition of the fins and engine shrouds increased the number of vehicle conic regions from 4 (as were considered in [1]) to 6. Again as in [1], quadratic polynomials were used to curve fit the mode shapes over the conic regions in evaluating the generalized forces associated with the bending modes.

Figures 1 - 12 give the Saturn V indicial and impulsive generalized aerodynamic forces associated with rigid body and the first four bending modes.* The curves are presented for a Mach number of 1.345 (70-sec. flight time). The indicial forcing functions are given in Figs. 1 through 6, while the impulsive forcing functions are shown in Figs. 7 through 12. The effects of penetration with lift growth, pure penetration and instantaneous immersion on the generalized forces can be easily seen from the figures. The impulsive forces resulting from instantaneous immersion considerations are not presented since they can only be described in an integrated sense.

The half cross section of the Saturn V configuration with simulated fins and engine shrouds is given at the bottom of each figure to facilitate interpretation of the growth functions. At zero time, the first region (escape tower) penetrates the gust front and the generalized force buildup begins. The succeeding conics encounter the gust at 0.0216, 0.0500, 0.0930, 0.2431 and 0.2523 sec. The pure penetration curves reach steady-state conditions at 0.2629 sec. The penetration with lift growth curves, in actuality, do not reach steady-state in a finite time. However, based on the numerical accuracy sought, these curves are assumed to reach steady-state at 0.4894 sec.

In [1], only the first four conic regions were considered in computing the aerodynamic forcing functions. The pure penetration and penetration with lift growth curves for a four conic configuration reach steady-state conditions at 0.1065 and 0.2895 sec., respectively. Including the effects of fins and engine shrouds in the aerodynamic formulation obviously causes the force buildup to be distributed over a longer response time than when only four conics are considered. Also, in comparison to the first four conic regions, the fins and engine shrouds yield a significant contribution to the steady-state forcing functions (see Figs. 1 through 6).

---

* The 70-sec. flight time indicial and impulsive forcing functions corresponding to translation and first and second bending are given in [1] for a configuration without fins and engine shrouds.

Instantaneous Immersion
Pure Penetration
Penetration with Lift Growth
M = 1.345

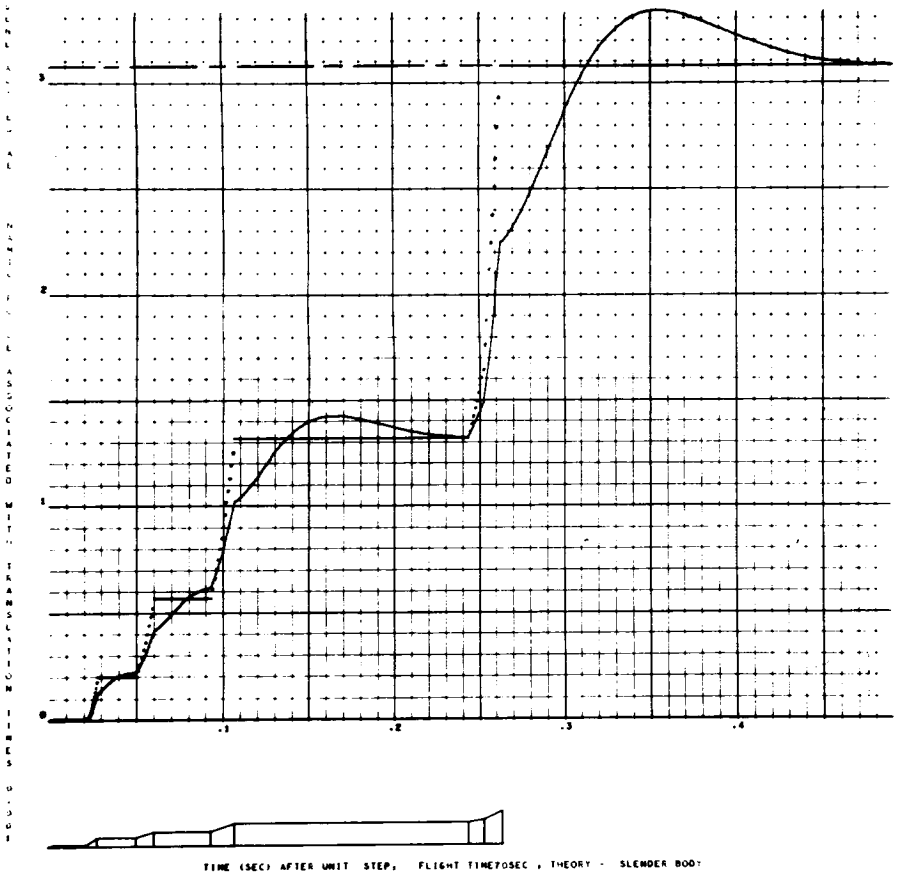

Fig. 1 - Indicial Normal Force Growth Functions for 70-sec. Flight Time

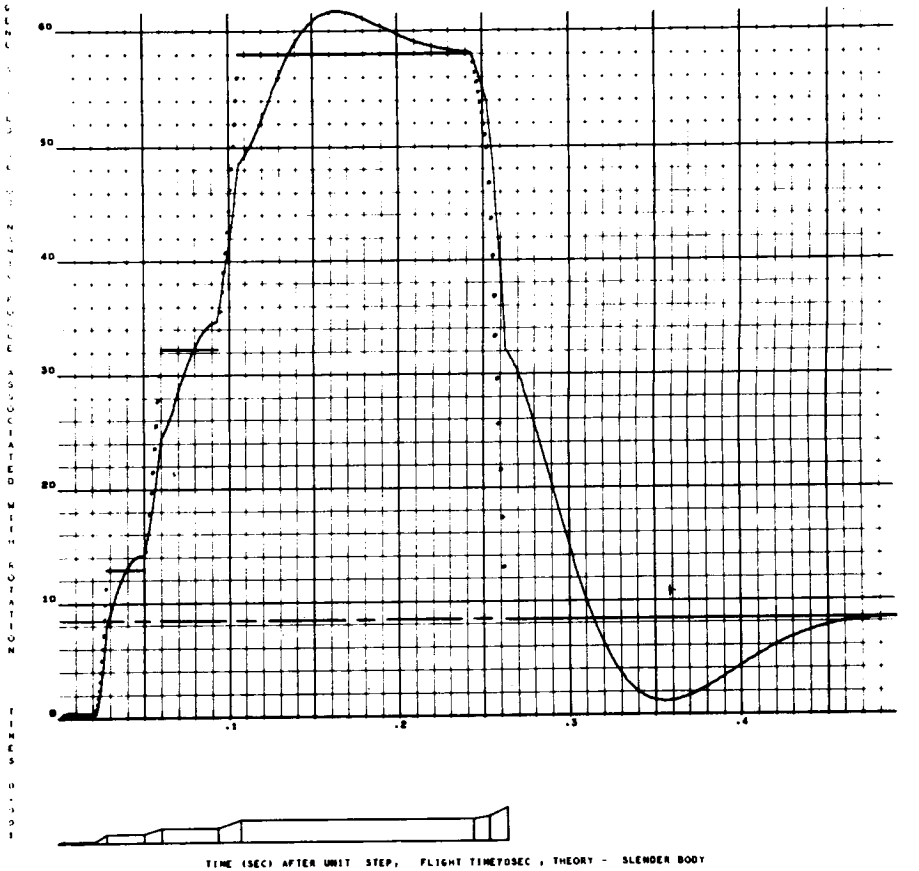

Fig. 2 - Indicial Rotational Moment Growth Functions for 70-sec. Flight Time

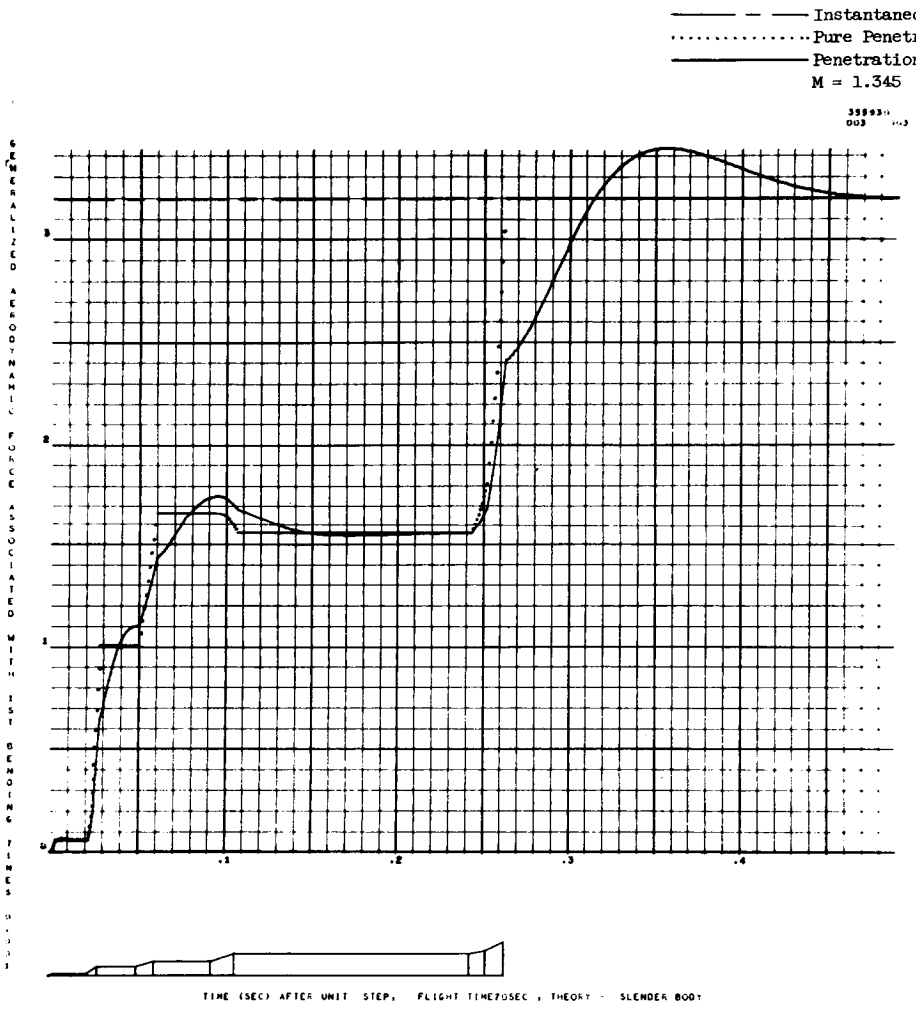

Fig. 3 - Indicial First Bending Moment Growth Functions for 70-sec. Flight Time

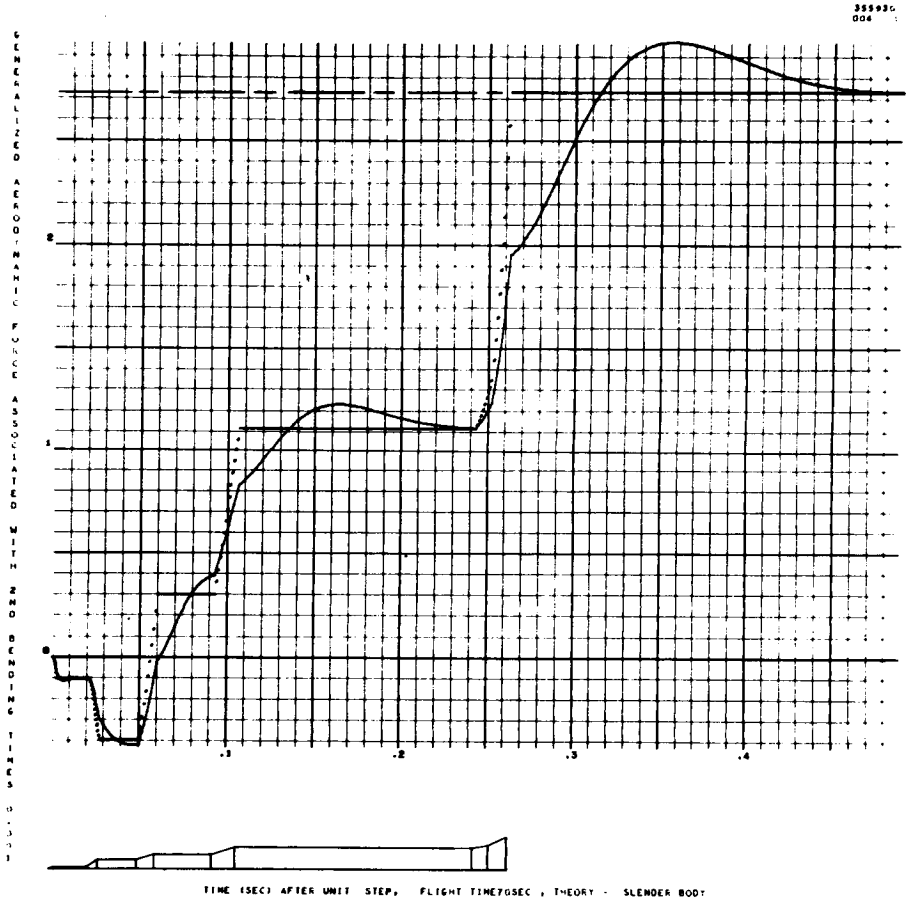

Fig. 4 - Indicial Second Bending Moment Growth Functions for 70-sec. Flight Time

Instantaneous Immersion
Pure Penetration
Penetration with Lift Growth
M = 1.345

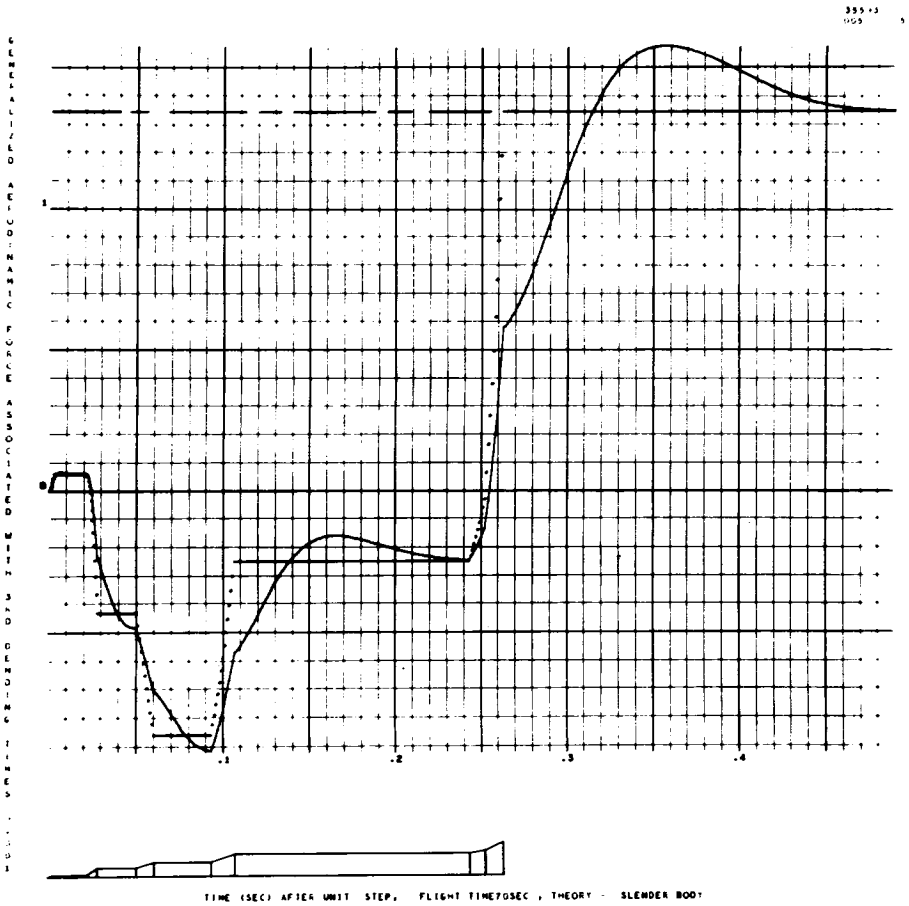

Fig. 5 - Indicial Third Bending Moment Growth Functions for 70-sec. Flight Time

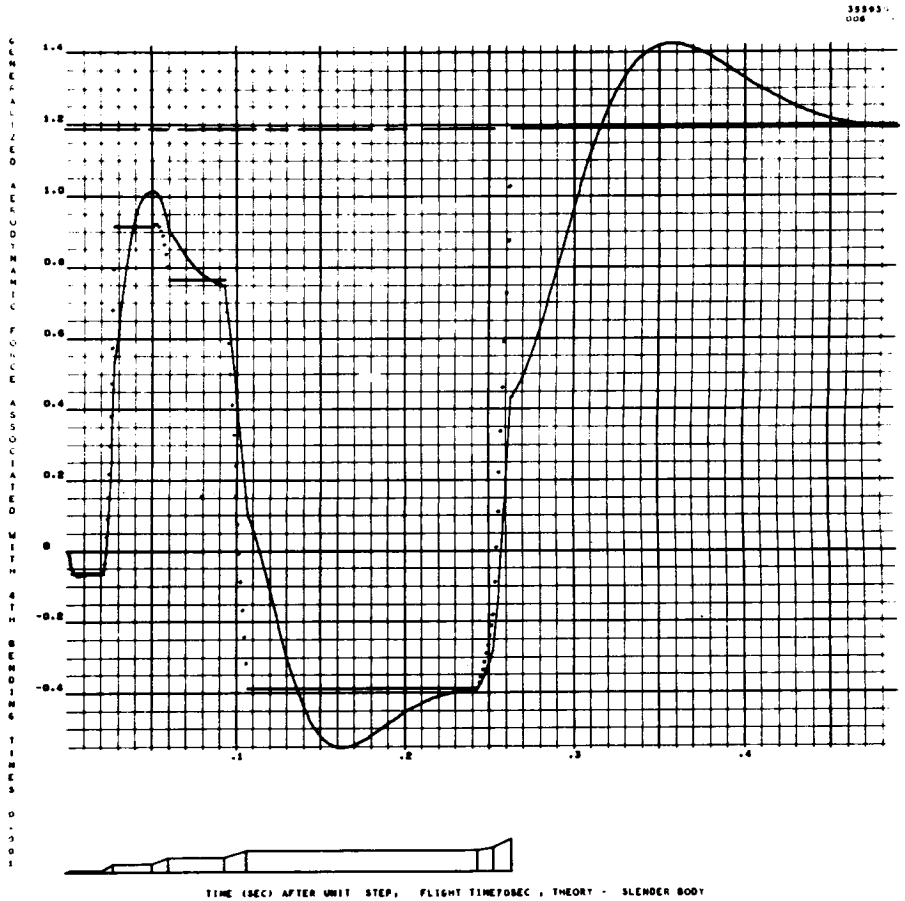

Fig. 6 - Indicial Fourth Bending Moment Growth Functions for 70-sec. Flight Time

..... Pure Penetration
———— Penetration with Lift Growth
M = 1.345

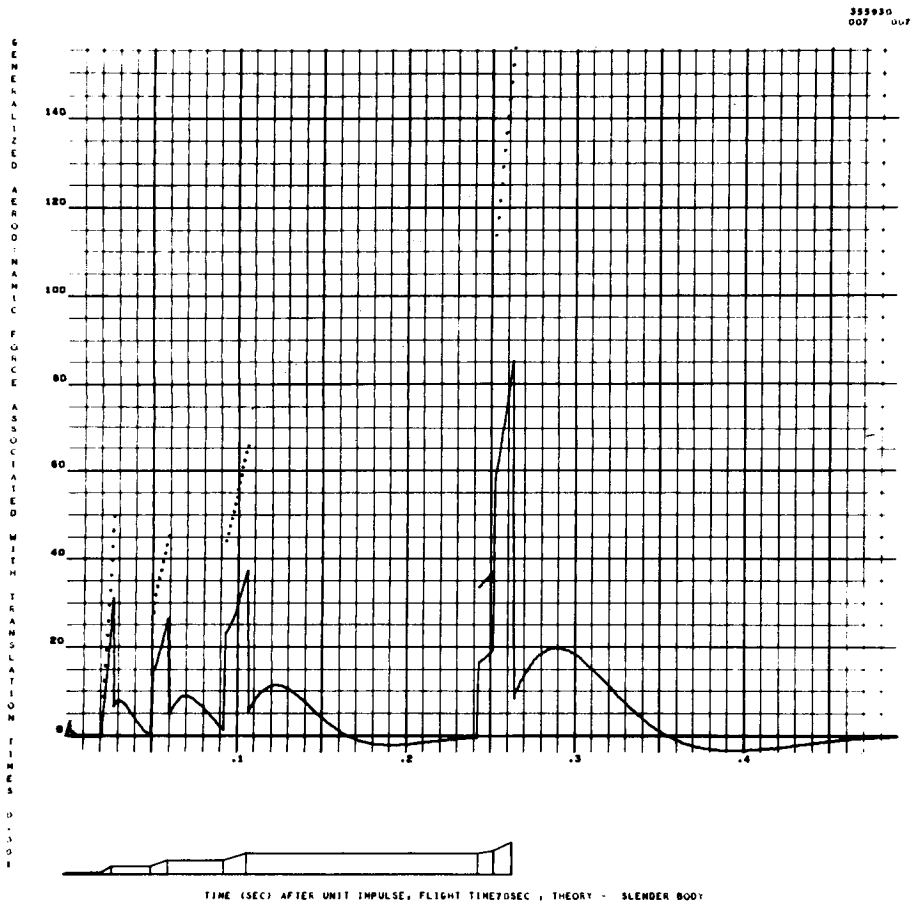

Fig. 7 - Impulsive Normal Force Growth Functions for 70-sec. Flight Time

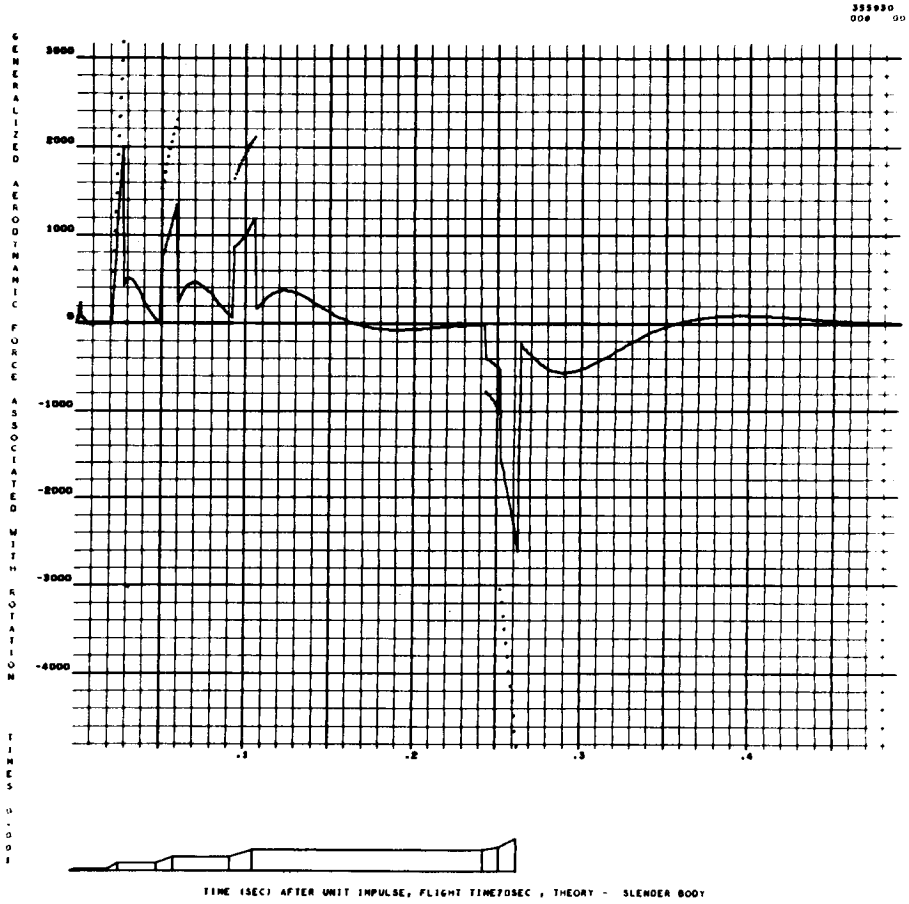

Fig. 8 - Impulsive Rotational Moment Growth Functions for 70-sec. Flight Time

·····Pure Penetration
————Penetration with Lift Growth
M = 1.345

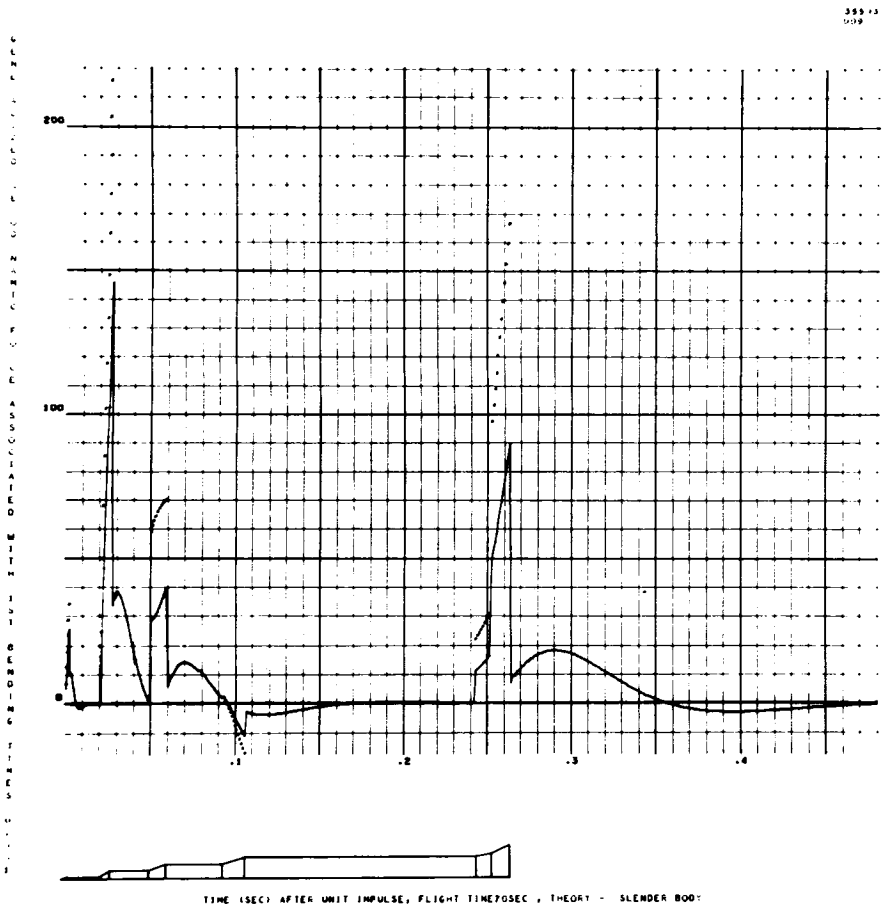

Fig. 9 - Impulsive First Bending Moment Growth Functions for 70-sec. Flight Time

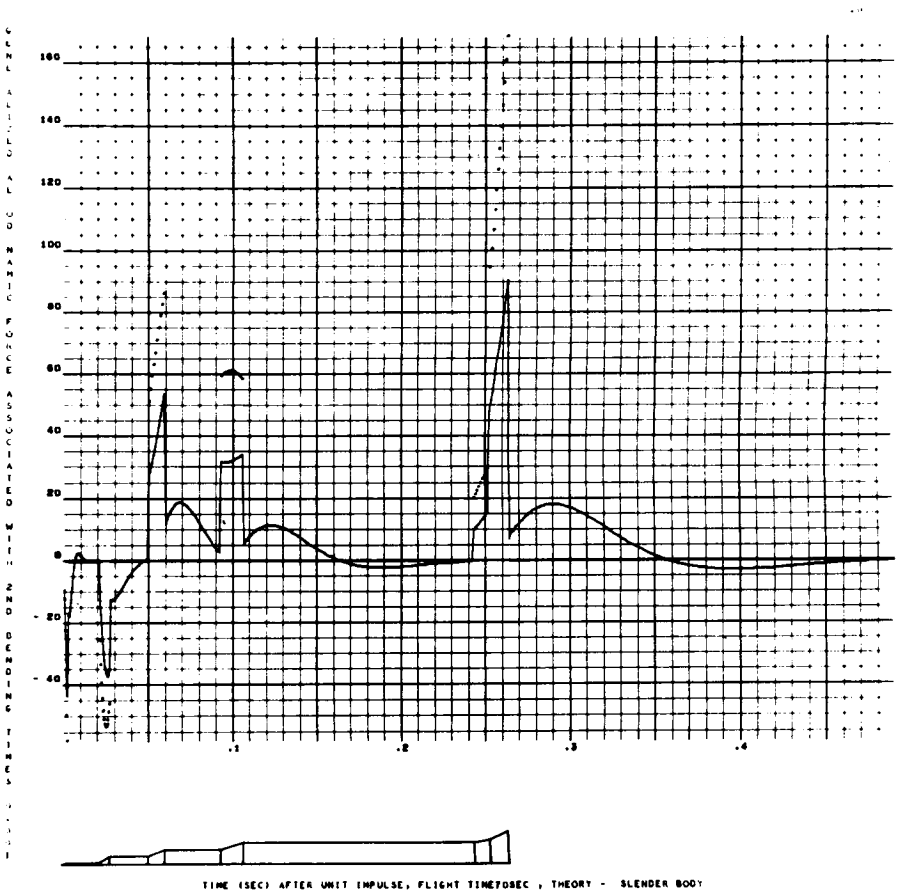

Fig. 10 - Impulsive Second Bending Moment Growth Functions for 70-sec. Flight Time

..... Pure Penetration
———— Penetration with Lift Growth
M = 1.345

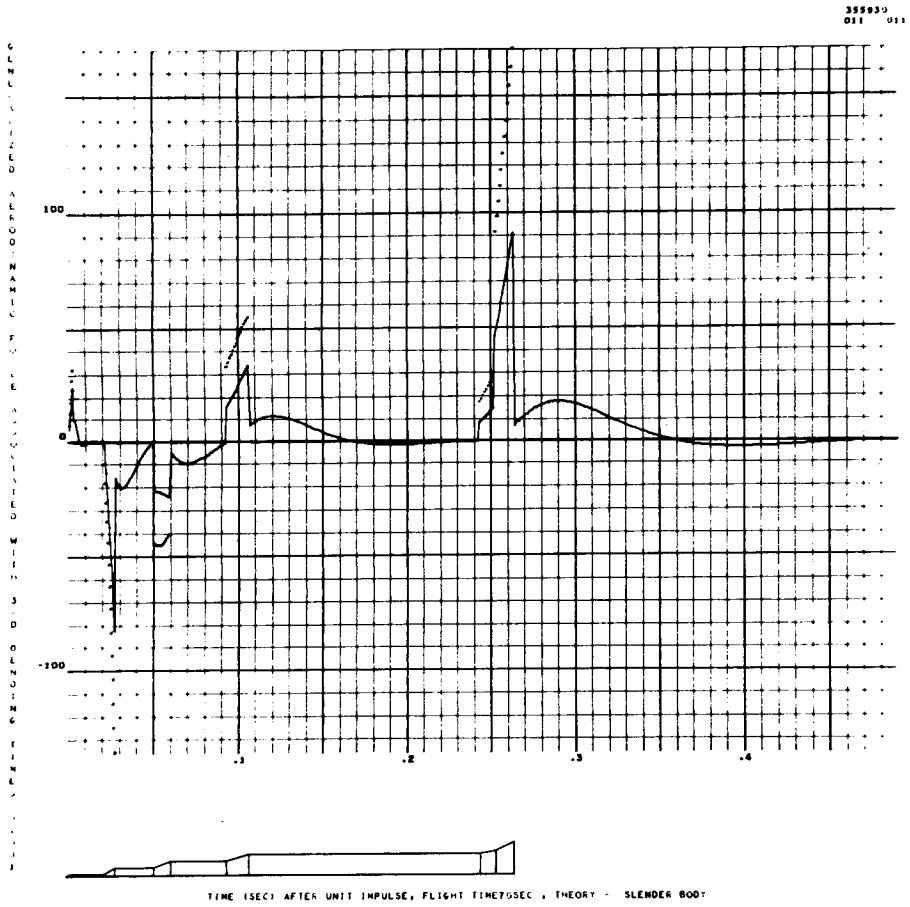

Fig. 11 - Impulsive Third Bending Moment Growth Functions for 70-sec. Flight Time

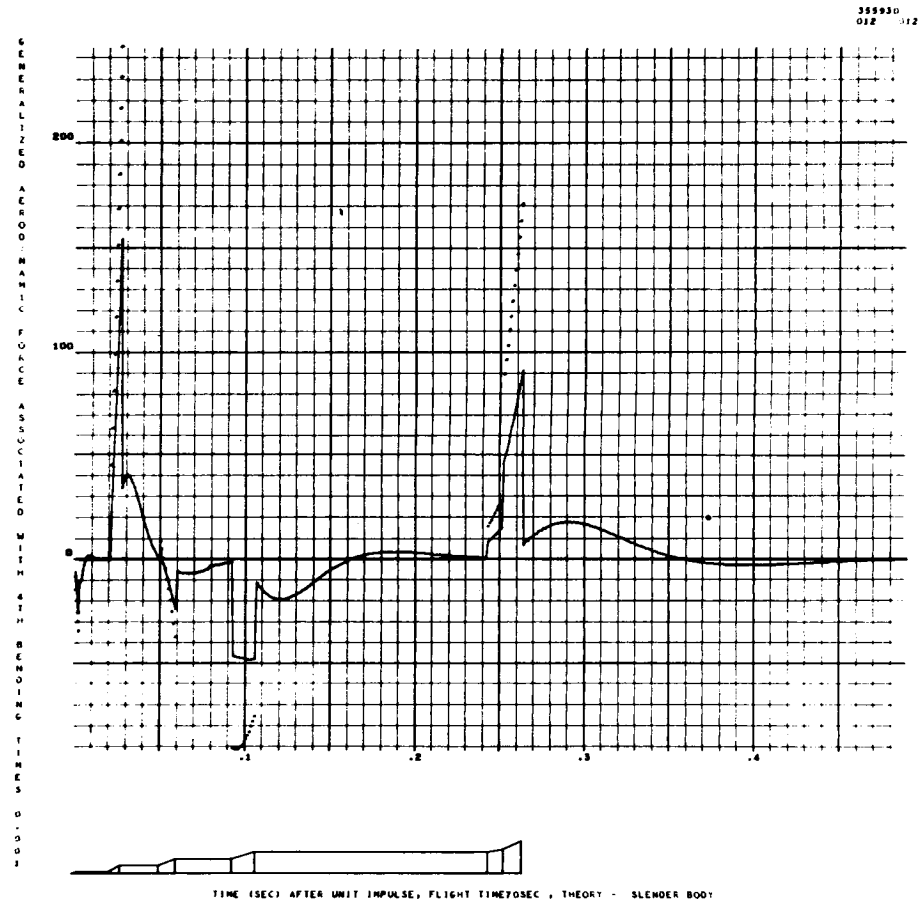

Fig. 12 - Impulsive Fourth Bending Moment Growth Functions for 70-sec. Flight Time

The moment distribution (generalized force due to rotation) is reduced to a relatively small steady-state value by the counteracting moment generated by the empennages.

The general form of the bending moment growth functions associated with the first four bending modes is similar to that of the rigid body forcing functions. The bending moment growth functions, however, reflect the character of the mode shapes. The negative growth functions in Figs. 9 through 12 correspond to regions of negative displacements of the respective bending modes. The integrated effects of the negative growth functions are given in the indicial forcing function plots. The mode shape influence on the growth functions in the region of the fins and engine shrouds in very weak. This is because the vehicle is extremely stiff in this region and all four mode shapes are normalized to one at the swivel point.

C. Method of Solution for Indicial and Impulsive Responses of Saturn V Configuration with Fins and Engine Shrouds

A fourth order* Runge-Kutta integration was used to numerically integrate the equations of motion. Responses were obtained for six different sets of aerodynamic environments. These six sets of forcing functions contain the indicial and impulsive aerodynamic forces** resulting from

1. Penetration with lift growth effects (abbreviated PWLG),
2. Pure penetration effects (abbreviated PP), and
3. Instantaneous immersion (abbreviated II).

---

* The Runge-Kutta integration expression used is considered to be of fourth-order accuracy. This is the same method used to compute the indicial and impulsive responses presented in [1].

** In [1] the aerodynamic forcing functions were calculated by the same computer program that obtained the indicial and impulsive responses. For this current investigation the aerodynamic subroutines were removed from the response program described in [1], and made into a completely separate main program. This aerodynamic program generated forcing function tapes which supplied a modified version of the response program with the necessary transient and steady-state aerodynamic wind forces. The use of externally generated aerodynamic tapes gave the response program greater flexibility in that the program was not tied directly to a specific aerodynamic theory or representation.

The Runge-Kutta integration process requires knowledge of the initial conditions (or starting values). The initial conditions for each of the six sets of forcing functions of both systems of equations were found through use of Laplace transform techniques. These techniques are discussed thoroughly in [1].

The indicial and impulsive responses of the Saturn V were computed at the 70- and 80-sec. flight times. The systems of equations are given in Appendix I and are described by a set of linear, differential equations with constant coefficients. Each set of coefficients, and consequently the associated responses, is applicable in a specific time interval.*.

Extremely fine time increments** were used in computing the indicial and impulsive responses of the deflections and their first derivatives. (Coarser increments were used in the printing and plotting of the output.)

In each flight time band, the responses were computed for a time interval of 20 sec. Twenty-second response records were computed for two purposes:

1. To insure that the responses achieved satisfactory steady-state values, and

2. To verify the assumption of using constant coefficients for a 10-sec. flight time band.

---

* The applicable interval of flight time for each set of these responses is taken as 10 sec. Thus, for example, the 70-sec. response calculations (obtained using the coefficients at 70 sec.) are considered valid between flight times of 65 and 75 sec.

** The selection of the increment size was based on the same two requirements used in [1]:

1. The increment size should be sufficiently small to permit a detailed description of the aerodynamic force distributions. (In this case, the aerodynamic forces are obtained from interpolation of data on the aerodynamic tapes.)

2. The increment size should permit 32 calculated response values per cycle for the highest frequency component of the system.

The impulsive responses for the 70-sec. flight time conditions converged at a faster rate than the 80-sec. responses. All of the 70-sec. impulsive responses (excluding translation) converged to within 1 percent or less of their maximum values at the end of 20 sec. In general, the 80-sec. impulsive responses also converged to within 1 percent of their maximum values with the exception of the higher bending modes, sloshing modes and control deflection. These latter responses had only decayed to within 5 percent at the end of 20 sec. In addition, the 80-sec. attitude control impulsive responses converged at a slower rate than the angle of attack control responses.

The assumption of constant coefficients was found to be valid for the 70-sec. flight time band responses. However, the use of constant coefficients in evaluating the 80-sec. responses was questionable. If, for each flight time band, the sloshing and fourth bending degrees of freedom were removed from both systems of equations, the responses of the remaining systems (excluding translation) would achieve satisfactory steady-state values within 10 sec. of response time. The sloshing and fourth bending modes are damped very lightly in comparison to the other modes of the system. Since coupled systems are considered, the response calculations for the generalized coordinates after about 7 or 8 sec. reflect the influence of sloshing and fourth bending*. The sloshing influence is governed basically by that part of the equations of motion which contain time invariant coefficients. The fourth bending mode, however, contains less damping at 80 sec. than at 70-sec. flight time (-0.3068 to -0.3338 rad/sec at 70 sec. compared to -0.1266 to -0.1593 rad/sec at 80 sec.). It is primarily this reduction in fourth bending damping that causes the 80-sec. responses to converge so slowly. For this reason, the 70-sec. responses are considered to be more reliable than the 80-sec. responses. Therefore, more emphasis will be given in this report to the 70-sec. responses than to the 80-sec. responses.

A considerable amount of indicial and impulsive response data were generated, plotted and analyzed in the investigation. Only a representative quantity of these data is presented in this report. Sample plots of the impulsive responses of several generalized coordinates are shown in Figs. 13 through 27 for the 70-sec. flight time band. These responses result from an angle of attack control system (Control 1) and reflect the three types of aerodynamic representation employed.

The numerics presented alongside the plots pertain to an analysis (see [1]) of the zero crossings, maximum and minimum values of the respective

* The effect of fourth bending was detected in all responses as early as 2 sec. after immersion into the gust.

SA-5 RESPØNSE TIME UNIT IMPULSE, I. I.,
70 SEC.F.T. CØNTRØL 1 ETA1, 1ST BENDING

0.00000	0.0000000E-39	CRØSS
0.16150	6.5980653E-03	MAX
0.43850	8.0696636E-06	CRØSS
0.69950	-5.5205663E-03	MIN
0.89150	-1.7068119E-06	CRØSS
1.05950	3.8420149E-03	MAX
1.17650	1.4684076E-05	CRØSS
1.23350	-1.0451792E-03	MIN
1.32049	-3.3587745E-04	MAX
1.45249	-2.1988033E-03	MIN
1.56649	-4.7036518E-05	CRØSS
1.60849	3.1120841E-04	MAX
1.67449	2.4976396E-06	CRØSS
1.68949	-2.5756396E-05	MIN
1.70149	-7.0974352E-06	CRØSS
1.80949	8.6627160E-04	MAX
1.89049	8.3476989E-06	CRØSS
1.94749	-4.5120762E-04	MIN
2.02849	-3.2590536E-06	CRØSS
2.03749	1.0395917E-05	MAX
2.04349	6.1152832E-06	CRØSS
2.17549	-1.4234545E-03	MIN
2.27749	-3.6988949E-05	CRØSS
2.31349	2.0450164E-04	MAX
2.34949	4.3274379E-06	CRØSS
2.42149	-5.7091810E-04	MIN
2.48149	-1.9749753E-05	CRØSS
2.55649	7.5497189E-04	MAX
2.64348	2.4084948E-05	CRØSS
2.67948	-1.3589998E-04	MIN
2.70948	-1.9183595E-05	CRØSS
2.79048	5.1122197E-04	MAX
2.86848	8.9747853E-06	CRØSS
2.91048	-1.8017792E-04	MIN
2.94648	-2.3579027E-05	CRØSS
3.03348	6.0047110E-04	MAX
3.12648	1.3962795E-05	CRØSS
3.15048	-4.8724784E-05	MIN
3.16848	-4.9658843E-06	CRØSS
3.27648	7.7575027E-04	MAX
3.37248	2.0161583E-05	CRØSS
3.40547	-1.0567773E-04	MIN
3.43547	-3.9287131E-06	CRØSS
3.51947	5.0198663E-04	MAX
3.59447	8.5123654E-06	CRØSS
3.65147	-3.0209894E-04	MIN
3.71147	-1.2432567E-05	CRØSS
3.76547	2.2919693E-04	MAX
3.81647	2.1444470E-05	CRØSS
3.88847	-3.4405032E-04	MIN
3.96047	-3.8063920E-06	CRØSS
4.00847	1.6835195E-04	MAX
4.05347	2.7365877E-07	CRØSS
4.12846	-3.6683672E-04	MIN
4.20346	-1.2031550E-05	CRØSS
4.25146	1.6355760E-04	MAX
4.29646	5.8655110E-06	CRØSS
4.37145	-3.5097754E-04	MIN
4.44345	-1.6039765E-05	CRØSS

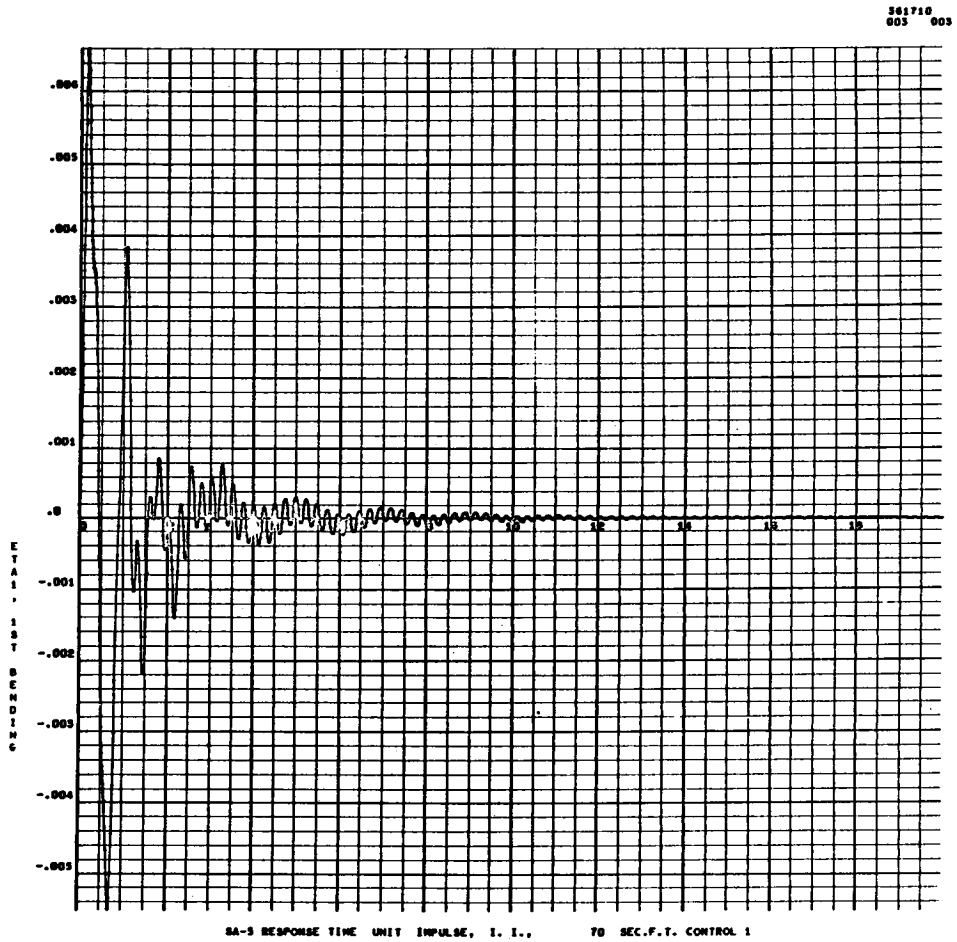

Fig. 13 - Impulsive Response of First Bending Considering Instantaneous Immersion - Angle of Attack Control, 70-sec. Flight Time

SA-5 RESPØNSE TIME UNIT IMPULSE, P. P.,
70 SEC.F.T. CØNTRØL 1 ETA1, 1ST BENDING

0.00000	0.0000000E-39	CRØSS
0.17250	5.3607514E-03	MAX
0.26350	3.3125399E-03	MIN
0.35350	4.2742389E-03	MAX
0.47550	3.5666366E-05	CRØSS
0.72650	-4.9096591E-03	MIN
0.98450	-1.0354164E-04	CRØSS
1.08350	2.7368673E-03	MAX
1.22450	1.6284372E-05	MIN
1.31449	7.9660375E-04	MAX
1.36549	6.9037168E-05	CRØSS
1.46149	-1.9781034E-03	MIN
1.59349	-9.0566712E-05	MAX
1.68649	-7.2348469E-04	MIN
1.74949	-4.2725092E-05	CRØSS
1.82149	8.0622598E-04	MAX
1.89349	1.0726035E-05	CRØSS
1.94149	-3.8027370E-04	MIN
1.99249	-1.9218525E-05	CRØSS
2.04649	3.7490829E-04	MAX
2.08849	1.6314974E-05	CRØSS
2.18149	-1.2776726E-03	MIN
2.28649	-4.3567020E-06	CRØSS
2.30749	8.7118922E-05	MAX
2.32849	1.0280843E-05	CRØSS
2.42149	-8.7508078E-04	MIN
2.49349	-4.0326795E-05	CRØSS
2.55649	6.1905620E-04	MAX
2.62848	3.8841499E-06	CRØSS
2.67348	-2.6522704E-04	MIN
2.71548	-2.0024422E-06	CRØSS
2.79348	6.3655720E-04	MAX
2.86848	2.2038202E-05	CRØSS
2.91348	-2.3288633E-04	MIN
2.95248	-1.9178550E-05	CRØSS
3.03348	6.3991824E-04	MAX
3.11748	1.7367217E-05	CRØSS
3.15048	-1.3624200E-04	MIN
3.18048	-2.3568832E-05	CRØSS
3.27648	7.9611948E-04	MAX
3.37548	7.9009874E-06	CRØSS
3.40247	-8.8918841E-05	MIN
3.42647	-1.6774806E-05	CRØSS
3.51947	6.3248657E-04	MAX
3.60047	1.9105010E-05	CRØSS
3.65147	-2.5673602E-04	MIN
3.69947	-1.5752865E-05	CRØSS
3.76547	3.4471226E-04	MAX
3.82547	1.6013125E-06	CRØSS
3.88847	-3.6586752E-04	MIN
3.95447	-2.2569634E-05	CRØSS
4.00847	2.2676803E-04	MAX
4.05647	1.2456301E-05	CRØSS
4.13146	-4.0097940E-04	MIN
4.20346	-7.7007992E-06	CRØSS
4.25146	1.9551743E-04	MAX
4.29646	2.0071524E-05	CRØSS
4.37445	-3.9264477E-04	MIN
4.44645	-8.4873548E-06	CRØSS

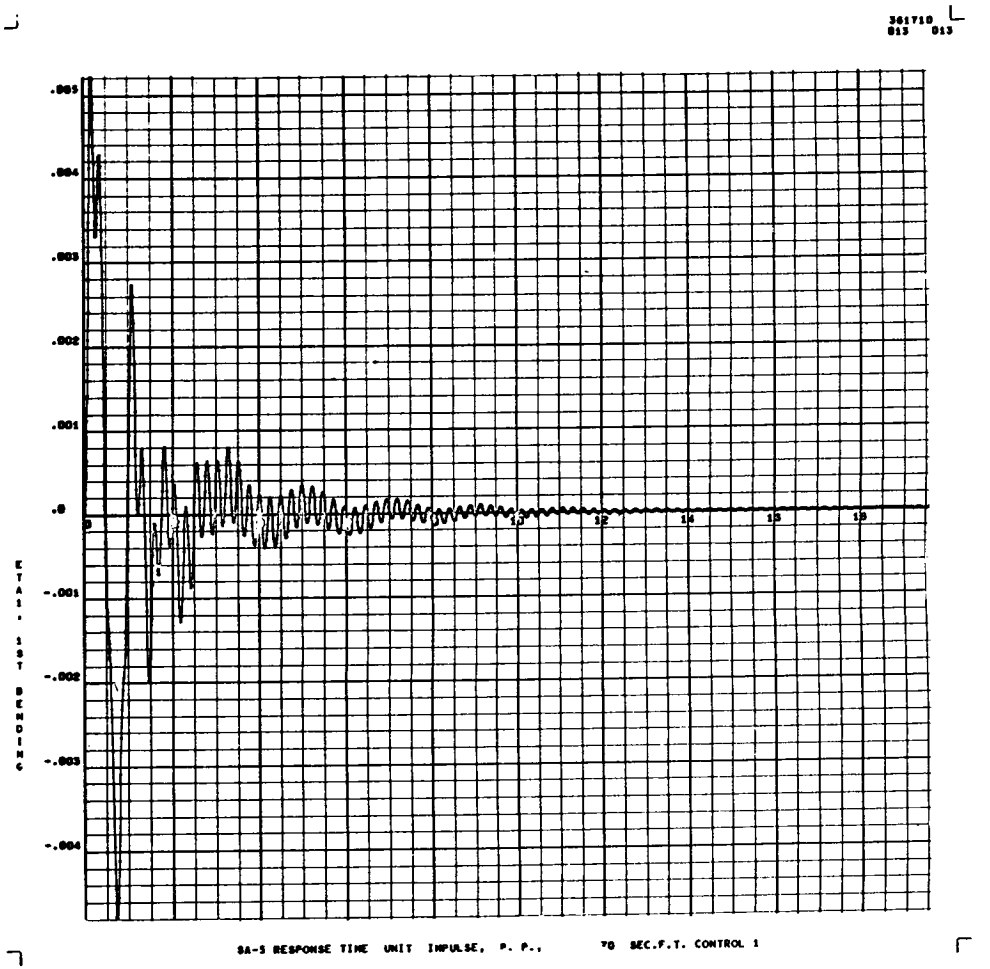

Fig. 14 - Impulsive Response of First Bending Considering Pure Penetration - Angle of Attack Control, 70-sec. Flight Time

SA-5 RESPØNSE TIME UNIT IMPULSE, P. W. L. G.,
70 SEC.F.T. CØNTRØL 1 ETA1, 1ST BENDING

0.00000	0.0000000E-39	CRØSS
0.17250	5.3988843E-03	MAX
0.27950	3.1992206E-03	MIN
0.36250	4.1859711E-03	MAX
0.47850	8.9374412E-06	CRØSS
0.72950	-4.8835310E-03	MIN
0.99050	-3.9125433E-05	CRØSS
1.08650	2.7471228E-03	MAX
1.20650	1.5818309E-06	CRØSS
1.22450	-9.3884461E-05	MIN
1.23950	-2.3426841E-05	CRØSS
1.32049	9.5353462E-04	MAX
1.37449	4.5246961E-05	CRØSS
1.46449	-2.0865475E-03	MIN
1.58449	-1.4661997E-05	CRØSS
1.59649	2.6657521E-05	MAX
1.60549	1.2297152E-05	CRØSS
1.69549	-7.7384982E-04	MIN
1.75849	-3.2187118E-06	CRØSS
1.82449	8.4473607E-04	MAX
1.89649	2.7066942E-05	CRØSS
1.94749	-4.2012625E-04	MIN
1.99849	-6.3443640E-06	CRØSS
2.04949	4.1704570E-04	MAX
2.09449	1.7256924E-05	CRØSS
2.18449	-1.3272523E-03	MIN
2.28049	-3.4755615E-05	CRØSS
2.31049	1.7083499E-04	MAX
2.34049	2.3346756E-06	CRØSS
2.42449	-9.4452315E-04	MIN
2.49949	-5.9972572E-06	CRØSS
2.56249	6.8928795E-04	MAX
2.63148	7.5164330E-06	CRØSS
2.67648	-3.2573687E-04	MIN
2.72148	-2.4584757E-05	CRØSS
2.79648	6.7931253E-04	MAX
2.87148	3.3710030E-05	CRØSS
2.91648	-2.7107567E-04	MIN
2.95848	-2.9676872E-05	CRØSS
3.03948	6.7312815E-04	MAX
3.12048	5.0722022E-06	CRØSS
3.15648	-1.8000180E-04	MIN
3.18948	-1.9233752E-05	CRØSS
3.28248	8.3370858E-04	MAX
3.37248	2.5223006E-05	CRØSS
3.40547	-1.4267213E-04	MIN
3.43847	-5.4443585E-06	CRØSS
3.52547	6.7173744E-04	MAX
3.60347	1.7226039E-05	CRØSS
3.65447	-3.0399106E-04	MIN
3.70547	-1.9755130E-05	CRØSS
3.76847	3.7800038E-04	MAX
3.82847	2.2949755E-05	CRØSS
3.89447	-4.0017743E-04	MIN
3.96047	-1.1842934E-05	CRØSS
4.01147	2.5457813E-04	MAX
4.06247	1.1599490E-05	CRØSS
4.13446	-4.3024696E-04	MIN
4.20646	-1.1416230E-05	CRØSS

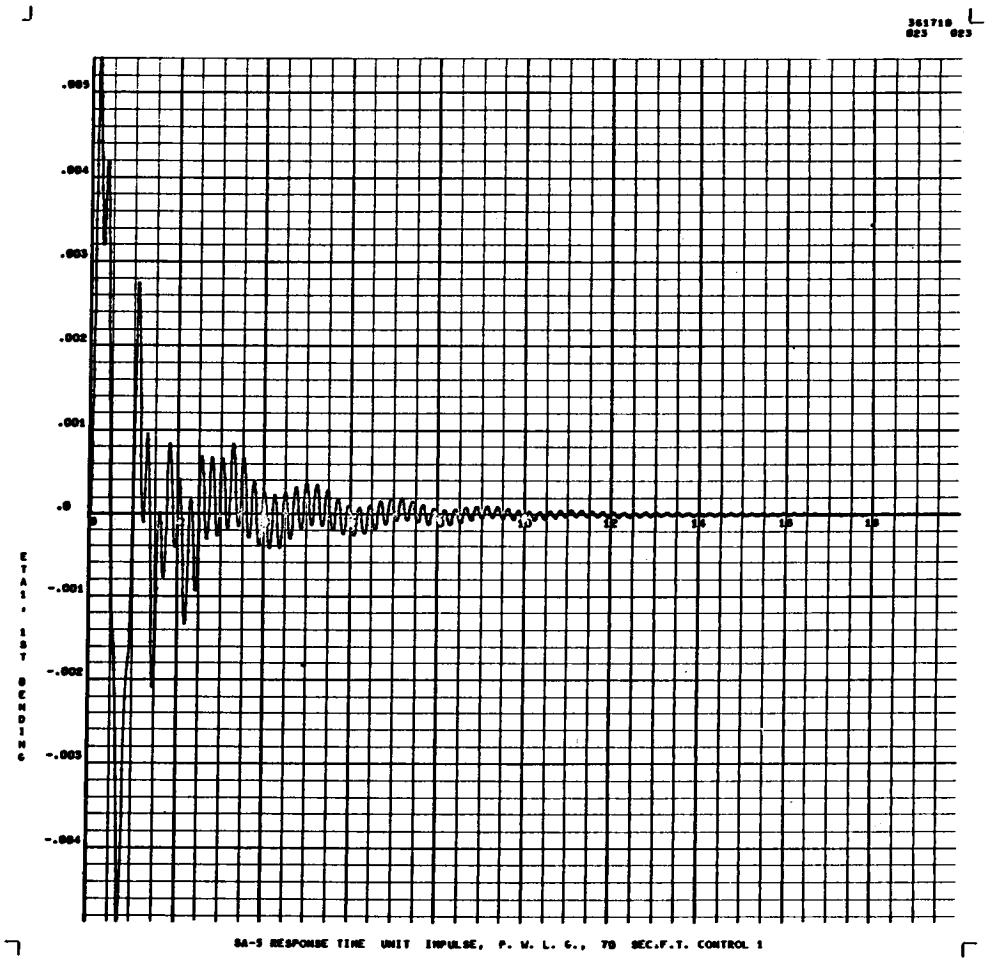

Fig. 15 - Impulsive Response of First Bending Considering Penetration With Lift Growth - Angle of Attack Control, 70-sec. Flight Time

SA-5 RESPØNSE TIME UNIT IMPULSE, I. I.,
70 SEC.F.T. CØNTRØL 1 ETA2, 2ND BENDING

0.00000	0.0000000E-39	CRØSS
0.13450	4.0798055E-03	MAX
0.22050	1.3657650E-05	CRØSS
0.29650	-2.7400594E-03	MIN
0.50450	-1.6160524E-05	CRØSS
0.60950	3.1720457E-03	MAX
0.71450	6.6829057E-05	CRØSS
0.91850	-2.6493699E-03	MIN
1.01150	-9.0954241E-05	CRØSS
1.08050	1.8178925E-03	MAX
1.15550	7.8629741E-05	CRØSS
1.20950	-9.2691647E-04	MIN
1.26050	-3.2238943E-05	CRØSS
1.33249	1.4680359E-03	MAX
1.40449	8.9716696E-06	CRØSS
1.46749	-1.1251422E-03	MIN
1.54249	-2.1011867E-05	CRØSS
1.58749	4.0989536E-04	MAX
1.62949	1.8241628E-05	CRØSS
1.70149	-8.2683211E-04	MIN
1.77949	-2.1733234E-05	CRØSS
1.81849	2.5589624E-04	MAX
1.85749	2.8967809E-05	CRØSS
1.92349	-5.4312740E-04	MIN
1.97749	-3.4982701E-05	CRØSS
2.04949	8.5810504E-04	MAX
2.11249	5.8761603E-05	CRØSS
2.17849	-8.4391113E-04	MIN
2.24449	-1.1202751E-05	CRØSS
2.30449	7.0513753E-04	MAX
2.36149	4.0502845E-05	CRØSS
2.43049	-8.1622002E-04	MIN
2.49649	-3.1936380E-05	CRØSS
2.55649	6.1963117E-04	MAX
2.62248	2.1143160E-05	CRØSS
2.67348	-3.8703466E-04	MIN
2.72448	-3.2966170E-05	CRØSS
2.79348	5.5344468E-04	MAX
2.86248	8.0788918E-06	CRØSS
2.91048	-3.1122499E-04	MIN
2.95848	-2.0537844E-05	CRØSS
3.03048	5.4228585E-04	MAX
3.09348	1.6295458E-05	CRØSS
3.15348	-4.5633360E-04	MIN
3.21048	-2.7417027E-06	CRØSS
3.27648	5.6720407E-04	MAX
3.34248	1.8392569E-05	CRØSS
3.40247	-4.4434960E-04	MIN
3.45947	-1.7426899E-05	CRØSS
3.52547	4.9179044E-04	MAX
3.58847	3.0190695E-05	CRØSS
3.64847	-3.8388183E-04	MIN
3.70847	-1.5664428E-05	CRØSS
3.76847	3.4048965E-04	MAX
3.82547	1.0382125E-05	CRØSS
3.88847	-3.6268900E-04	MIN
3.95147	-1.7197453E-06	CRØSS
4.00847	3.0046247E-04	MAX
4.06247	2.0266126E-05	CRØSS

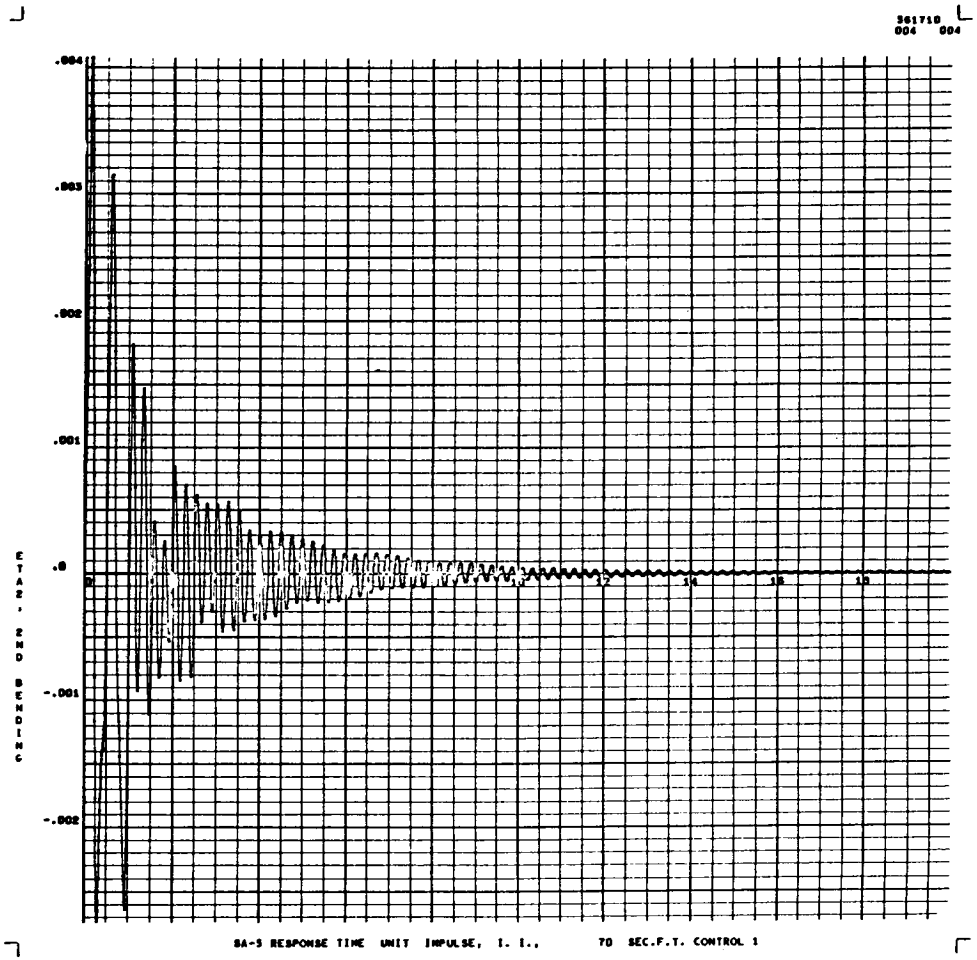

Fig. 16 - Impulsive Response of Second Bending Considering Instantaneous Immersion - Angle of Attack Control, 70-sec. Flight Time

SA-5 RESPØNSE TIME UNIT IMPULSE, P. P.,
70 SEC.F.T. CØNTRØL 1 ETA2, 2ND BENDING

0.00000	0.0000000E-39	CRØSS
0.03150	-1.9612131E-05	MIN
0.04150	-1.6208162E-07	CRØSS
0.15450	3.3658786E-03	MAX
0.23950	2.6629142E-05	CRØSS
0.28250	-1.0117910E-03	MIN
0.36750	-6.5993255E-05	MAX
0.47550	-1.7095756E-03	MIN
0.54350	-8.4152161E-06	CRØSS
0.61850	1.9496530E-03	MAX
0.72350	3.0214460E-05	CRØSS
0.74750	-9.4990118E-05	MIN
0.77150	-4.5416039E-06	CRØSS
0.81050	1.8670076E-04	MAX
0.83750	2.1411032E-05	CRØSS
0.94850	-2.2954593E-03	MIN
1.03550	-2.7153622E-05	CRØSS
1.08650	9.5320389E-04	MAX
1.13750	8.0683970E-05	CRØSS
1.20350	-1.1794803E-03	MIN
1.26050	-3.4189350E-05	CRØSS
1.33249	1.5881697E-03	MAX
1.40449	3.4447898E-05	CRØSS
1.46149	-1.0160883E-03	MIN
1.52449	-6.1625910E-05	CRØSS
1.57849	6.9509777E-04	MAX
1.63249	1.2735441E-05	CRØSS
1.70149	-9.8350803E-04	MIN
1.77349	-3.6787578E-05	CRØSS
1.81849	4.0084537E-04	MAX
1.86049	3.7188124E-05	CRØSS
1.92949	-7.9792164E-04	MIN
1.99249	-1.1197697E-05	CRØSS
2.05549	8.4095635E-04	MAX
2.11549	6.0554693E-05	CRØSS
2.18149	-8.3196283E-04	MIN
2.24149	-2.6937556E-05	CRØSS
2.30449	7.8717605E-04	MAX
2.36149	5.2561321E-05	CRØSS
2.42749	-8.6145810E-04	MIN
2.49349	-5.2837068E-05	CRØSS
2.55349	6.4870910E-04	MAX
2.61348	3.3104522E-05	CRØSS
2.67348	-5.5046458E-04	MIN
2.72748	-3.5447012E-05	CRØSS
2.79348	6.4211462E-04	MAX
2.85948	2.6674918E-05	CRØSS
2.91348	-4.0990074E-04	MIN
2.96148	-3.3166349E-05	CRØSS
3.03348	6.3866691E-04	MAX
3.09648	3.4716330E-05	CRØSS
3.15648	-4.8660531E-04	MIN
3.21048	-1.5667856E-05	CRØSS
3.27648	6.1764329E-04	MAX
3.34248	2.1339375E-05	CRØSS
3.40247	-4.8346617E-04	MIN
3.45947	-3.9362635E-06	CRØSS
3.52547	5.5046014E-04	MAX
3.58847	1.9202530E-05	CRØSS

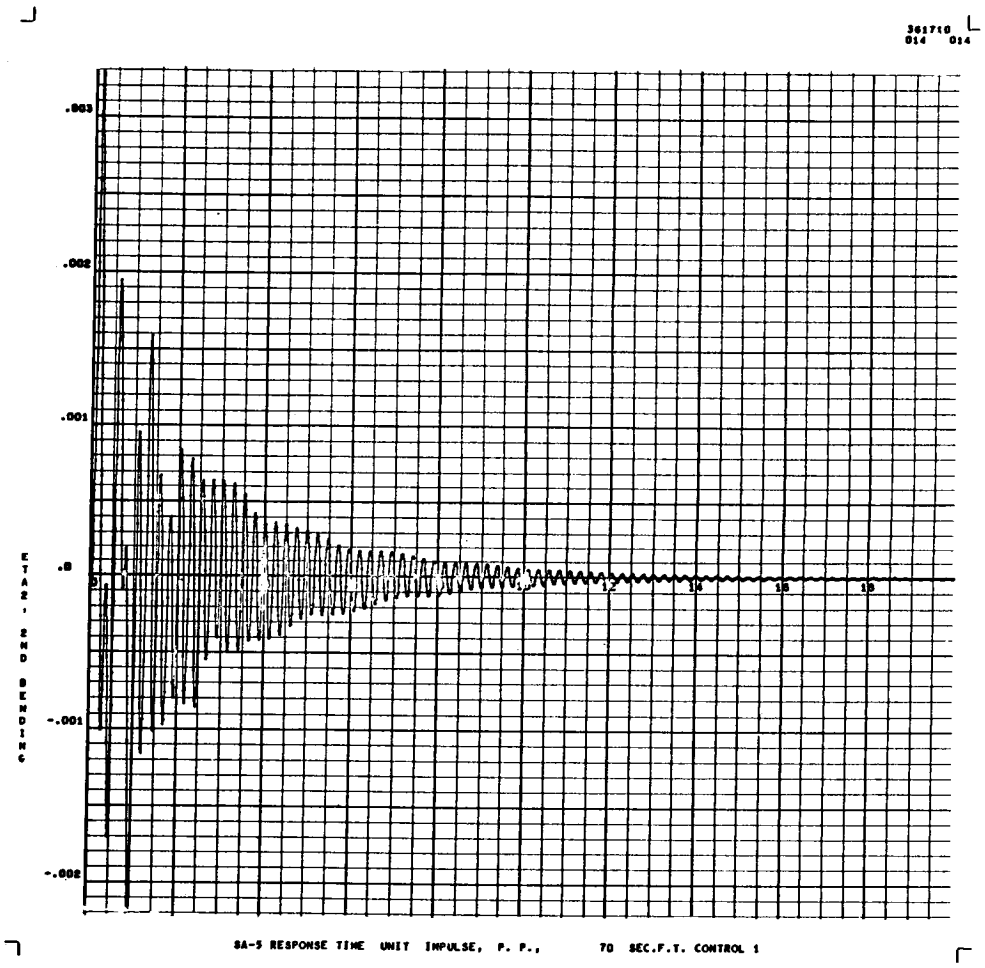

Fig. 17 - Impulsive Response of Second Bending Considering Pure Penetration - Angle of Attack Control, 70-sec. Flight Time

SA-5 RESPØNSE TIME UNIT IMPULSE, P. W. L. G.,
70 SEC.F.T. CØNTRØL 1 ETA2, 2ND BENDING

0.00000	0.0000000E-39	CRØSS
0.03050	-1.6471559E-05	MIN
0.04050	-9.9978698E-07	CRØSS
0.15650	3.3253909E-03	MAX
0.24050	2.7814776E-05	CRØSS
0.28850	-1.1921446E-03	MIN
0.36250	-8.4190173E-06	CRØSS
0.37850	8.1597526E-05	MAX
0.39350	5.9955005E-07	CRØSS
0.48350	-1.6063286E-03	MIN
0.54750	-2.9839494E-05	CRØSS
0.62150	1.9478412E-03	MAX
0.71450	4.0951675E-05	CRØSS
0.74750	-2.7212614E-04	MIN
0.78950	-3.9021168E-06	CRØSS
0.82250	1.8655619E-04	MAX
0.84650	2.5417360E-05	CRØSS
0.95450	-2.2289921E-03	MIN
1.03550	-6.6212570E-05	CRØSS
1.08950	1.0278784E-03	MAX
1.14050	3.2438771E-05	CRØSS
1.20650	-1.3751468E-03	MIN
1.26350	-9.1191967E-05	CRØSS
1.33549	1.7826878E-03	MAX
1.40749	6.2041262E-05	CRØSS
1.46749	-1.1774034E-03	MIN
1.53049	-3.9988449E-05	CRØSS
1.58449	8.1812700E-04	MAX
1.63849	4.6410400E-05	CRØSS
1.70749	-1.0650837E-03	MIN
1.77949	-2.0703494E-05	CRØSS
1.82449	4.5685829E-04	MAX
1.86949	8.8815664E-06	CRØSS
1.93549	-8.3226502E-04	MIN
1.99549	-4.1492203E-05	CRØSS
2.06149	8.9492032E-04	MAX
2.12149	6.3105708E-06	CRØSS
2.18449	-9.1458581E-04	MIN
2.24449	-4.2471604E-05	CRØSS
2.30749	8.8607297E-04	MAX
2.36749	2.4495480E-05	CRØSS
2.43349	-9.5879447E-04	MIN
2.49949	-1.8614273E-05	CRØSS
2.55949	7.3919022E-04	MAX
2.61948	2.2946685E-05	CRØSS
2.67648	-6.2259739E-04	MIN
2.73348	-4.2036397E-05	CRØSS
2.79948	6.9659754E-04	MAX
2.86548	1.0446034E-05	CRØSS
2.91648	-4.5658193E-04	MIN
2.96748	-3.3986579E-05	CRØSS
3.03648	6.8186485E-04	MAX
3.10248	5.3528315E-06	CRØSS
3.15948	-5.3891698E-04	MIN
3.21348	-4.3330339E-05	CRØSS
3.28248	6.7371155E-04	MAX
3.34548	3.5388739E-05	CRØSS
3.40547	-5.4547690E-04	MIN
3.46247	-3.3304096E-05	CRØSS

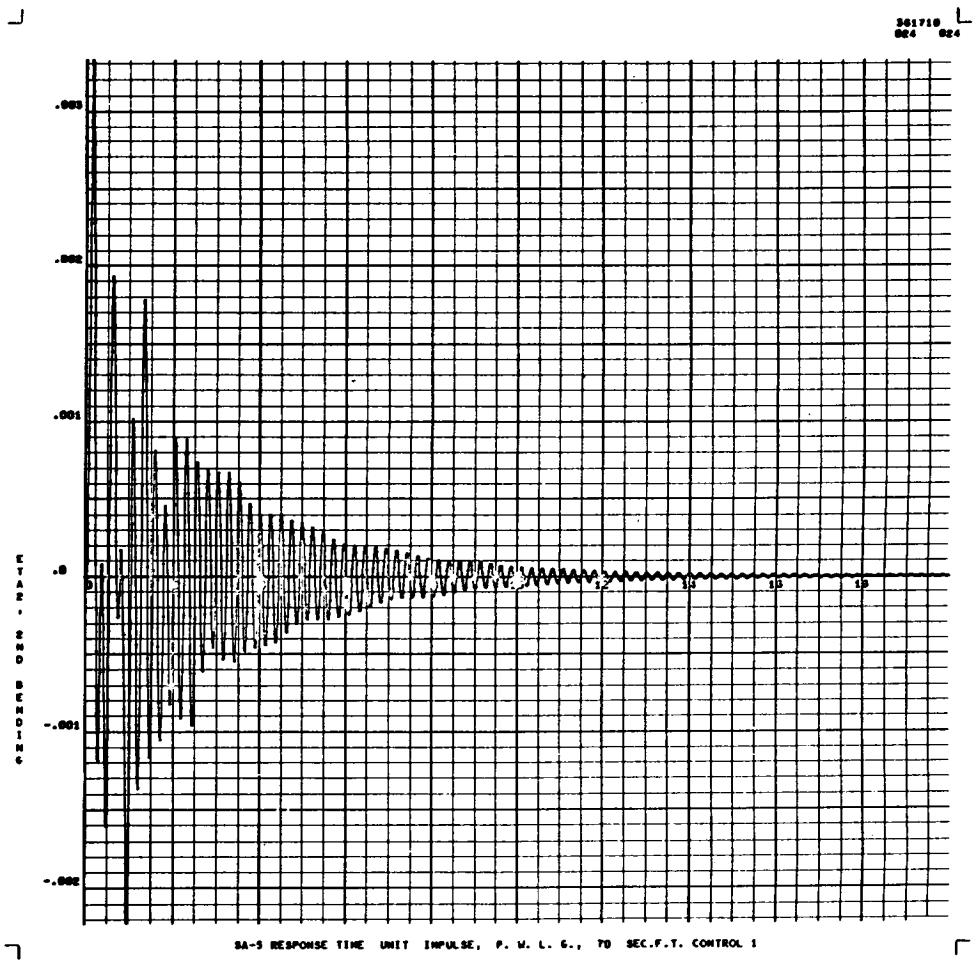

Fig. 18 - Impulsive Response of Second Bending Considering Penetration With Lift Growth - Angle of Attack Control, 70-sec. Flight Time

SA-5 RESPØNSE TIME UNIT IMPULSE, I. I.,
70 SEC.F.T. CØNTRØL 1 ETA3, 3RD BENDING

0.00000	0.0000000E-39	CRØSS
0.11650	3.2710698E-03	MAX
0.17350	5.0034270E-05	CRØSS
0.24750	-5.7374564E-03	MIN
0.31450	-6.6761986E-05	CRØSS
0.38650	6.2133525E-03	MAX
0.46550	9.2987721E-05	CRØSS
0.53650	-4.1032694E-03	MIN
0.64850	-9.6909177E-05	CRØSS
0.77750	3.4839374E-03	MAX
0.84950	1.5028382E-04	CRØSS
0.93650	-5.7821202E-03	MIN
1.00850	-1.2852055E-04	CRØSS
1.07750	5.2419722E-03	MAX
1.14650	4.0722571E-05	CRØSS
1.21250	-4.7131538E-03	MIN
1.27849	-2.8738768E-04	CRØSS
1.34749	4.1372674E-03	MAX
1.41949	9.0032579E-05	CRØSS
1.48249	-2.7181901E-03	MIN
1.56049	-2.3360658E-05	CRØSS
1.60549	8.7847782E-04	MAX
1.66249	1.2715435E-05	CRØSS
1.70149	-3.9317288E-04	MIN
1.73749	-6.2483837E-06	CRØSS
1.79449	8.0361182E-04	MAX
1.83949	6.4338892E-05	CRØSS
1.91449	-1.9529666E-03	MIN
1.97449	-1.5566013E-04	CRØSS
2.04649	2.5788278E-03	MAX
2.11249	1.4437925E-05	CRØSS
2.17849	-2.6765252E-03	MIN
2.24449	-8.9275258E-05	CRØSS
2.31049	2.4408931E-03	MAX
2.37649	6.0215561E-05	CRØSS
2.43949	-1.9729839E-03	MIN
2.50549	-5.2766771E-05	CRØSS
2.56549	1.3852459E-03	MAX
2.62848	3.8782627E-05	CRØSS
2.67948	-8.2605420E-04	MIN
2.73048	-5.9366781E-05	CRØSS
2.79048	8.9158100E-04	MAX
2.84448	3.6608835E-05	CRØSS
2.90448	-9.6922948E-04	MIN
2.95848	-2.0422458E-06	CRØSS
3.02448	1.3870370E-03	MAX
3.08748	4.4587359E-06	CRØSS
3.15048	-1.4743749E-03	MIN
3.21348	-2.9724764E-05	CRØSS
3.27948	1.5269927E-03	MAX
3.34248	5.6108394E-05	CRØSS
3.40547	-1.3441149E-03	MIN
3.46847	-4.7163420E-05	CRØSS
3.53147	1.1450968E-03	MAX
3.59147	6.8390509E-05	CRØSS
3.65147	-9.1743151E-04	MIN
3.71147	-2.9323964E-05	CRØSS
3.76847	7.7220006E-04	MAX
3.82547	2.6998994E-05	CRØSS

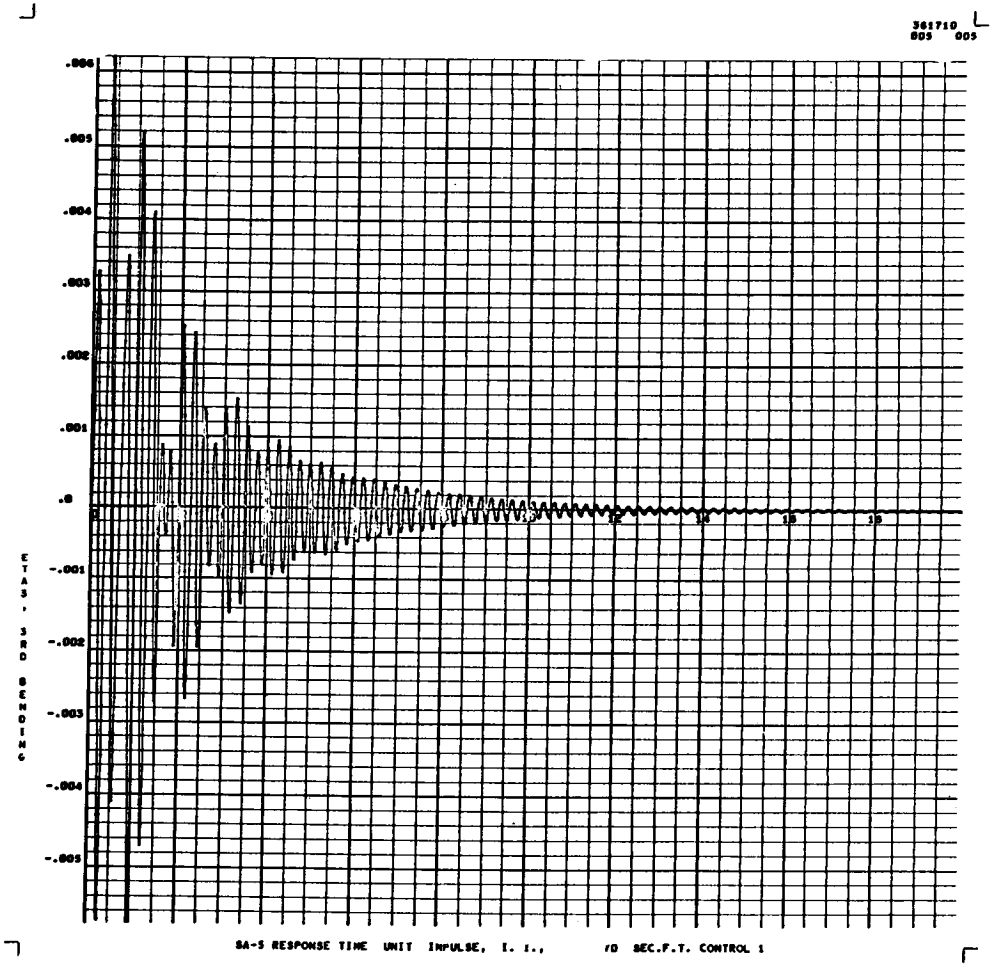

Fig. 19 - Impulsive Response of Third Bending Considering Instantaneous Immersion - Angle of Attack Control, 70-Sec. Flight Time

SA-5 RESPØNSE TIME UNIT IMPULSE, P. P.,
70 SEC.F.T. CØNTRØL 1 ETA3, 3RD BENDING

0.00000	0.0000000E-39	CRØSS
0.02500	1.7935545E-05	MAX
0.03250	8.2419361E-06	MIN
0.13750	2.9974382E-03	MAX
0.19150	1.1416106E-05	CRØSS
0.25750	-4.7944541E-03	MIN
0.31750	-3.5590210E-06	CRØSS
0.38350	4.8802217E-03	MAX
0.45750	6.0364967E-05	CRØSS
0.51650	-2.8083393E-03	MIN
0.60350	-2.5413001E-05	CRØSS
0.63050	2.7534338E-04	MAX
0.66050	2.0414009E-06	CRØSS
0.69650	-3.4427258E-04	MIN
0.72350	-3.5203489E-05	CRØSS
0.81050	2.6294008E-03	MAX
0.86750	1.9250440E-04	CRØSS
0.94550	-4.4647216E-03	MIN
1.01150	-2.6268937E-04	CRØSS
1.07750	4.2382748E-03	MAX
1.14050	2.6397702E-04	CRØSS
1.20950	-4.4424066E-03	MIN
1.27550	-1.8894621E-04	CRØSS
1.34149	3.8761794E-03	MAX
1.41049	9.7592443E-05	CRØSS
1.47049	-2.6537622E-03	MIN
1.53649	-1.0142178E-04	CRØSS
1.59049	1.5100144E-03	MAX
1.64449	6.7225493E-05	CRØSS
1.69849	-1.2882805E-03	MIN
1.75249	-8.1902304E-05	CRØSS
1.80949	1.2592417E-03	MAX
1.85749	8.0974734E-05	CRØSS
1.92649	-2.0602754E-03	MIN
1.98649	-2.7488419E-05	CRØSS
2.05249	2.4226728E-03	MAX
2.11249	1.7394684E-04	CRØSS
2.17849	-2.5469919E-03	MIN
2.24449	-7.4429845E-06	CRØSS
2.30749	2.4058513E-03	MAX
2.37049	1.4933866E-04	CRØSS
2.43349	-2.0576415E-03	MIN
2.49649	-1.3022252E-04	CRØSS
2.55649	1.6243801E-03	MAX
2.61948	4.0146345E-05	CRØSS
2.67648	-1.2476273E-03	MIN
2.73048	-8.8934066E-05	CRØSS
2.79048	1.2626326E-03	MAX
2.85048	2.8263379E-05	CRØSS
2.91048	-1.2133937E-03	MIN
2.96448	-3.4313817E-05	CRØSS
3.03048	1.5190081E-03	MAX
3.09048	6.1932829E-05	CRØSS
3.15348	-1.5116039E-03	MIN
3.21348	-6.7571940E-05	CRØSS
3.27948	1.5816279E-03	MAX
3.34248	1.4832220E-05	CRØSS
3.40247	-1.4182098E-03	MIN
3.46547	-3.7909140E-05	CRØSS

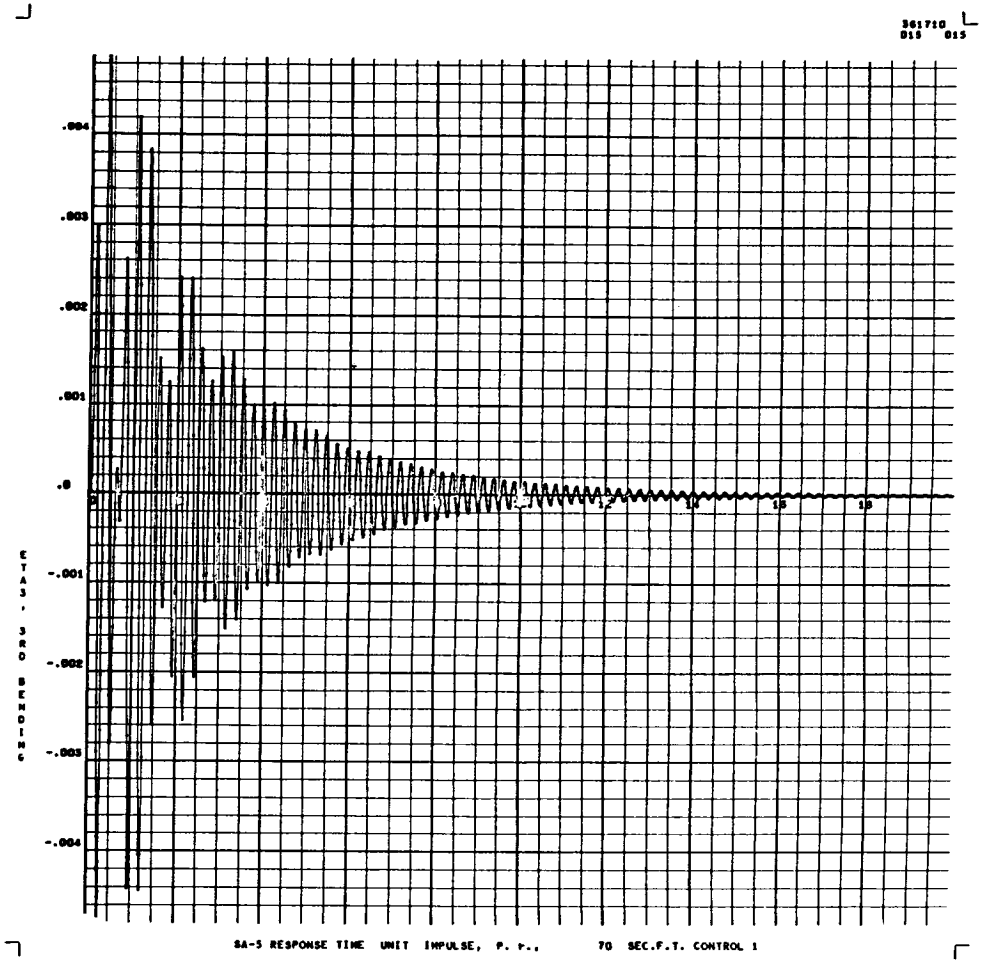

Fig. 20 - Impulsive Response of Third Bending Considering Pure Penetration - Angle of Attack Control, 70-sec. Flight Time

SA-5 RESPØNSE TIME UNIT IMPULSE, P. W. L. G.,
70 SEC.F.T. CØNTRØL 1 ETA3, 3RD BENDING

0.00000	0.0000000E-39	CRØSS
0.02700	2.1210886E-05	MAX
0.02900	2.0999438E-05	MIN
0.13750	2.9041168E-03	MAX
0.19150	1.5803446E-05	CRØSS
0.25850	-4.7632182E-03	MIN
0.31950	-3.5044206E-05	CRØSS
0.38750	5.4121056E-03	MAX
0.45950	2.6771891E-05	CRØSS
0.52050	-3.5093405E-03	MIN
0.60350	-7.6901015E-06	CRØSS
0.64250	7.4420536E-04	MAX
0.70850	8.0810002E-05	MIN
0.81350	2.3735614E-03	MAX
0.86750	1.3623726E-04	CRØSS
0.94550	-4.6261213E-03	MIN
1.01150	-2.8104358E-04	CRØSS
1.08050	4.7666033E-03	MAX
1.14350	1.5960482E-04	CRØSS
1.21250	-5.1129611E-03	MIN
1.27849	-2.0890394E-04	CRØSS
1.34449	4.5278879E-03	MAX
1.41349	1.7265155E-04	CRØSS
1.47349	-3.1941151E-03	MIN
1.54249	-9.7571527E-05	CRØSS
1.59649	1.8529876E-03	MAX
1.65349	1.2261593E-04	CRØSS
1.70749	-1.3692862E-03	MIN
1.76149	-6.9971734E-05	CRØSS
1.81549	1.2241209E-03	MAX
1.86349	9.7377051E-06	CRØSS
1.92949	-2.1042127E-03	MIN
1.98949	-9.3067138E-06	CRØSS
2.05549	2.6044050E-03	MAX
2.11549	1.6502547E-04	CRØSS
2.18449	-2.8314621E-03	MIN
2.24749	-1.4691659E-05	CRØSS
2.31049	2.7336804E-03	MAX
2.37649	3.2405045E-05	CRØSS
2.43949	-2.3698958E-03	MIN
2.50249	-8.6028967E-05	CRØSS
2.56249	1.8758581E-03	MAX
2.62548	5.0263605E-05	CRØSS
2.68248	-1.4090992E-03	MIN
2.73948	-2.3913831E-05	CRØSS
2.79948	1.3506999E-03	MAX
2.85648	1.9410044E-05	CRØSS
2.91348	-1.2870515E-03	MIN
2.96748	-9.9223060E-05	CRØSS
3.03348	1.6194572E-03	MAX
3.09348	9.4110854E-05	CRØSS
3.15648	-1.6553516E-03	MIN
3.21648	-1.0814801E-04	CRØSS
3.28248	1.7548132E-03	MAX
3.34548	5.2688934E-05	CRØSS
3.40847	-1.6017718E-03	MIN
3.46847	-1.0275633E-04	CRØSS
3.53147	1.4554682E-03	MAX
3.59447	2.8687478E-05	CRØSS

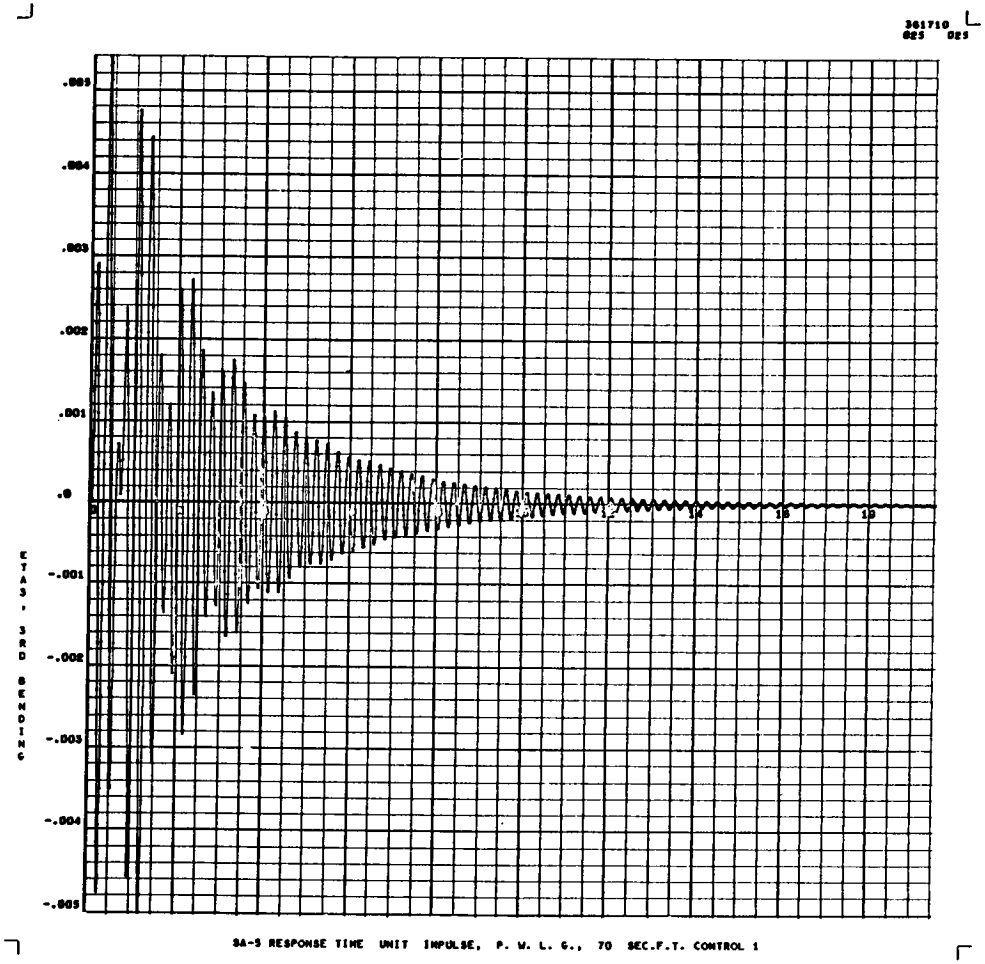

Fig. 21 - Impulsive Response of Third Bending Considering Penetration With Lift Growth - Angle of Attack Control, 70-sec. Flight Time

SA-5 RESPØNSE TIME UNIT IMPULSE, I. I.,
70 SEC.F.T. CØNTRØL 1 ETA4, 4TH BENDING

0.00000	0.0000000E-39	CRØSS
0.10450	9.1046832E-04	MAX
0.15250	7.7912923E-06	CRØSS
0.22150	-2.1098189E-03	MIN
0.27650	-3.1369698E-05	CRØSS
0.34450	3.2278676E-03	MAX
0.40450	1.1269767E-05	CRØSS
0.46950	-3.8408936E-03	MIN
0.53150	-1.2713525E-05	CRØSS
0.59550	4.1535340E-03	MAX
0.65750	1.4918430E-04	CRØSS
0.72350	-4.1875698E-03	MIN
0.78650	-6.3207335E-06	CRØSS
0.84950	3.9162805E-03	MAX
0.91250	5.2404364E-05	CRØSS
0.97550	-3.5383696E-03	MIN
1.03850	-1.8741840E-04	CRØSS
1.09850	2.6667764E-03	MAX
1.15850	8.7093729E-05	CRØSS
1.21550	-2.1649145E-03	MIN
1.27250	-5.5681865E-05	CRØSS
1.33249	2.1572566E-03	MAX
1.38949	1.9558485E-05	CRØSS
1.44949	-2.3292251E-03	MIN
1.50949	-3.6075893E-05	CRØSS
1.57249	2.4947159E-03	MAX
1.62949	1.7731095E-04	CRØSS
1.69549	-2.7065625E-03	MIN
1.75849	-1.1791253E-05	CRØSS
1.82149	2.5968185E-03	MAX
1.88149	1.2984612E-04	CRØSS
1.94449	-2.4258292E-03	MIN
2.00749	-3.5893685E-05	CRØSS
2.06749	2.1526379E-03	MAX
2.13049	4.8923175E-06	CRØSS
2.19049	-1.8810109E-03	MIN
2.24749	-1.2911650E-04	CRØSS
2.30749	1.7271764E-03	MAX
2.36749	5.8245414E-05	CRØSS
2.42749	-1.6902216E-03	MIN
2.48749	-2.6566227E-05	CRØSS
2.54749	1.7313583E-03	MAX
2.60749	9.7795708E-05	CRØSS
2.67048	-1.7451429E-03	MIN
2.73048	-5.9449065E-05	CRØSS
2.79348	1.7768306E-03	MAX
2.85348	1.2798315E-04	CRØSS
2.91648	-1.6720746E-03	MIN
2.97648	-1.1421074E-04	CRØSS
3.03948	1.5870304E-03	MAX
3.10248	2.1623855E-06	CRØSS
3.16248	-1.4421780E-03	MIN
3.22248	-4.5578933E-05	CRØSS
3.28248	1.3436745E-03	MAX
3.34248	6.9464671E-05	CRØSS
3.40547	-1.2682998E-03	MIN
3.46247	-7.2230803E-05	CRØSS
3.52547	1.2408879E-03	MAX
3.58547	3.4984241E-06	CRØSS

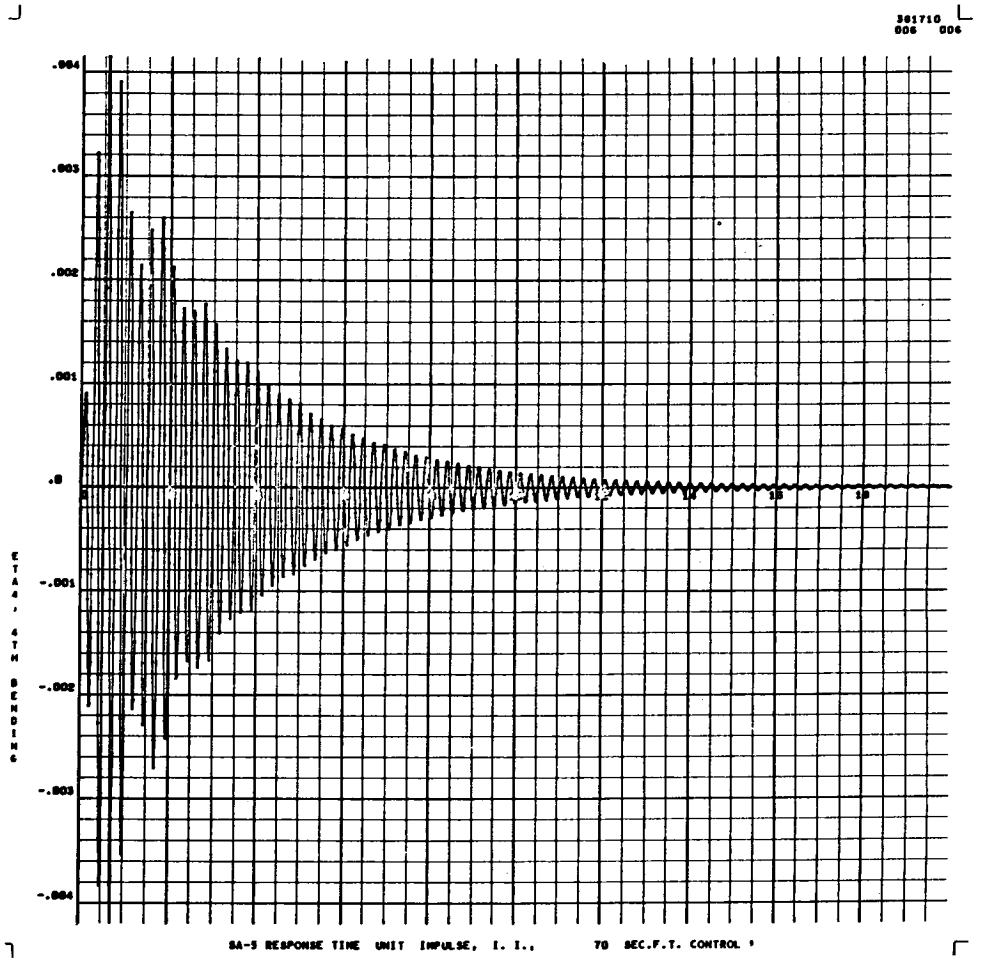

Fig. 22 - Impulsive Response of Fourth Bending Considering Instantaneous Immersion - Angle of Attack Control, 70-Sec. Flight Time

SA-5 RESPØNSE TIME UNIT IMPULSE, P. P.,
70 SEC.F.T. CØNTRØL 1 ETA4, 4TH BENDING

0.00000	0.0000000E-39	CRØSS
0.02050	-4.1206121E-06	MIN
0.02500	-5.8382935E-07	CRØSS
0.11450	1.0766399E-03	MAX
0.16350	7.7687250E-06	CRØSS
0.23250	-2.3175789E-03	MIN
0.28450	-4.7773055E-05	CRØSS
0.35050	3.4862123E-03	MAX
0.40950	3.1063907E-05	CRØSS
0.47350	-4.0262621E-03	MIN
0.53350	-8.4097586E-05	CRØSS
0.59750	4.3502594E-03	MAX
0.65750	2.6992344E-04	CRØSS
0.72350	-4.3932509E-03	MIN
0.78350	-2.7365940E-04	CRØSS
0.84650	4.1484683E-03	MAX
0.90950	1.6201819E-04	CRØSS
0.97250	-3.8054922E-03	MIN
1.03550	-8.1502585E-05	CRØSS
1.09550	3.1312802E-03	MAX
1.15550	4.6896275E-07	CRØSS
1.21250	-2.8385643E-03	MIN
1.27250	-1.1421847E-04	CRØSS
1.33249	2.7210739E-03	MAX
1.39249	2.4836740E-05	CRØSS
1.45249	-2.7369300E-03	MIN
1.51249	-3.5152021E-05	CRØSS
1.57549	2.8111320E-03	MAX
1.63249	1.5868816E-04	CRØSS
1.69549	-2.9266572E-03	MIN
1.75849	-6.7000632E-05	CRØSS
1.82149	2.7944373E-03	MAX
1.88149	7.7544655E-05	CRØSS
1.94449	-2.6764574E-03	MIN
2.00449	-1.2964083E-04	CRØSS
2.06749	2.4379803E-03	MAX
2.12749	6.2249806E-05	CRØSS
2.18749	-2.2256218E-03	MIN
2.24749	-9.5388976E-05	CRØSS
2.30749	2.0825395E-03	MAX
2.36749	9.7229942E-05	CRØSS
2.43049	-2.0092112E-03	MIN
2.48749	-1.1055510E-04	CRØSS
2.55049	1.9967160E-03	MAX
2.61049	3.2906304E-05	CRØSS
2.67048	-1.9693320E-03	MIN
2.73048	-1.2405010E-04	CRØSS
2.79348	1.9676915E-03	MAX
2.85648	1.4655379E-06	CRØSS
2.91648	-1.8595462E-03	MIN
2.97648	-1.0034522E-04	CRØSS
3.03948	1.7911173E-03	MAX
3.09948	9.7051723E-05	CRØSS
3.16248	-1.6532036E-03	MIN
3.22248	-1.7884171E-05	CRØSS
3.28248	1.5696103E-03	MAX
3.34248	7.4610943E-05	CRØSS
3.40547	-1.4841108E-03	MIN
3.46247	-1.0019840E-04	CRØSS

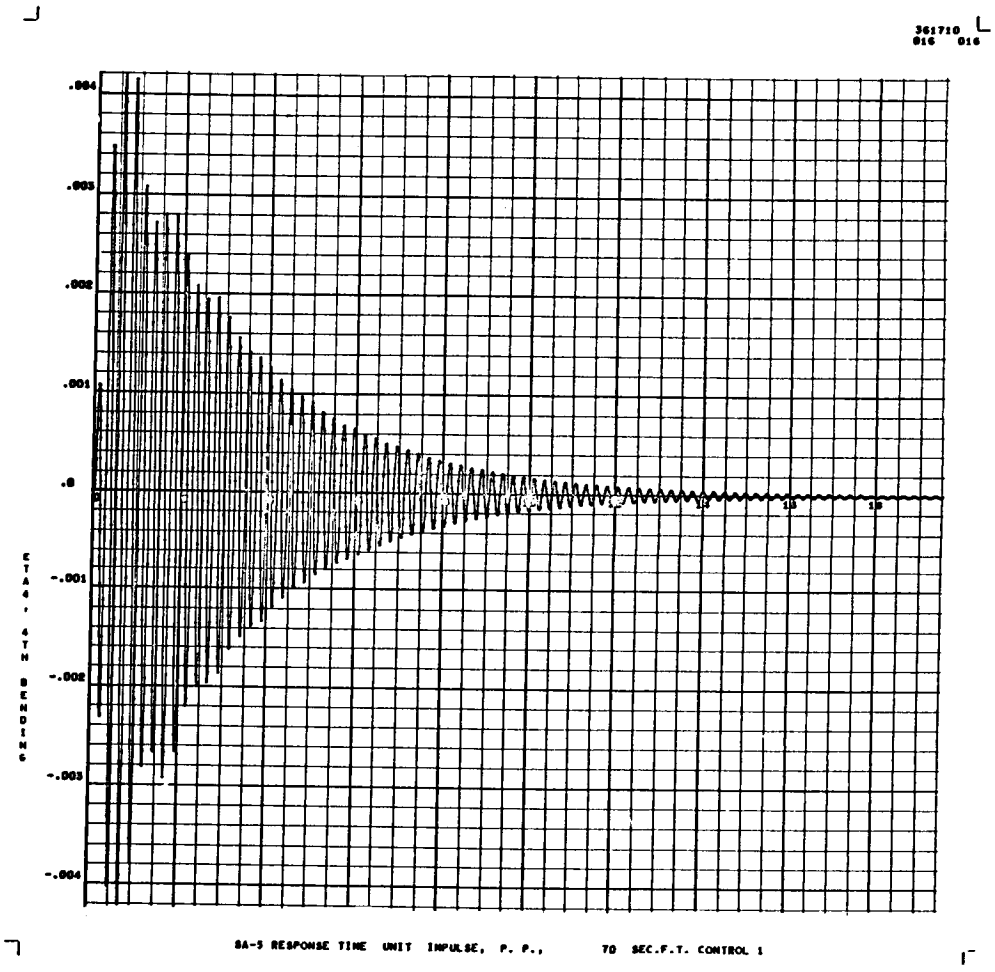

Fig. 23 - Impulsive Response of Fourth Bending Considering Pure Penetration - Angle of Attack Control, 70-Sec. Flight Time

SA-5 RESPØNSE TIME UNIT IMPULSE, P. W. L. G.,
70 SEC.F.T. CØNTRØL 1 ETA4, 4TH BENDING

0.00000	0.0000000E-39	CRØSS
0.02050	-4.4219840E-06	MIN
0.02600	-3.6661902E-07	CRØSS
0.11550	1.1234620E-03	MAX
0.16350	1.4630783E-05	CRØSS
0.23250	-2.3847326E-03	MIN
0.28650	-3.6358369E-05	CRØSS
0.35350	3.6758154E-03	MAX
0.41250	2.2434533E-05	CRØSS
0.47650	-4.3642662E-03	MIN
0.53750	-1.8599282E-05	CRØSS
0.60050	4.7885687E-03	MAX
0.66350	1.9213767E-05	CRØSS
0.72650	-4.8884791E-03	MIN
0.78950	-6.3326501E-05	CRØSS
0.85250	4.6574909E-03	MAX
0.91250	3.3643262E-04	CRØSS
0.97550	-4.2850488E-03	MIN
1.03850	-2.6533604E-04	CRØSS
1.09850	3.5485086E-03	MAX
1.15850	2.3185188E-04	CRØSS
1.21850	-3.1552429E-03	MIN
1.27849	-1.0835464E-04	CRØSS
1.33849	2.9610990E-03	MAX
1.39549	2.0227211E-04	CRØSS
1.45849	-2.9582588E-03	MIN
1.51549	-1.6548187E-04	CRØSS
1.57849	3.0601073E-03	MAX
1.63849	3.9245435E-05	CRØSS
1.70149	-3.2105050E-03	MIN
1.76149	-1.6544139E-04	CRØSS
1.82449	3.1028823E-03	MAX
1.88449	1.9332418E-04	CRØSS
1.94749	-2.9850297E-03	MIN
2.01049	-4.4443044E-05	CRØSS
2.07049	2.7262021E-03	MAX
2.13349	1.0921904E-06	CRØSS
2.19349	-2.4775716E-03	MIN
2.25349	-5.6608016E-05	CRØSS
2.31349	2.2989850E-03	MAX
2.37349	5.8142796E-05	CRØSS
2.43349	-2.2022408E-03	MIN
2.49349	-6.0194789E-05	CRØSS
2.55349	2.1813755E-03	MAX
2.61348	1.2844371E-04	CRØSS
2.67648	-2.1624542E-03	MIN
2.73648	-5.5054910E-05	CRØSS
2.79948	2.1674192E-03	MAX
2.85948	7.9994834E-05	CRØSS
2.92248	-2.0620225E-03	MIN
2.98248	-4.0660718E-05	CRØSS
3.04548	1.9864411E-03	MAX
3.10548	4.5568231E-05	CRØSS
3.16548	-1.8369512E-03	MIN
3.22548	-1.0971178E-04	CRØSS
3.28848	1.7364240E-03	MAX
3.34848	3.7302352E-05	CRØSS
3.40847	-1.6372683E-03	MIN
3.46847	-6.6202234E-05	CRØSS

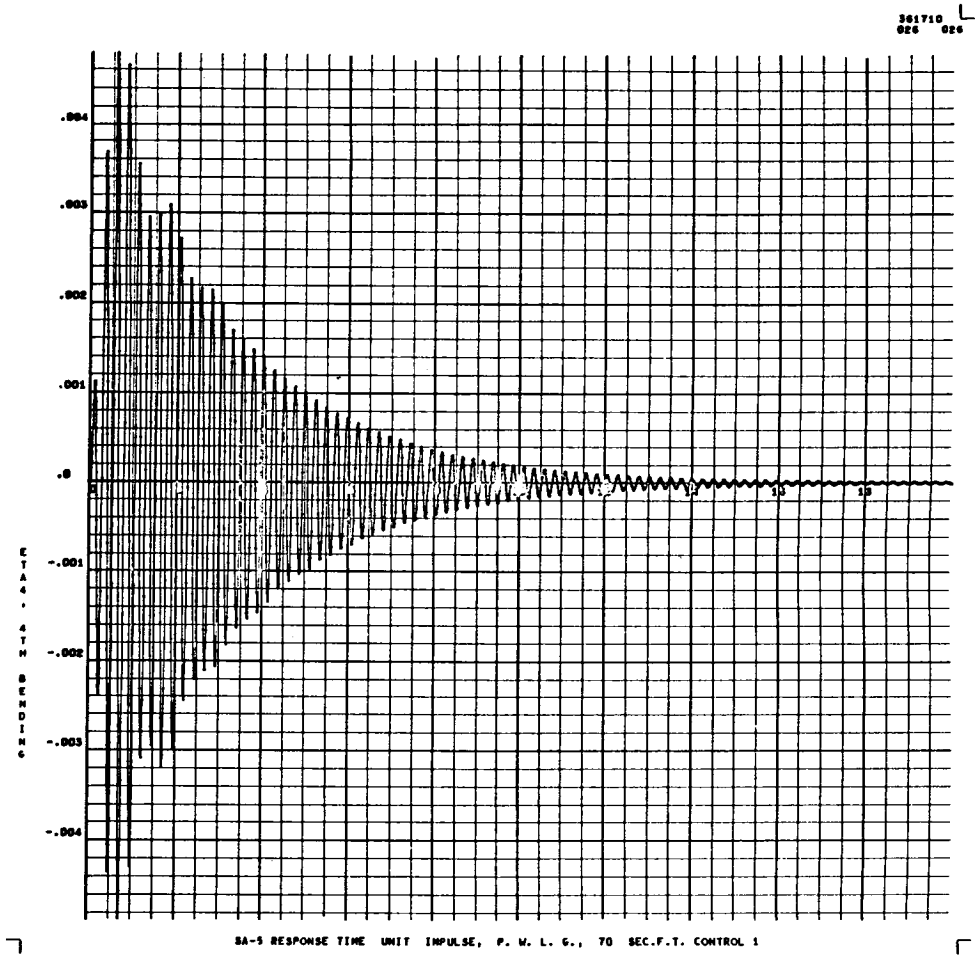

Fig. 24 - Impulsive Response of Fourth Bending Considering Penetration with Lift Growth - Angle of Attack Control, 70-Sec. Flight Time

SA-5 RESPØNSE TIME UNIT IMPULSE, I. I.,
70 SEC.F.T. CØNTRØL 1 BETAC, CØNTRØL DEFLECTIØN

0.00000	0.0000000E-39	CRØSS
0.00050	0.0000000E-39	CRØSS
0.00050	0.0000000E-39	MIN
0.06050	2.3478657E-02	MAX
0.10450	4.8392991E-04	CRØSS
0.15450	-1.9944716E-02	MIN
0.21350	-2.6719306E-04	CRØSS
0.27050	1.5059480E-02	MAX
0.33950	2.0594555E-04	CRØSS
0.38750	-6.8541853E-03	MIN
0.44450	-1.8458290E-05	CRØSS
0.49350	4.9277716E-03	MAX
0.54450	3.9386450E-06	CRØSS
0.60650	-6.5512870E-03	MIN
0.66650	-3.1072863E-04	CRØSS
0.72650	5.8897155E-03	MAX
0.78650	9.8023182E-05	CRØSS
0.85250	-6.1216120E-03	MIN
0.95150	-2.5931550E-04	MAX
1.05950	-8.9394652E-03	MIN
1.12550	-5.5019767E-04	CRØSS
1.20050	1.0832728E-02	MAX
1.27250	1.0899531E-04	CRØSS
1.33249	-7.3749693E-03	MIN
1.39249	-2.7165108E-05	CRØSS
1.45249	7.0787536E-03	MAX
1.51549	1.3787480E-04	CRØSS
1.58149	-7.3930202E-03	MIN
1.65349	-3.0245162E-04	CRØSS
1.70449	3.5997230E-03	MAX
1.75549	2.1702116E-04	CRØSS
1.81849	-4.2823091E-03	MIN
1.87849	-1.5634816E-04	CRØSS
1.93549	3.6158336E-03	MAX
1.98949	2.2729401E-04	CRØSS
2.05249	-4.1125854E-03	MIN
2.10949	-2.6920326E-05	CRØSS
2.17249	4.9786313E-03	MAX
2.23249	3.5025939E-04	CRØSS
2.30149	-5.4956659E-03	MIN
2.36449	-1.2124005E-04	CRØSS
2.42749	4.8213050E-03	MAX
2.48749	1.7281568E-04	CRØSS
2.55049	-4.4243048E-03	MIN
2.61049	-1.0380539E-04	CRØSS
2.67348	4.3597883E-03	MAX
2.73948	2.4383786E-04	CRØSS
2.79348	-2.7431312E-03	MIN
2.84748	-4.9744631E-06	CRØSS
2.91348	3.6173881E-03	MAX
2.97648	1.2172902E-04	CRØSS
3.03348	-2.6396636E-03	MIN
3.08448	-1.3945112E-04	CRØSS
3.15048	3.5613524E-03	MAX
3.21348	2.2693136E-04	CRØSS
3.27348	-3.0689618E-03	MIN
3.33048	-2.1873834E-04	CRØSS
3.39647	3.5972890E-03	MAX
3.46247	7.7241053E-05	CRØSS

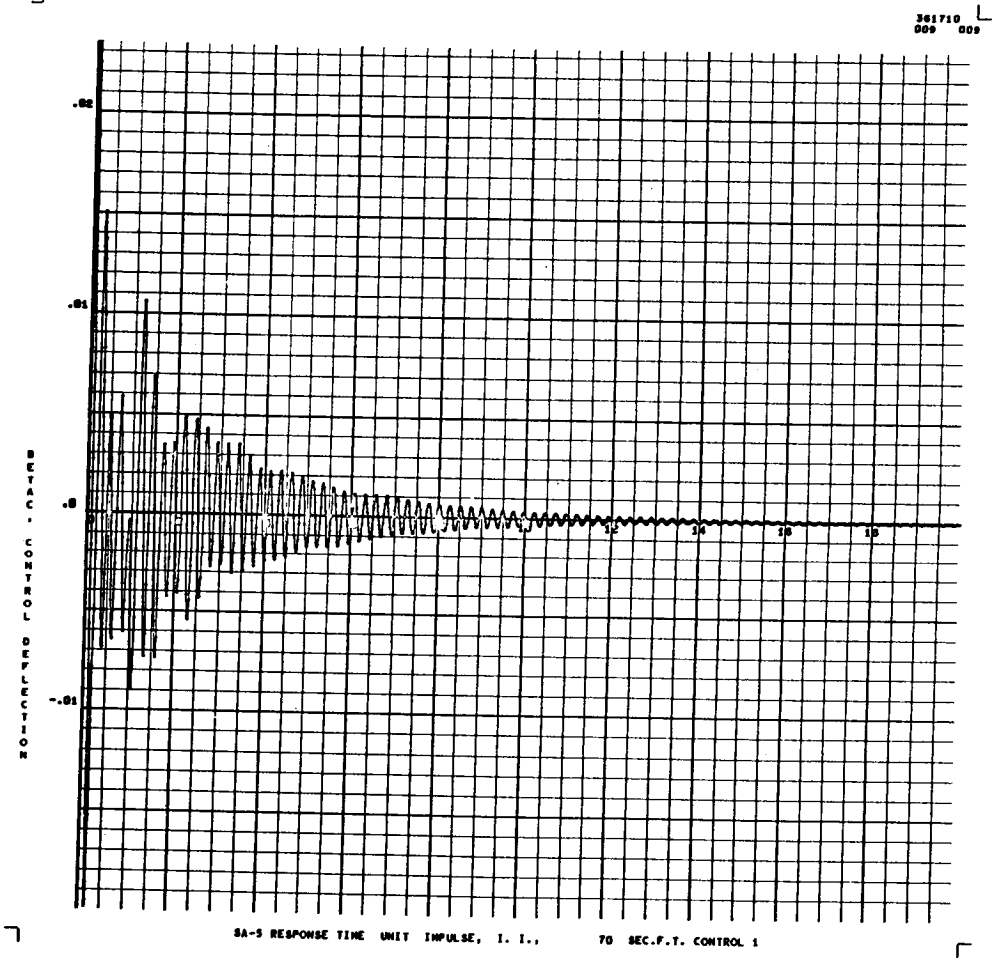

Fig. 25 - Impulsive Response of Control Deflection Considering Instantaneous Immersion - Angle of Attack Control, 70-sec. Flight Time

SA-5 RESPØNSE TIME UNIT IMPULSE, P. P.,
70 SEC.F.T. CØNTRØL 1 BETAC, CØNTRØL DEFLECTIØN

0.00000	0.0000000E-39	CRØSS
0.00050	0.0000000E-39	CRØSS
0.00050	0.0000000E-39	MIN
0.06350	2.6449027E-02	MAX
0.11150	6.7297713E-04	CRØSS
0.16350	-2.0160131E-02	MIN
0.22450	-2.3460931E-04	CRØSS
0.27950	1.3821424E-02	MAX
0.33450	2.9914734E-04	CRØSS
0.38350	-9.3601377E-03	MIN
0.43850	-1.1277570E-04	CRØSS
0.49350	8.2606445E-03	MAX
0.55050	2.1604138E-04	CRØSS
0.60950	-7.9066945E-03	MIN
0.66950	-5.1236153E-04	CRØSS
0.72650	6.2270281E-03	MAX
0.78350	1.0538689E-04	CRØSS
0.84650	-6.7621078E-03	MIN
0.91250	-1.4396487E-04	CRØSS
0.95450	3.0297968E-03	MAX
0.99050	3.4123930E-04	CRØSS
1.07150	-1.0156487E-02	MIN
1.14050	-4.1942166E-04	CRØSS
1.20350	8.7284135E-03	MAX
1.26650	4.8622912E-04	CRØSS
1.32649	-7.5012381E-03	MIN
1.38649	-2.4299529E-04	CRØSS
1.45249	8.2698287E-03	MAX
1.51549	2.6610789E-04	CRØSS
1.57849	-7.4864132E-03	MIN
1.64449	-4.5862682E-04	CRØSS
1.69849	4.6775726E-03	MAX
1.75249	2.1435387E-04	CRØSS
1.81849	-5.7990741E-03	MIN
1.88149	-1.2579482E-04	CRØSS
1.93849	4.4170136E-03	MAX
1.99249	1.3862829E-04	CRØSS
2.05549	-5.1093745E-03	MIN
2.11249	-3.6926321E-04	CRØSS
2.17849	5.4288410E-03	MAX
2.23549	4.1238703E-04	CRØSS
2.30149	-5.6739693E-03	MIN
2.36449	-5.6466055E-05	CRØSS
2.42449	5.1597927E-03	MAX
2.48449	3.1263447E-04	CRØSS
2.54749	-5.0183298E-03	MIN
2.61049	-4.0979834E-05	CRØSS
2.67348	4.7313774E-03	MAX
2.73648	7.3477986E-05	CRØSS
2.79348	-3.5417966E-03	MIN
2.84748	-7.9776812E-05	CRØSS
2.91348	4.3257158E-03	MAX
2.97648	2.0590581E-04	CRØSS
3.03348	-3.1689348E-03	MIN
3.08748	-6.1373474E-05	CRØSS
3.15348	4.1274804E-03	MAX
3.21648	1.9592714E-04	CRØSS
3.27648	-3.3808129E-03	MIN
3.33348	-3.8715749E-05	CRØSS

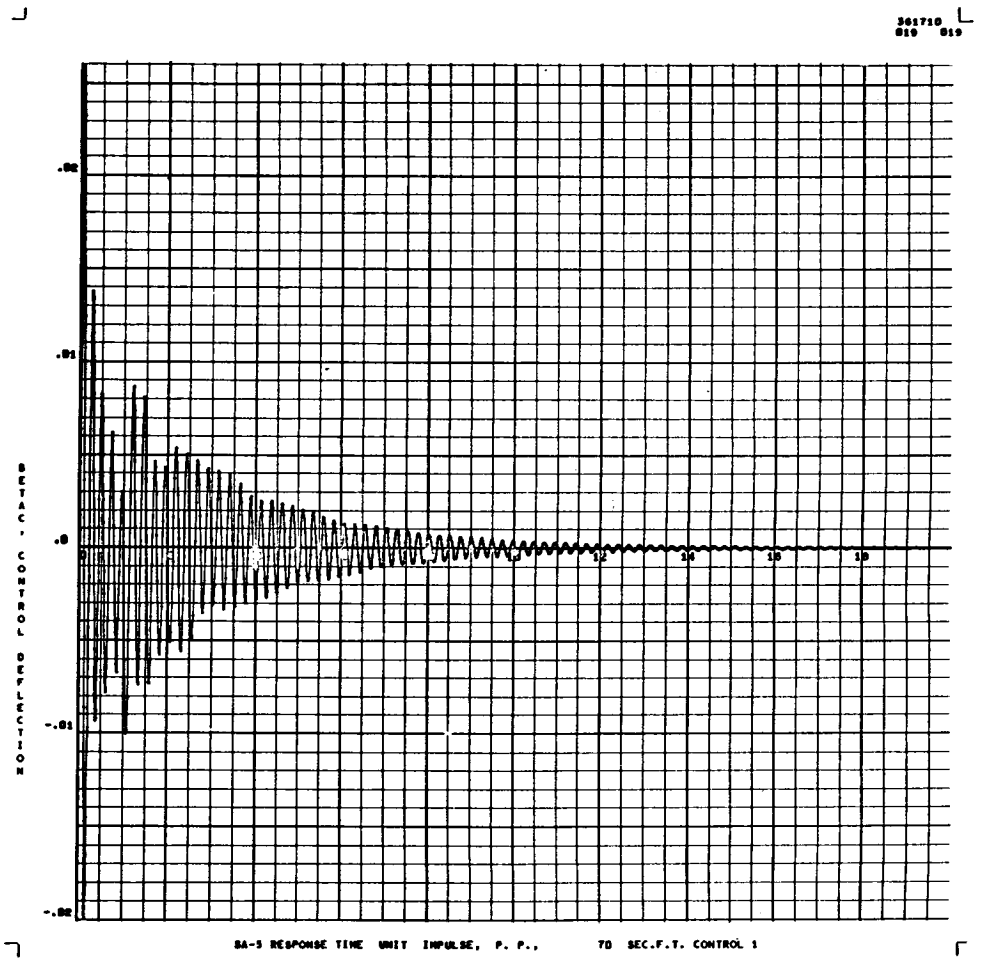

Fig. 26 - Impulsive Response of Control Deflection Considering Pure Penetration - Angle of Attack Control, 70-sec. Flight Time

SA-5 RESPØNSE TIME UNIT IMPULSE, P. W. L. G.,
70 SEC.F.T. CØNTRØL 1 BETAC, CØNTRØL DEFLECTIØN

0.00000	0.0000000E-39	CRØSS
0.00050	0.0000000E-39	CRØSS
0.00050	0.0000000E-39	MIN
0.06350	2.6455277E-02	MAX
0.11250	1.0991760E-05	CRØSS
0.16350	-2.0213204E-02	MIN
0.22450	-3.7340217E-04	CRØSS
0.28050	1.3842495E-02	MAX
0.33950	1.5207447E-04	CRØSS
0.39050	-9.8245769E-03	MIN
0.44650	-1.2965699E-04	CRØSS
0.50150	8.7428654E-03	MAX
0.55850	1.8481813E-04	CRØSS
0.61550	-8.2003908E-03	MIN
0.67550	-4.4295310E-04	CRØSS
0.73250	6.6892446E-03	MAX
0.78650	5.2779591E-04	CRØSS
0.85250	-7.3483639E-03	MIN
0.91850	-1.5335147E-05	CRØSS
0.96050	3.4170142E-03	MAX
0.99950	5.7784830E-05	CRØSS
1.07750	-1.0392436E-02	MIN
1.14350	-4.0208386E-04	CRØSS
1.20650	9.4220740E-03	MAX
1.26950	3.9543725E-04	CRØSS
1.33249	-8.5666698E-03	MIN
1.38949	-5.3514279E-04	CRØSS
1.45549	9.3612925E-03	MAX
1.52149	9.2546397E-06	CRØSS
1.58449	-8.4184961E-03	MIN
1.65049	-2.4211672E-04	CRØSS
1.70449	5.4401152E-03	MAX
1.75849	3.5371540E-04	CRØSS
1.82449	-6.3149642E-03	MIN
1.88749	-6.0714407E-05	CRØSS
1.94149	4.8167848E-03	MAX
1.99849	7.9665238E-05	CRØSS
2.06149	-5.4702958E-03	MIN
2.11849	-1.7639691E-04	CRØSS
2.18149	5.8792019E-03	MAX
2.24149	1.4911933E-04	CRØSS
2.30449	-6.2226442E-03	MIN
2.36749	-1.9049153E-04	CRØSS
2.43049	5.7746131E-03	MAX
2.49049	1.2390047E-04	CRØSS
2.55349	-5.6197392E-03	MIN
2.61348	-2.9408728E-04	CRØSS
2.67648	5.2759996E-03	MAX
2.73948	2.8948341E-04	CRØSS
2.79648	-4.0082559E-03	MIN
2.85348	-8.4939700E-05	CRØSS
2.91648	4.6916037E-03	MAX
2.98248	8.3462372E-05	CRØSS
3.03948	-3.5112273E-03	MIN
3.09348	-6.0074199E-06	CRØSS
3.15948	4.4503925E-03	MAX
3.22248	1.7295602E-05	CRØSS
3.27948	-3.7455785E-03	MIN
3.33648	-2.2568356E-04	CRØSS

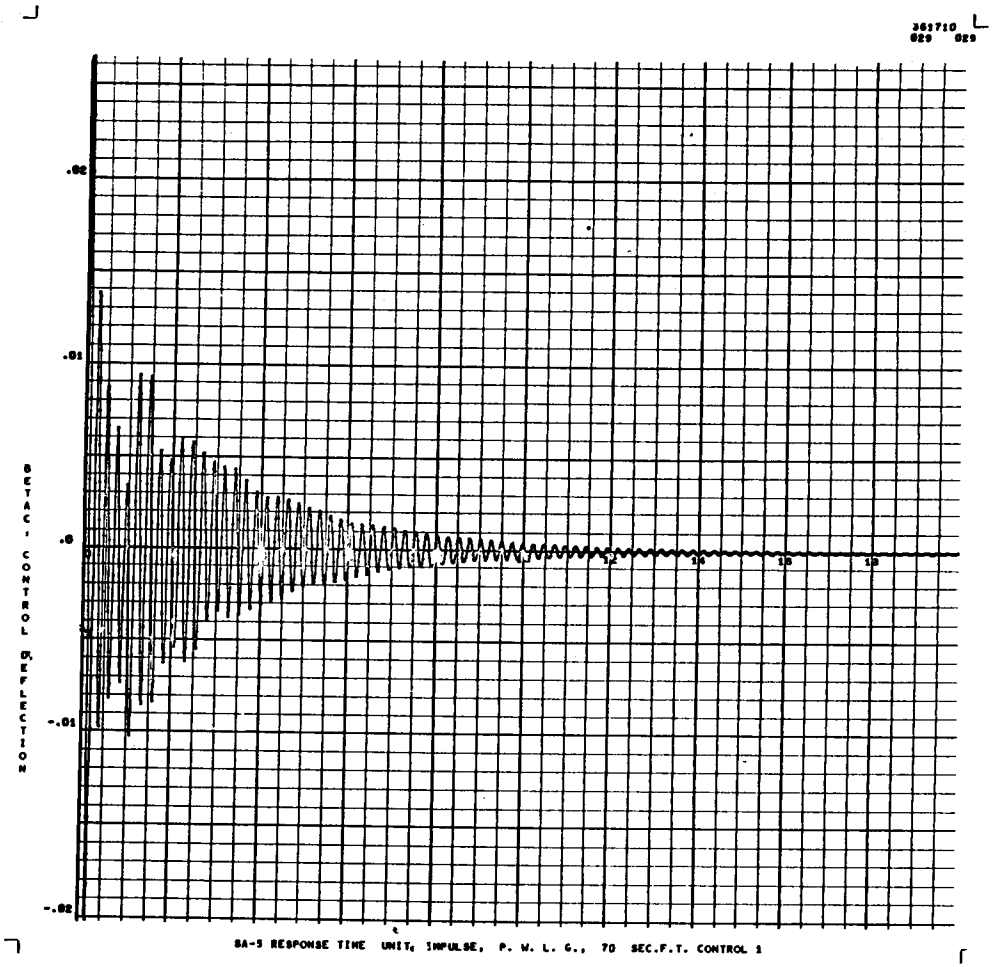

Fig. 27 - Impulsive Response of Control Deflection Considering Penetration With Lift Growth - Angle of Attack Control, 70-sec. Flight Time

coordinate response. The format of the information presented is as follows:

Response Time	Response Value	Response Maximum, Minimum or Crossing

The maximum, minimum and zero crossing values are the calulcated points which precede (in time) the event.

The evaluation of the wind-induced responses (both generalized coordinates and bending moments) can be determined from either the indicial or impulsive responses. In a past investigation (see [1]), the impulsive responses were shown to have better convergence characteristics than the indicial responses. Thus, the impulsive responses were selected for use in the calculation of the wind-induced responses. The evaluation of these wind-induced responses is presented in the next section.

D. Wind-Induced Responses

This section presents the method used and procedures followed in computing the wind-induced responses of the Saturn V generalized coordinates and bending moments. A sample of the numerical computations is presented for illustrative purposes. The responses of the vehicle to an arbitrary side wind input are formulated as Duhamel integrals (see [1]). The kernel function of these integrals is written in terms of the impulsive responses. Thus, the wind-induced responses are given by

$$R(t) = \int_0^t R_i(t-\tau) v_y(\tau) d\tau \tag{1}$$

where $R_i(\tau)$ is a generalized coorinate or a bending moment response (see Appendix III) to a unit impulse wind, $v_y(\tau)$ is an arbitrary side wind profile, and $R(t)$ is the generalized coordinate or bending moment response to the wind, $v_y(t)$. Descriptions of the wind environment used in the above integral are given in Appendix IV.

The two phases of the investigation aré defined in terms of the purpose and use of the wind-induced responses sought and the types of wind environment used in computing the responses.

In phase I, the wind-induced responses of the generalized coordinates were evaluated to determine the effects and importance of penetration and growth of lift on the vehicle responses.

The responses considered were the nine generalized coordinates plus the local angle of attack*, α_L . NASA's Sinusoidal Gust Criteria was used as the wind environment in phase I. The basic constituents of the Sinusoidal Gust Criteria are the wavelength, λ , and amplitude, A , of the sinusoids (see Appendix IV). The relationship between a given wavelength and its associated amplitude is presented in tabular form in [6]. For the response calculations in phase I, four wavelengths were considered for each flight time condition investigated. These wavelengths corresponded to the first four bending frequencies (coupled) of vehicle system.

In phase II, the wind-induced responses of both the generalized coordinates (including local angle of attack) and bending moments were computed in investigating the influence of methods of control on vehicle responses and load alleviation when gust penetration effects are considered. Responses to NASA's Imbedded Gust Criteria were compared for two aerodynamic considerations: instantaneous immersion and pure penetration. Two types of vehicle control systems were investigated: (1) angle of attack and (2) attitude (see Appendix I).

The development of the bending moment equations used in this report is discussed in Appendix III. These equations were formulated from three basic approaches: (1) a total bending moment obtained by a summation of moments technique, (2) a reduced, or simplified form of (1), and (3) the mode displacement method. According to the first technique, the bending moment at any station, x_k , along the vehicle length is derived by considering the aerodynamic, thrust and inertia forces acting on a free body segment of the vehicle. The reduced bending moment equation is obtained from the total by neglecting terms that are small compared to those retained. The bending moment arising from the third method is computed from elementary beam theory considerations.

---

* In phase I, α_L is the rigid body angle of attack at the vehicle's nose defined as

$$\alpha_L(t) = \phi - \frac{\dot{y}}{U} - \frac{x_g}{U}\dot{\phi} + \frac{v_y(t)}{U} .$$

Here, x_g is the location of the vehicle's center of gravity, measured from the nose.

From Appendix III, the total bending moment equation is given by,

$$M_{B_T}(x_k,t) = M_{GUST}(x_k,t) + M'_{\phi}(x_k)\phi(t) + M'_{\alpha}(x_k)\alpha(t)$$

$$+ M'_{\beta_C}(x_k)\beta_C(t) + M'_{\dot{\phi}}(x_k)\dot{\phi}(t) + \sum_{i=1}^{4} M'_{\eta_i}(x_k)\eta_i(t)$$

$$+ \sum_{i=1}^{4} M'_{\dot{\eta}_i}(x_k)\dot{\eta}_i(t) + \sum_{i=1}^{4} M'_{\ddot{\eta}_i}(x_k)\ddot{\eta}_i(t) \quad ; \tag{2}$$

the reduced bending moment equation is given by

$$M_{B_R}(x_k,t) = M_{GUST}(x_k,t) + M'_{\alpha}(x_k)\alpha(t) + M'_{\beta_C}(x_k)\beta_C(t)$$

$$+ \sum_{i=1}^{4} M'_{\ddot{\eta}_i}(x_k)\ddot{\eta}_i(t) \quad ; \tag{3}$$

and the mode displacement bending moment equation is

$$M_{B_M}(x_k,t) = - \sum_{i=1}^{n} \omega_{Bi}^2 I_i(x_k)\eta_i \quad . \tag{4}$$

The entities in the above equations are defined in Appendix III.

The wind-induced bending moment response comparisons given in this report are based on the reduced bending moment expression. Of the three bending moment equations, the reduced expression affords the greatest numerical reliability. Numerical difficulties were encountered in evaluating some of the weighting coefficients, $M'(x_k)$, in the total bending moment equation and convergence uncertainties existed in the mode displacement method since only four modes were considered.

The bending moment and local angle of attack* responses were evaluated at three vehicle stations:

Station 1 - Located at the base of the command module (x_k = 12 meters),**

Station 2 - Located at the base of the instrument unit (x_k = 25 meters), and

Station 3 - Located at the mid-point of the LOX tank of the S-1C stage (x_k = 76.2 meters).

The wind-induced responses for each phase were computed in the 70- and 80-sec. flight time bands. Each band was initially chosen to encompass 10 sec. of flight time with the vehicle parameters evaluated at the band midpoint. In other words, the 70-sec. band would extend from 65 to 75 sec. Subsequently, each band was extended 5 sec. so that, for instance, the 70-sec. band extended from 65 to 80 sec. The computation of the extra 5 sec. of response records were made to insure that the maximum wind responses would be recorded and that the responses would exhibit some convergence toward their steady-state value. In order to conserve computer running time, computation of responses were made only over the flight time intervals of 70 to 80 sec. and 80 to 90 sec. Responses to the buildup rate of the wind profiles were considered a secondary feature of the wind response traces.

The numerical increments used in each band to calculate the responses were chosen to provide sufficient resolution to adequately define the highest frequency component of the system. The computer programs employed to obtain the wind induced responses are modified versions of those discussed in [1].

A representative sample of the 70-sec. flight time band wind-induced response is presented in this report. Several coordinate responses to the Sinusoidal Gust profiles, shown in Fig. 28, are presented in Figs. 29 through 43. These responses result from an angle of attack control system and reflect the three types of aerodynamic representation employed. The wavelength of the sinusoidal gust corresponds to the second bending frequency.

---

* In phase II, the expression used for the local angle of attack is

$$\alpha_L(x_k,t) = \phi - \frac{\dot{y}}{U} + \frac{(x_k - x_g)}{U}\dot{\phi} + \frac{v_y(x_k,t)}{U} \quad .$$

For $x_k = 0$, this equation reduces to the local angle of attack expression used in phase I.

** The values for x_k are measured aft from the top of the vehicle's excape tower.

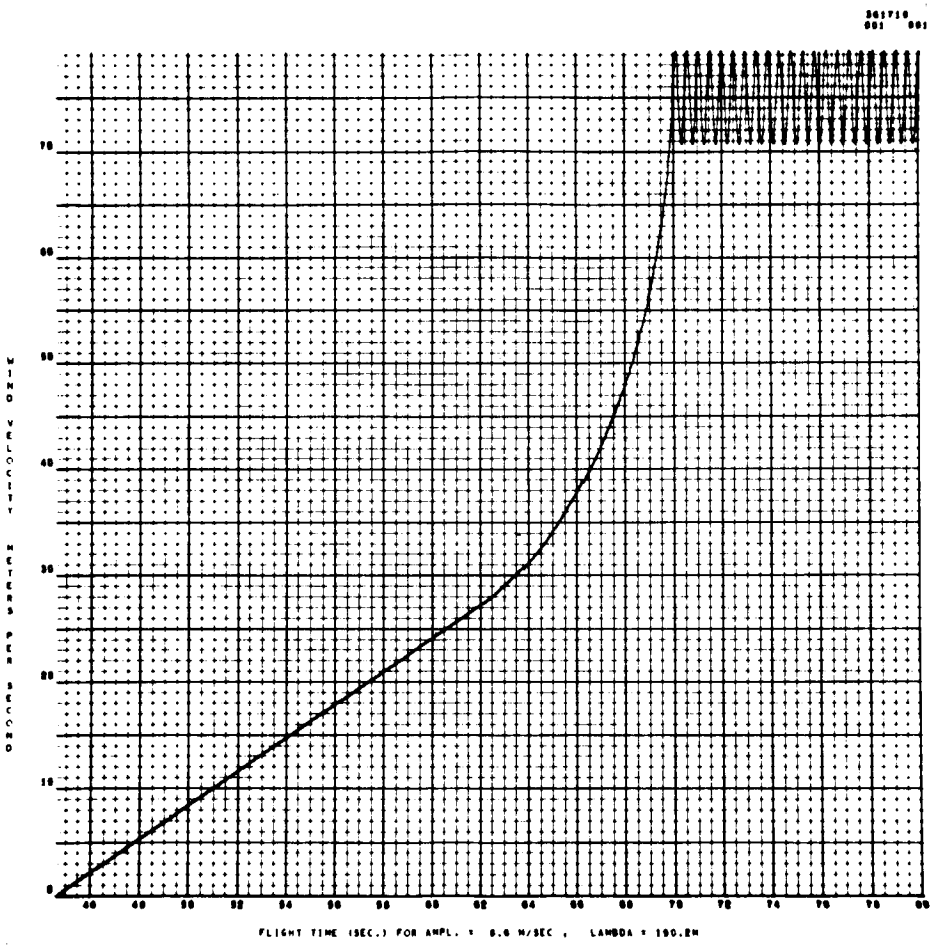

Fig. 28 - Sinusoidal Gust Profile, A = 8.6 m/sec, λ = 190.2 m

SA-5 WIND RESPØNSE TIME, INSTANTANEØUS IMMERSIØN
70 SEC.F.T. CØNTRØL 1 ETA1, 1ST BENDING

70.27189	4.2843825E-02	MAX
70.64535	2.6783220E-02	MIN
71.14329	3.2076838E-02	MAX
71.45450	2.5739861E-02	MIN
71.70347	2.9804265E-02	MAX
71.95245	2.6306942E-02	MIN
72.13917	2.8575842E-02	MAX
72.35702	2.6023523E-02	MIN
72.63711	3.0567676E-02	MAX
72.85496	2.8038632E-02	MIN
73.10393	3.2251582E-02	MAX
73.32178	2.9520006E-02	MIN
73.57075	3.2734894E-02	MAX
73.81972	2.9256120E-02	MIN
74.03757	3.2346894E-02	MAX
74.28654	2.9029658E-02	MIN
74.53551	3.2424615E-02	MAX
74.75336	2.9471092E-02	MIN
75.00233	3.2975286E-02	MAX
75.22018	2.9792523E-02	MIN
75.46915	3.2950649E-02	MAX
75.71812	2.9495118E-02	MIN
75.93597	3.2530473E-02	MAX
76.18494	2.9161961E-02	MIN
76.40279	3.2441583E-02	MAX
76.65176	2.9322786E-02	MIN
76.90073	3.2725575E-02	MAX
77.11858	2.9591903E-02	MIN
77.36755	3.2868097E-02	MAX
77.58540	2.9572203E-02	MIN
77.83437	3.2740480E-02	MAX
78.08334	2.9442847E-02	MIN
78.30119	3.2692648E-02	MAX
78.55016	2.9502010E-02	MIN
78.76801	3.2837095E-02	MAX
79.01698	2.9671972E-02	MIN
79.26595	3.2964743E-02	MAX
79.48380	2.9724240E-02	MIN
79.73277	3.2958751E-02	MAX
79.95062	2.9689444E-02	MIN

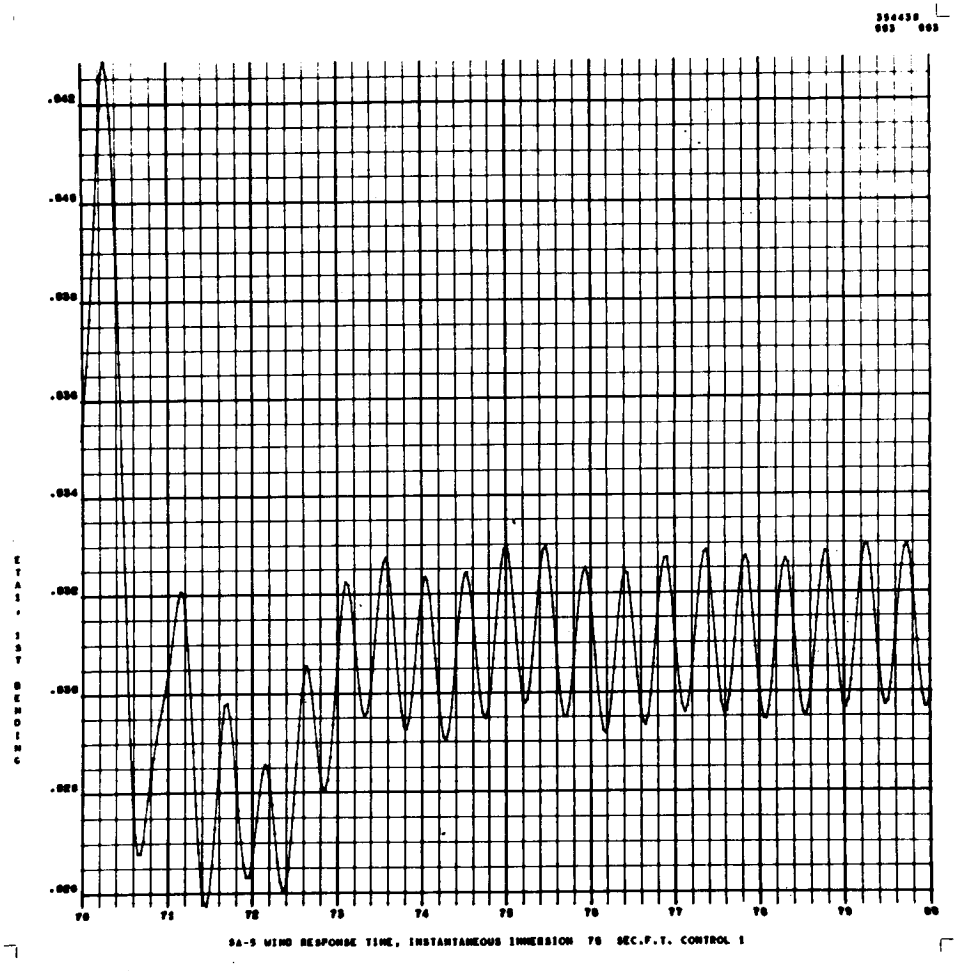

Fig. 29 - Sinusoidal Wind-Induced Response of First Bending Considering Instantaneous Immersion - Angle of Attack Control, 70-sec. Flight Time

SA-5 WIND RESPØNSE TIME, PURE PENETRATIØN

70 SEC.F.T. CØNTRØL 1 ETA1, 1ST BENDING

70.30302	4.0566308E-02	MAX
70.80096	2.6928116E-02	MIN
71.20553	3.0070426E-02	MAX
71.51675	2.5033681E-02	MIN
71.73460	2.7543795E-02	MAX
71.98357	2.5114781E-02	MIN
72.17029	2.6610025E-02	MAX
72.41926	2.4820508E-02	MIN
72.69936	2.8288547E-02	MAX
72.88608	2.6856691E-02	MIN
73.16617	3.0126665E-02	MAX
73.35290	2.8492073E-02	MIN
73.60187	3.0813510E-02	MAX
73.85084	2.8363769E-02	MIN
74.09981	3.0449110E-02	MAX
74.31766	2.8126686E-02	MIN
74.56663	3.0529690E-02	MAX
74.78448	2.8531933E-02	MIN
75.03345	3.1069194E-02	MAX
75.28242	2.8923987E-02	MIN
75.50027	3.1106748E-02	MAX
75.74924	2.8639471E-02	MIN
75.96709	3.0685618E-02	MAX
76.21606	2.8301899E-02	MIN
76.46503	3.0584684E-02	MAX
76.68288	2.8448493E-02	MIN
76.93185	3.0889761E-02	MAX
77.14970	2.8763706E-02	MIN
77.39867	3.1056655E-02	MAX
77.64764	2.8749592E-02	MIN
77.86549	3.0936252E-02	MAX
78.11446	2.8616115E-02	MIN
78.36343	3.0875047E-02	MAX
78.58128	2.8690821E-02	MIN
78.83025	3.1062354E-02	MAX
79.04810	2.8900688E-02	MIN
79.29707	3.1224366E-02	MAX
79.54604	2.8983445E-02	MIN
79.76389	3.1221927E-02	MAX

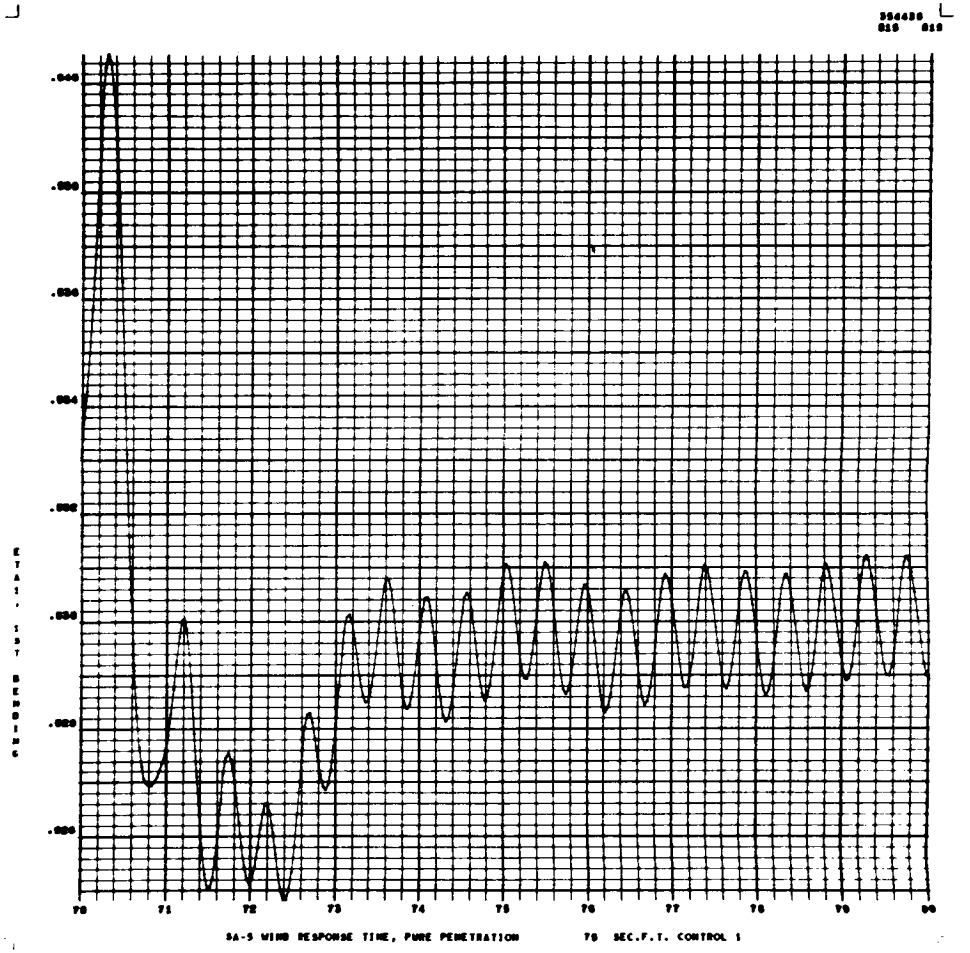

Fig. 30 - Sinusoidal Wind-Induced Response of First Bending Considering Pure Penetration - Angle of Attack Control, 70-sec. Flight Time

SA-5 WIND RESPØNSE TIME, PENETRATIØN WITH LIFT
70 SEC.F.T. CØNTRØL 1 ETA1, 1ST BENDING

70.30302	4.1278900E-02	MAX
70.83208	2.7814155E-02	MIN
71.20553	3.0986045E-02	MAX
71.51675	2.6027477E-02	MIN
71.73460	2.8417293E-02	MAX
71.98357	2.6094185E-02	MIN
72.17029	2.7517429E-02	MAX
72.38814	2.5755564E-02	MIN
72.59936	2.9125137E-02	MAX
72.88608	2.7754533E-02	MIN
73.16617	3.0919257E-02	MAX
73.35290	2.9349031E-02	MIN
73.60187	3.1591634E-02	MAX
73.35084	2.9218143E-02	MIN
74.09981	3.1213674E-02	MAX
74.31766	2.8969876E-02	MIN
74.56663	3.1282074E-02	MAX
74.78448	2.9358414E-02	MIN
75.03345	3.1810923E-02	MAX
75.28242	2.9749069E-02	MIN
75.50027	3.1846010E-02	MAX
75.74924	2.9460971E-02	MIN
75.96709	3.1424717E-02	MAX
76.21606	2.9116600E-02	MIN
76.46503	3.1308561E-02	MAX
76.68288	2.9251553E-02	MIN
76.93185	3.1605254E-02	MAX
77.14970	2.9557174E-02	MIN
77.39867	3.1768195E-02	MAX
77.64764	2.9543341E-02	MIN
77.86549	3.1644663E-02	MAX
78.11446	2.9401861E-02	MIN
78.36343	3.1568330E-02	MAX
78.58128	2.9464843E-02	MIN
78.83025	3.1746623E-02	MAX
79.04810	2.9664106E-02	MIN
79.29707	3.1903134E-02	MAX
79.54604	2.9745902E-02	MIN
79.76389	3.1897061E-02	MAX

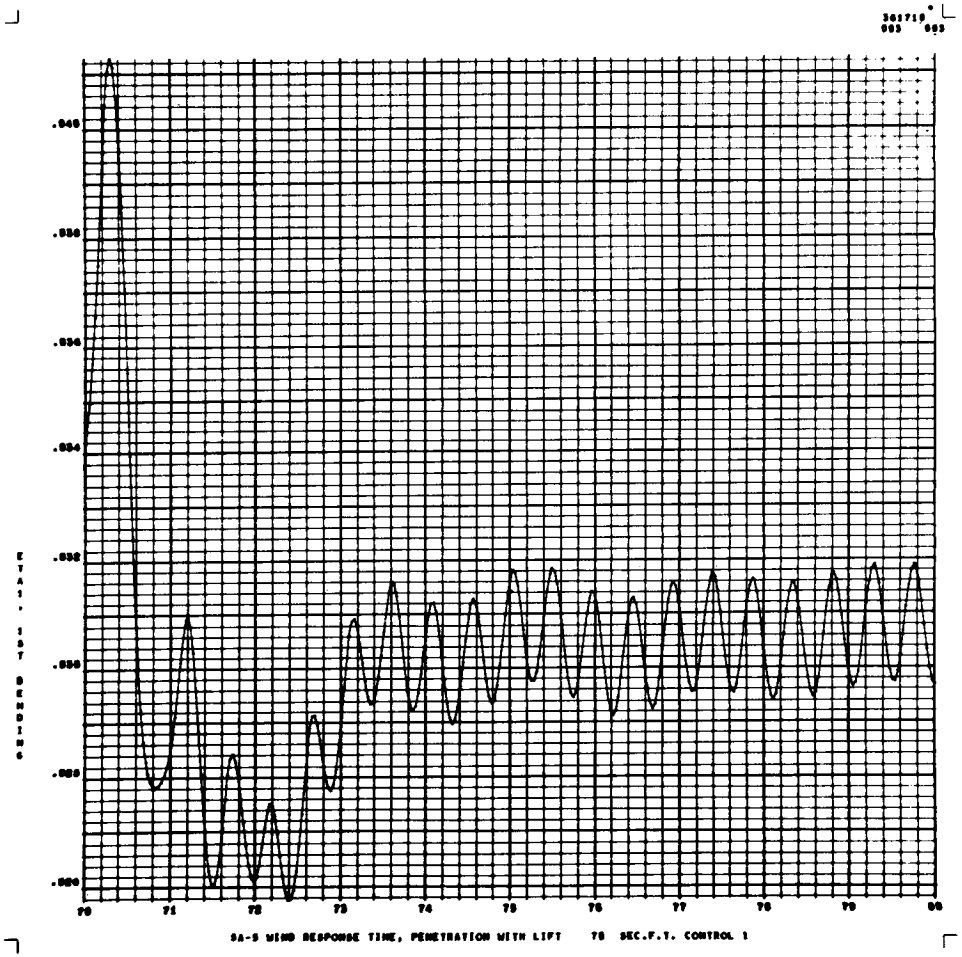

Fig. 31 - Sinusoidal Wind-Induced Response of First Bending Considering Penetration With Lift Growth - Angle of Attack Control, 70-sec. Flight Time

SA-5 WIND RESPØNSE TIME, INSTANTANEØUS IMMERSIØN
70 SEC.F.T. CØNTRØL 1 ETA2, 2ND BENDING

70.20965	1.2205074E-02	MAX
70.45862	6.4268062E-03	MIN
70.70759	1.3894115E-02	MAX
70.95656	2.1546807E-03	MIN
71.20553	1.4206587E-02	MAX
71.42338	2.3928684E-03	MIN
71.67235	1.3081861E-02	MAX
71.92132	2.0353135E-03	MIN
72.13917	1.3560392E-02	MAX
72.38814	2.0561688E-03	MIN
72.60599	1.3819204E-02	MAX
72.85496	2.7361375E-03	MIN
73.10393	1.4374185E-02	MAX
73.32178	2.9773350E-03	MIN
73.57075	1.4523607E-02	MAX
73.78860	3.0245800E-03	MIN
74.03757	1.4466633E-02	MAX
74.28654	3.0102005E-03	MIN
74.50439	1.4514494E-02	MAX
74.75336	3.0770879E-03	MIN
74.97121	1.4558351E-02	MAX
75.22018	3.1091709E-03	MIN
75.46915	1.4562658E-02	MAX
75.68700	3.0498548E-03	MIN
75.93597	1.4507945E-02	MAX
76.18494	3.0651478E-03	MIN
76.40279	1.4513066E-02	MAX
76.65176	3.0440451E-03	MIN
76.86961	1.4546342E-02	MAX
77.11858	3.0663013E-03	MIN
77.36755	1.4510454E-02	MAX
77.58540	3.0604986E-03	MIN
77.83437	1.4553726E-02	MAX
78.05222	3.0893234E-03	MIN
78.30119	1.4584427E-02	MAX
78.55016	3.1387413E-03	MIN
78.76801	1.4612109E-02	MAX
79.01698	3.1159966E-03	MIN
79.23483	1.4579320E-02	MAX
79.48380	3.1044216E-03	MIN
79.73277	1.4580107E-02	MAX
79.95062	3.1185508E-03	MIN

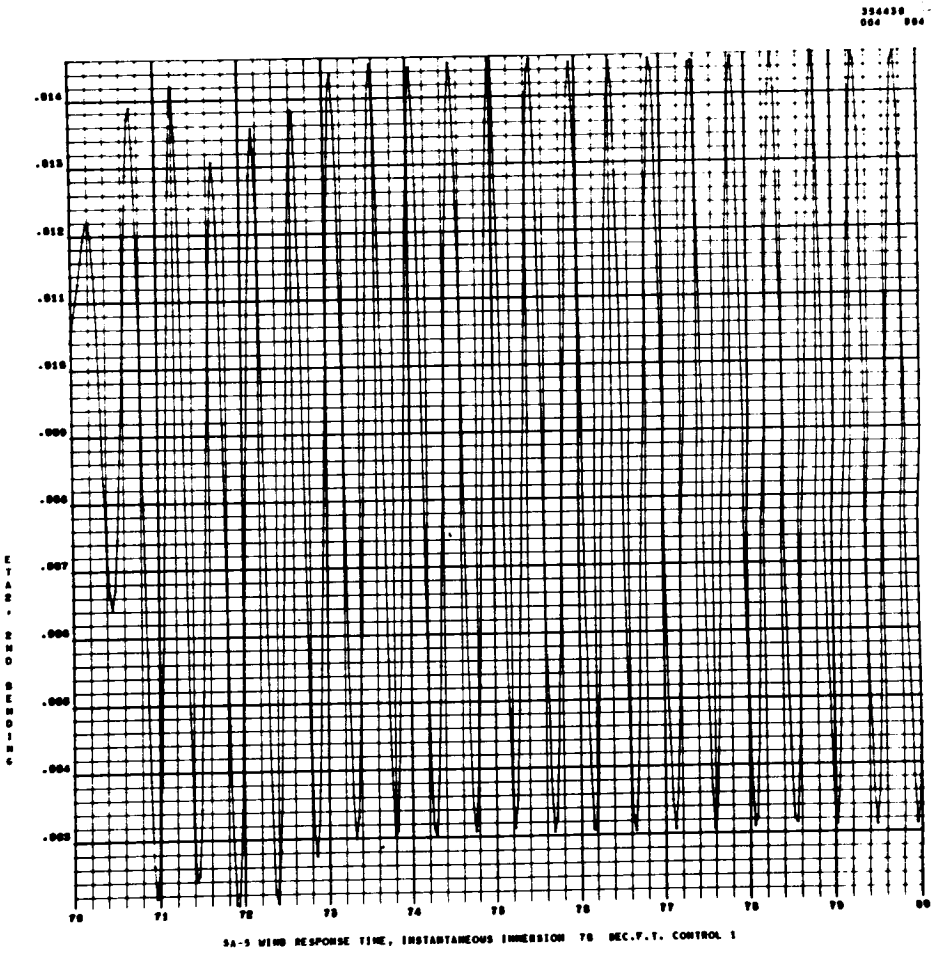

Fig. 32 - Sinusoidal Wind-Induced Response of Second Bending Considering Instantaneous Immersion - Angle of Attack Control, 70-sec. Flight Time

SA-5 WIND RESPØNSE TIME, PURE PENETRATIØN
70 SEC.F.T. CØNTRØL 1 ETA2, 2ND BENDING

70.24077	1.1640849E-02	MAX
70.52086	7.6779250E-03	MIN
70.73871	1.1716434E-02	MAX
71.01881	4.5814189E-03	MIN
71.23665	1.0960476E-02	MAX
71.48563	4.8739988E-03	MIN
71.70347	1.0068047E-02	MAX
71.95245	4.3605223E-03	MIN
72.20142	1.0340769E-02	MAX
72.41926	4.5882909E-03	MIN
72.66823	1.0759682E-02	MAX
72.88608	5.2775659E-03	MIN
73.13505	1.1319508E-02	MAX
73.38402	5.6119300E-03	MIN
73.60187	1.1444780E-02	MAX
73.85084	5.5657303E-03	MIN
74.06869	1.1339876E-02	MAX
74.31766	5.5524888E-03	MIN
74.56663	1.1448973E-02	MAX
74.78448	5.6814751E-03	MIN
75.03345	1.1584344E-02	MAX
75.25130	5.7769482E-03	MIN
75.50027	1.1544930E-02	MAX
75.74924	5.6471791E-03	MIN
75.96709	1.1416742E-02	MAX
76.21606	5.5569479E-03	MIN
76.46503	1.1381562E-02	MAX
76.68288	5.6115667E-03	MIN
76.93185	1.1498344E-02	MAX
77.14970	5.7050062E-03	MIN
77.39867	1.1543962E-02	MAX
77.64764	5.7137989E-03	MIN
77.86549	1.1510955E-02	MAX
78.11446	5.6563771E-03	MIN
78.33231	1.1482775E-02	MAX
78.58128	5.6748221E-03	MIN
78.83025	1.1526844E-02	MAX
79.04810	5.7371493E-03	MIN
79.29707	1.1596576E-02	MAX
79.51492	5.7896644E-03	MIN
79.76389	1.1607197E-02	MAX

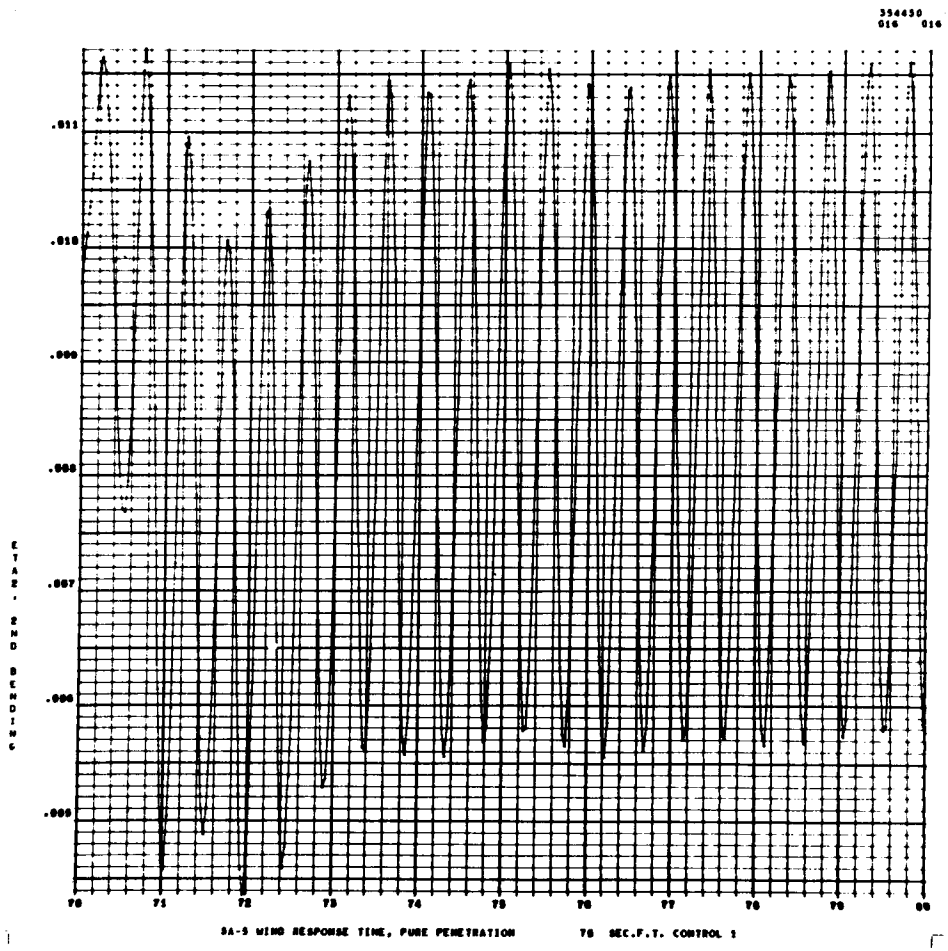

Fig. 33 - Sinusoidal Wind-Induced Response of Second Bending Considering Pure Penetration - Angle of Attack Control, 70-sec. Flight Time

SA-5 WIND RESPØNSE TIME, PENETRATIØN WITH LIFT
70 SEC.F.T. CØNTRØL 1 ETA2, 2ND BENDING

70.24077	1.1739163E-02	MAX
70.52086	7.9374529E-03	MIN
70.73871	1.1727009E-02	MAX
71.01881	4.9962793E-03	MIN
71.23665	1.0901704E-02	MAX
71.48563	5.3505281E-03	MIN
71.70347	1.0016788E-02	MAX
71.95245	4.8090342E-03	MIN
72.17029	1.0267609E-02	MAX
72.41926	5.0308769E-03	MIN
72.66823	1.0656671E-02	MAX
72.88608	5.6851209E-03	MIN
73.13505	1.1213430E-02	MAX
73.35290	6.0267115E-03	MIN
73.60187	1.1336152E-02	MAX
73.85084	5.9848950E-03	MIN
74.06869	1.1238977E-02	MAX
74.31766	5.9596009E-03	MIN
74.56663	1.1313735E-02	MAX
74.78448	6.0747132E-03	MIN
75.03345	1.1452041E-02	MAX
75.25130	6.1580486E-03	MIN
75.50027	1.1419708E-02	MAX
75.74924	6.0598578E-03	MIN
75.96709	1.1300983E-02	MAX
76.21606	5.9620183E-03	MIN
76.43391	1.1259012E-02	MAX
76.68288	6.0062961E-03	MIN
76.93185	1.1356179E-02	MAX
77.14970	6.0885842E-03	MIN
77.39867	1.1407649E-02	MAX
77.61652	6.1198116E-03	MIN
77.86549	1.1382147E-02	MAX
78.11446	6.0589985E-03	MIN
78.33231	1.1362026E-02	MAX
78.58128	6.0679165E-03	MIN
78.83025	1.1374133E-02	MAX
79.04810	6.1191542E-03	MIN
79.29707	1.1447360E-02	MAX
79.51492	6.1591921E-03	MIN
79.76389	1.1463700E-02	MAX

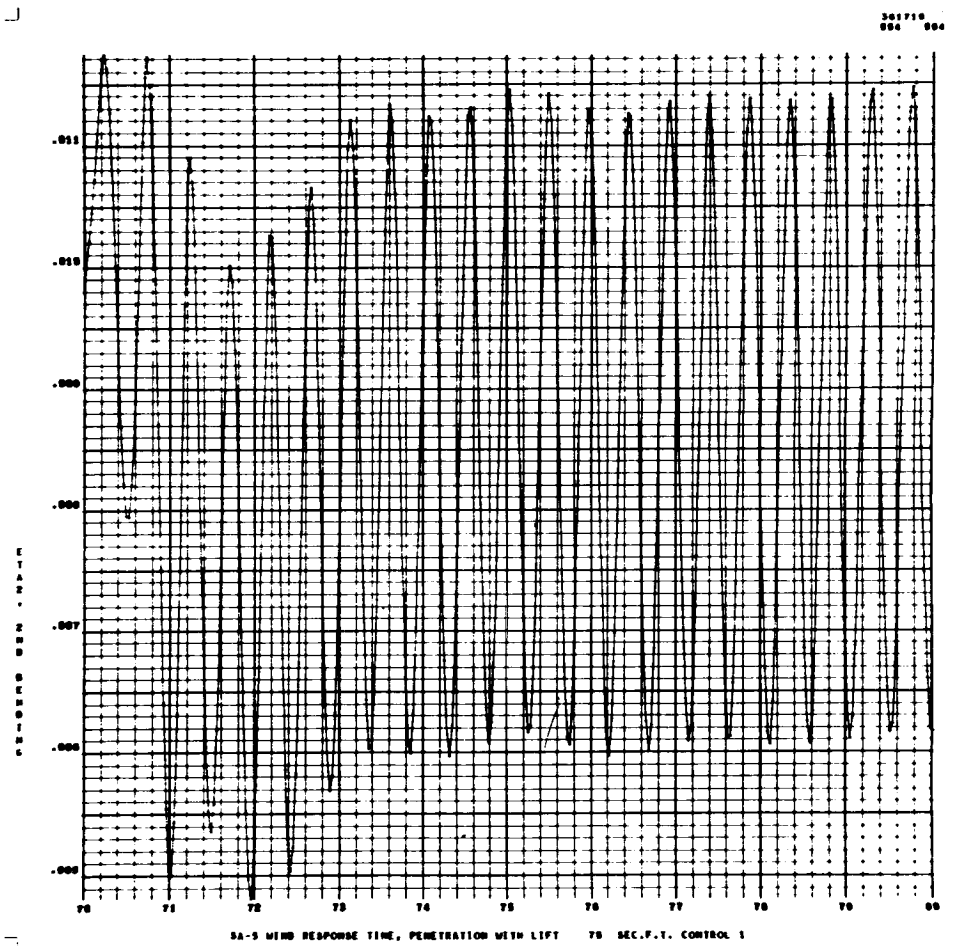

Fig. 34 - Sinusoidal Wind-Induced Response of Second Bending Considering Penetration With Lift Growth - Angle of Attack Control, 70-sec. Flight Time

SA-5 WIND RESPØNSE TIME, INSTANTANEØUS IMMERSIØN
70 SEC.F.T. CØNTRØL 1 ETA3, 3RD BENDING

70.17853	4.8738666E-03	MAX
70.36526	2.2617883E-03	MIN
70.55199	5.8696744E-03	MAX
70.76984	1.0917762E-03	MIN
70.95656	4.6822923E-03	MAX
71.14329	1.4171921E-03	MIN
71.45450	4.2061475E-03	MAX
71.67235	5.4937274E-04	MIN
71.89020	4.4509143E-03	MAX
72.10805	1.0046338E-03	MIN
72.38814	4.4066960E-03	MAX
72.60599	1.1937641E-03	MIN
72.85496	4.9715382E-03	MAX
73.07281	1.5396959E-03	MIN
73.32178	4.9472698E-03	MAX
73.53963	1.5314782E-03	MIN
73.78860	4.9819243E-03	MAX
74.03757	1.5497658E-03	MIN
74.25542	4.9483395E-03	MAX
74.50439	1.5752113E-03	MIN
74.72224	5.0496968E-03	MAX
74.97121	1.6394602E-03	MIN
75.22018	5.0435489E-03	MAX
75.43803	1.6022843E-03	MIN
75.68700	5.0016334E-03	MAX
75.93597	1.5654744E-03	MIN
76.15382	4.9822236E-03	MAX
76.40279	1.5637789E-03	MIN
76.62054	5.0264607E-03	MAX
76.86961	1.6073659E-03	MIN
77.08746	5.0306797E-03	MAX
77.33643	1.6170499E-03	MIN
77.58540	5.0380094E-03	MAX
77.80325	1.6148319E-03	MIN
78.05222	5.0389444E-03	MAX
78.30119	1.6222306E-03	MIN
78.51904	5.0544342E-03	MAX
78.76801	1.6283211E-03	MIN
78.98586	5.0546409E-03	MAX
79.23483	1.6309969E-03	MIN
79.48380	5.0545330E-03	MAX
79.70165	1.6290931E-03	MIN
79.95062	5.0638661E-03	MAX

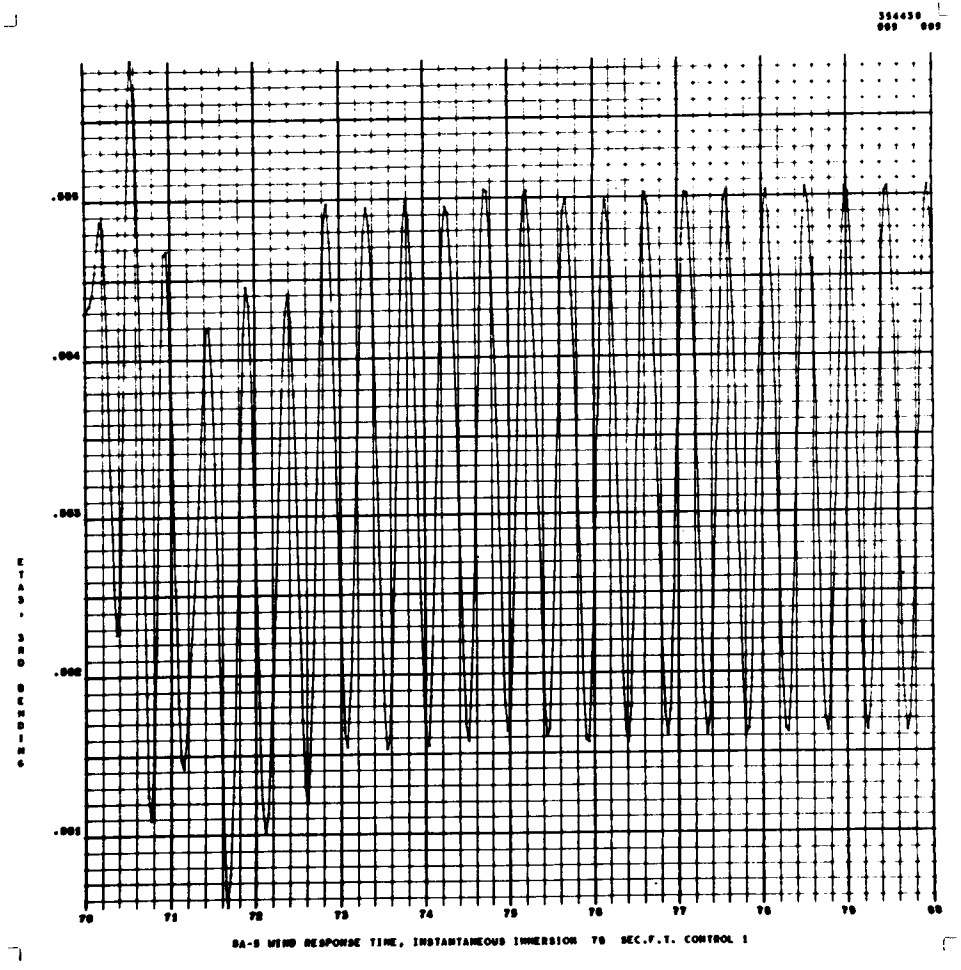

Fig. 35 - Sinusoidal Wind-Induced Response of Third Bending Considering Instantaneous Immersion - Angle of Attack Control, 70-sec. Flight Time

SA-5 WIND RESPØNSE TIME, PURE PENETRATIØN
70 SEC.F.T. CØNTRØL 1 ETA3, 3RD BENDING

70.20965	4.6377584E-03	MAX
70.36526	2.9716948E-03	MIN
70.55199	4.8320310E-03	MAX
70.76984	2.1014555E-03	MIN
70.95656	3.8767057E-03	MAX
71.14329	1.9962739E-03	MIN
71.23665	2.1466530E-03	MAX
71.26778	2.1221786E-03	MIN
71.45450	3.6197418E-03	MAX
71.70347	1.2125389E-03	MIN
71.92132	3.4299249E-03	MAX
72.13917	1.6308906E-03	MIN
72.41926	3.6331504E-03	MAX
72.60599	1.7724365E-03	MIN
72.88608	4.0520087E-03	MAX
73.10393	2.1813468E-03	MIN
73.35290	4.1610118E-03	MAX
73.57075	2.1402761E-03	MIN
73.81972	4.1316321E-03	MAX
74.03757	2.1407999E-03	MIN
74.31766	4.1164553E-03	MAX
74.53551	2.1871950E-03	MIN
74.78448	4.1945722E-03	MAX
75.00233	2.2427942E-03	MIN
75.25130	4.1968152E-03	MAX
75.46915	2.1901632E-03	MIN
75.71812	4.1282153E-03	MAX
75.93597	2.1475434E-03	MIN
76.18494	4.0989979E-03	MAX
76.43391	2.1451470E-03	MIN
76.65176	4.1431145E-03	MAX
76.90073	2.1923621E-03	MIN
77.11858	4.1716765E-03	MAX
77.36755	2.2072395E-03	MIN
77.61652	4.1643601E-03	MAX
77.83437	2.2033403E-03	MIN
78.08334	4.1662369E-03	MAX
78.33231	2.2103916E-03	MIN
78.55016	4.1901566E-03	MAX
78.79913	2.2306012E-03	MIN
79.01698	4.2088776E-03	MAX
79.26595	2.2436280E-03	MIN
79.51492	4.2041377E-03	MAX
79.73277	2.2429893E-03	MIN
79.98174	4.2117052E-03	MAX

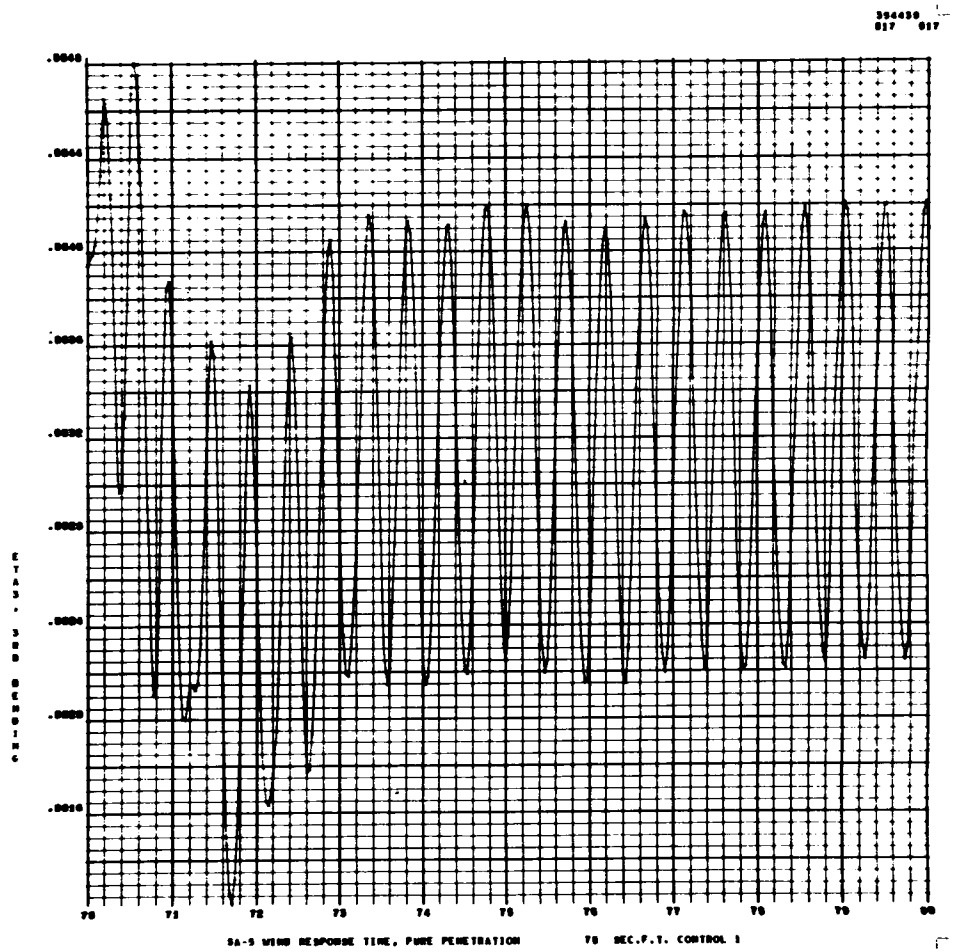

Fig. 36 - Sinusoidal Wind-Induced Response of Third Bending Considering Pure Penetration - Angle of Attack Control, 70-sec. Flight Time

SA-5 WIND RESPØNSE TIME, PENETRATIØN WITH LIFT
70 SEC.F.T. CØNTRØL 1 ETA3, 3RD BENDING

70.20965	4.6858C89E-03	MAX
70.36526	3.0146171E-03	MIN
70.55199	4.9836504E-03	MAX
70.76984	2.1749415E-03	MIN
70.92544	4.0554276E-03	MAX
71.11217	1.9618013E-03	MIN
71.23665	2.3706703E-03	MAX
71.29890	2.3199195E-03	MIN
71.45450	3.7062548E-03	MAX
71.70347	1.3492609E-03	MIN
71.92132	3.4965331E-03	MAX
72.10805	1.7228397E-03	MIN
72.41926	3.6837173E-03	MAX
72.60599	1.8441493E-03	MIN
72.88608	4.0774164E-03	MAX
73.07281	2.2694141E-03	MIN
73.35290	4.1849144E-03	MAX
73.57075	2.2302254E-03	MIN
73.81972	4.1547457E-03	MAX
74.03757	2.2321331E-03	MIN
74.28654	4.1324936E-03	MAX
74.50439	2.2863882E-03	MIN
74.75336	4.2135920E-03	MAX
75.00233	2.3500506E-03	MIN
75.25130	4.2102282E-03	MAX
75.46915	2.2926975E-03	MIN
75.71812	4.1497014E-03	MAX
75.93597	2.2478932E-03	MIN
76.18494	4.1281575E-03	MAX
76.43391	2.2639866E-03	MIN
76.65176	4.1799765E-03	MAX
76.90073	2.3077936E-03	MIN
77.11858	4.2161623E-03	MAX
77.36755	2.3180412E-03	MIN
77.58540	4.1997207E-03	MAX
77.83437	2.3082629E-03	MIN
78.08334	4.1926677E-03	MAX
78.30119	2.3222152E-03	MIN
78.55016	4.2211860E-03	MAX
78.79913	2.3479789E-03	MIN
79.01698	4.2447605E-03	MAX
79.26595	2.3543929E-03	MIN
79.48380	4.2382162E-03	MAX
79.73277	2.3466349E-03	MIN
79.98174	4.2299169E-03	MAX

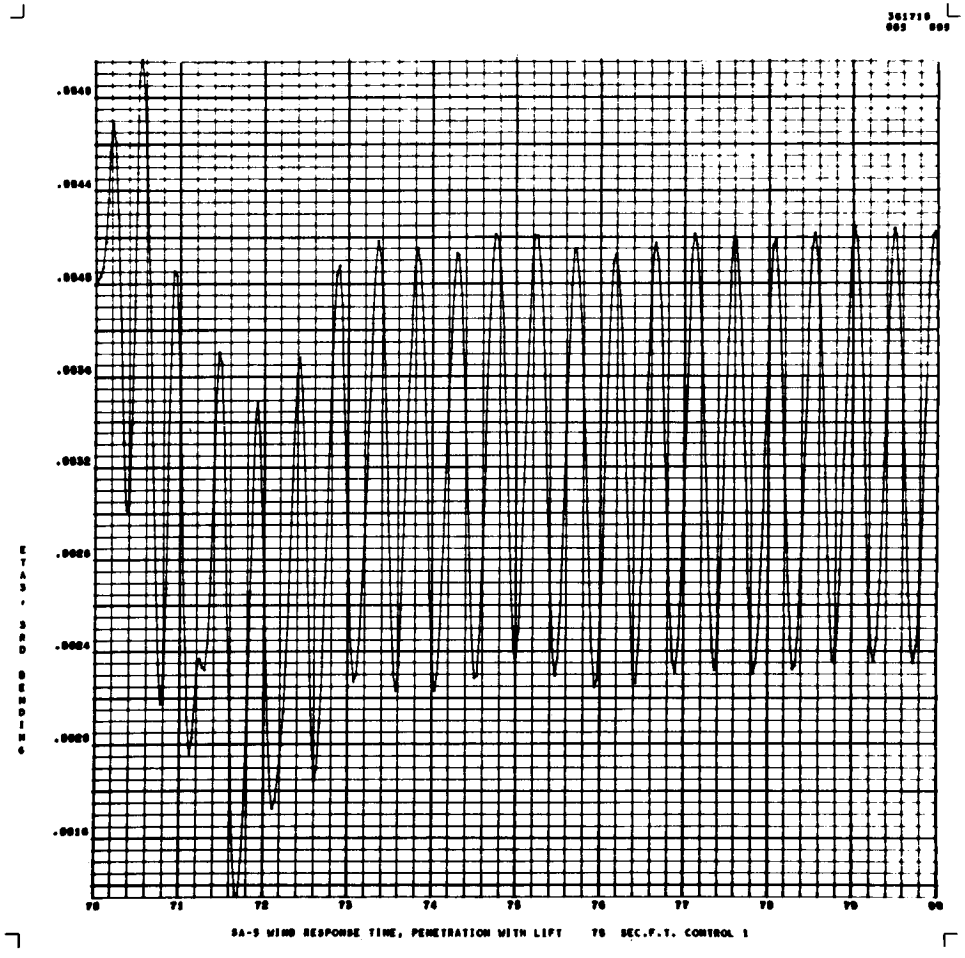

Fig. 37 - Sinusoidal Wind-Induced Response of Third Bending Considering Penetration With Lift Growth - Angle of Attack Control, 70-sec. Flight Time

SA-5 WIND RESPØNSE TIME, INSTANTANEØUS IMMERSIØN
70 SEC.F.T. CØNTRØL 1 ETA4, 4TH BENDING

70.02292	9.6373633E-04	MIN
70.17853	1.1704506E-03	MAX
70.33414	5.2986862E-04	MIN
70.45862	1.3525064E-03	MAX
70.61423	6.0274073E-04	MIN
70.70759	9.8523223E-04	MAX
70.83208	3.4760801E-04	MIN
70.98768	1.0233717E-03	MAX
71.14329	3.4648808E-04	MIN
71.42338	1.0168371E-03	MAX
71.57899	1.9882659E-04	MIN
71.70347	4.9891389E-04	MAX
71.76572	4.3903138E-04	MIN
71.92132	9.5110931E-04	MAX
72.07693	2.3173091E-04	MIN
72.38814	9.6530801E-04	MAX
72.57487	3.3555708E-04	MIN
72.88608	1.0473345E-03	MAX
73.04169	3.7875760E-04	MIN
73.35290	1.0155854E-03	MAX
73.53963	3.9921650E-04	MIN
73.81972	9.8463688E-04	MAX
74.00645	3.8864967E-04	MIN
74.28654	9.7893018E-04	MAX
74.50439	4.3167177E-04	MIN
74.72224	1.0033283E-03	MAX
74.97121	4.4063796E-04	MIN
75.18906	1.0215737E-03	MAX
75.43803	4.4560736E-04	MIN
75.65588	1.0168500E-03	MAX
75.93597	4.3885286E-04	MIN
76.12270	1.0233768E-03	MAX
76.40279	4.5578540E-04	MIN
76.62064	1.0417274E-03	MAX
76.86961	4.7561172E-04	MIN
77.08746	1.0555154E-C3	MAX
77.33643	4.8403932E-04	MIN
77.55428	1.0498263E-03	MAX
77.80325	4.8452167E-04	MIN
78.05222	1.0476356E-C3	MAX
78.27007	4.8877750E-04	MIN
78.51904	1.0547265E-03	MAX
78.76801	4.9208845E-04	MIN
78.98586	1.0550864E-C3	MAX
79.23483	4.8886517E-04	MIN
79.45268	1.0463131E-03	MAX
79.70165	4.8214915E-04	MIN
79.95062	1.0464794E-C3	MAX

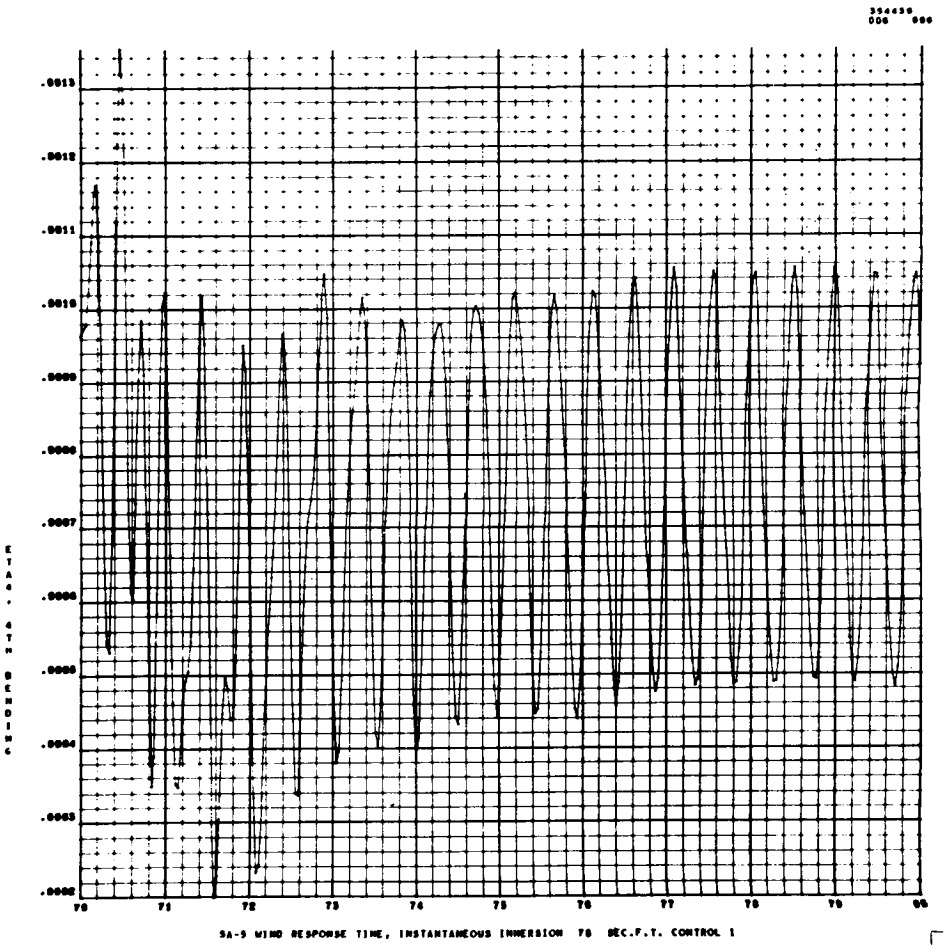

Fig. 38 - Sinusoidal Wind-Induced Response of Fourth Bending Considering Instantaneous Immersion - Angle of Attack Control, 70-sec. Flight Time

SA-5 WIND RESPØNSE TIME, PURE PENETRATIØN
70 SEC.F.T. CØNTRØL 1 ETA4, 4TH BENDING

70.02292	8.9801793E-04	MIN
70.17853	1.1209258E-03	MAX
70.33414	4.8301235E-04	MIN
70.45862	1.2959707E-03	MAX
70.61423	6.1353589E-04	MIN
70.70759	9.8029530E-04	MAX
70.83208	2.8005096E-04	MIN
70.98768	1.0081084E-03	MAX
71.11217	3.7003895E-04	MIN
71.20553	4.6786361E-04	MAX
71.29890	3.2236972E-04	MIN
71.45450	9.2859782E-04	MAX
71.57899	2.9152855E-04	MIN
71.67235	4.3200760E-04	MAX
71.79684	2.1388643E-04	MIN
71.95245	8.7531719E-04	MAX
72.10805	2.6967631E-04	MIN
72.20142	4.1229617E-04	MAX
72.26366	3.8738639E-04	MIN
72.41926	9.0646825E-04	MAX
72.57487	3.5174059E-04	MIN
72.69936	5.2513540E-04	MAX
72.73048	5.1205446E-04	MIN
72.91720	9.9459375E-04	MAX
73.07281	4.0569911E-04	MIN
73.38402	9.8884254E-04	MAX
73.53963	4.1860744E-04	MIN
73.85084	9.6382465E-04	MAX
74.03757	3.9455313E-04	MIN
74.34878	9.4110061E-04	MAX
74.50439	4.2099013E-04	MIN
74.81560	9.4467252E-04	MAX
75.00233	4.2630450E-04	MIN
75.28242	9.1671119E-04	MAX
75.46915	4.1753512E-04	MIN
75.74924	8.8599588E-04	MAX
75.96709	4.0619919E-04	MIN
76.18494	8.8519016E-04	MAX
76.43391	4.1475861E-04	MIN
76.65176	9.0697379E-04	MAX
76.90073	4.3678294E-04	MIN
77.11858	9.2385528E-04	MAX
77.39867	4.4391493E-04	MIN
77.58540	9.2511763E-04	MAX
77.86549	4.4464342E-04	MIN
78.08334	9.3237834E-04	MAX
78.33231	4.5453087E-04	MIN
78.55016	9.4310872E-04	MAX
78.79913	4.6776353E-04	MIN
79.01698	9.4755042E-04	MAX
79.26595	4.7545787E-04	MIN
79.51492	9.5007606E-04	MAX
79.76389	4.7658809E-04	MIN
79.98174	9.5074389E-04	MAX

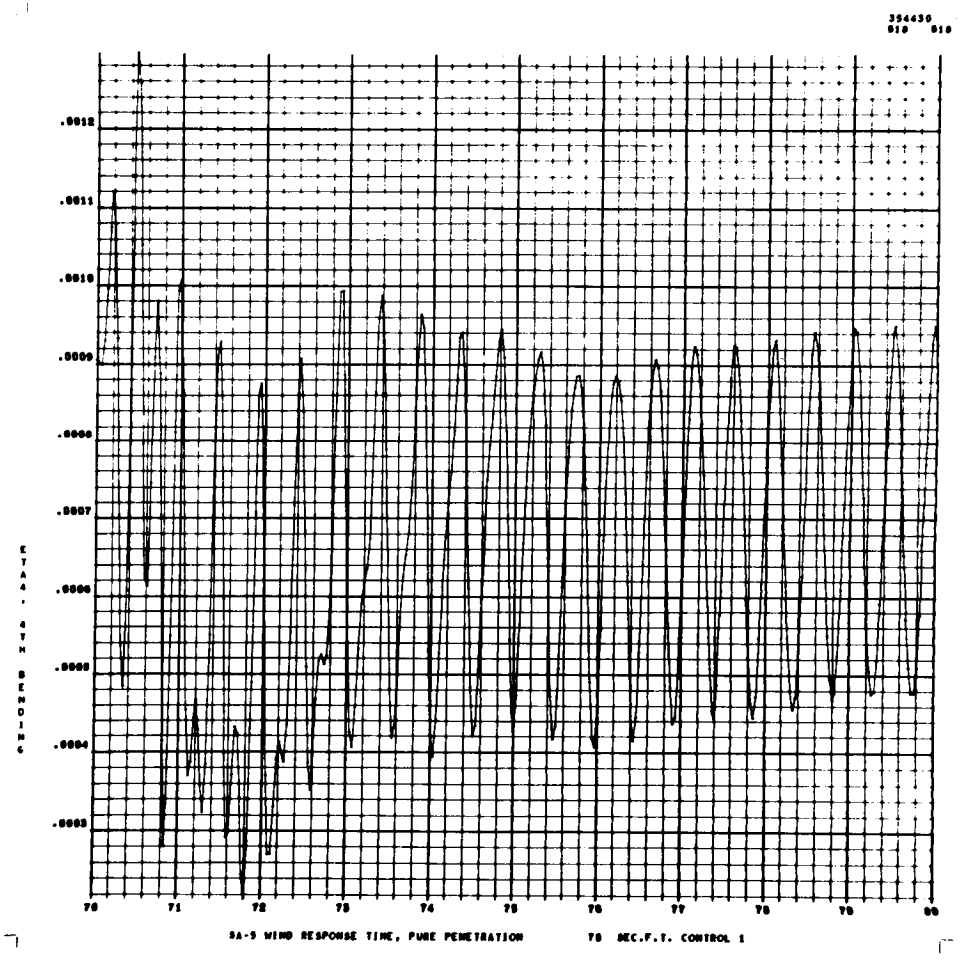

Fig. 39 - Sinusoidal Wind-Induced Response of Fourth Bending Considering Pure Penetration - Angle of Attack Control, 70-sec. Flight Time

SA-5 WIND RESPØNSE TIME, PENETRATIØN WITH LIFT
70 SEC.F.T. CØNTRØL 1 ETA4, 4TH BENDING

70.05405	9.3004802E-04	MIN
70.17853	1.1562706E-03	MAX
70.33414	4.8865092E-04	MIN
70.45862	1.3744589E-03	MAX
70.61423	5.9486472E-04	MIN
70.70759	1.0392239E-03	MAX
70.83208	2.9202120E-04	MIN
70.98768	1.1043854E-03	MAX
71.11217	3.6406931E-04	MIN
71.20553	5.1024261E-04	MAX
71.29890	3.8046287E-04	MIN
71.45450	9.8502605E-04	MAX
71.57899	3.0758871E-04	MIN
71.70347	4.9263189E-04	MAX
71.79684	2.4814926E-04	MIN
71.95245	9.4424565E-04	MAX
72.10805	2.7659782E-04	MIN
72.20142	4.7652510E-04	MAX
72.26366	4.4536800E-04	MIN
72.41926	9.5184120E-04	MAX
72.57487	3.6821993E-04	MIN
72.69936	5.8588263E-04	MAX
72.76160	5.6538465E-04	MIN
72.91720	1.0454666E-03	MAX
73.07281	4.1944024E-04	MIN
73.38402	1.0255342E-03	MAX
73.53963	4.3896130E-04	MIN
73.85084	9.9496431E-04	MAX
74.03757	4.1460010E-04	MIN
74.34878	9.7254723E-04	MAX
74.50439	4.4585128E-04	MIN
74.81560	9.7209911E-04	MAX
75.00233	4.5181659E-04	MIN
75.28242	9.4153814E-04	MAX
75.46915	4.4722215E-04	MIN
75.71812	9.1440321E-04	MAX
75.96709	4.3639102E-04	MIN
76.18494	9.1871099E-04	MAX
76.43391	4.4758349E-04	MIN
76.65176	9.4381292E-04	MAX
76.90073	4.7189079E-04	MIN
77.11859	9.6295604E-04	MAX
77.39867	4.7932620E-04	MIN
77.58540	9.6515138E-04	MAX
77.86549	4.8146037E-04	MIN
78.08334	9.6961195E-04	MAX
78.33231	4.9170605E-04	MIN
78.55016	9.8039246E-04	MAX
78.79913	5.0440685E-04	MIN
79.01698	9.8431016E-04	MAX
79.26595	5.1105499E-04	MIN
79.51492	9.8510529E-04	MAX
79.73277	5.1126625E-04	MIN
79.98174	9.8529385E-04	MAX

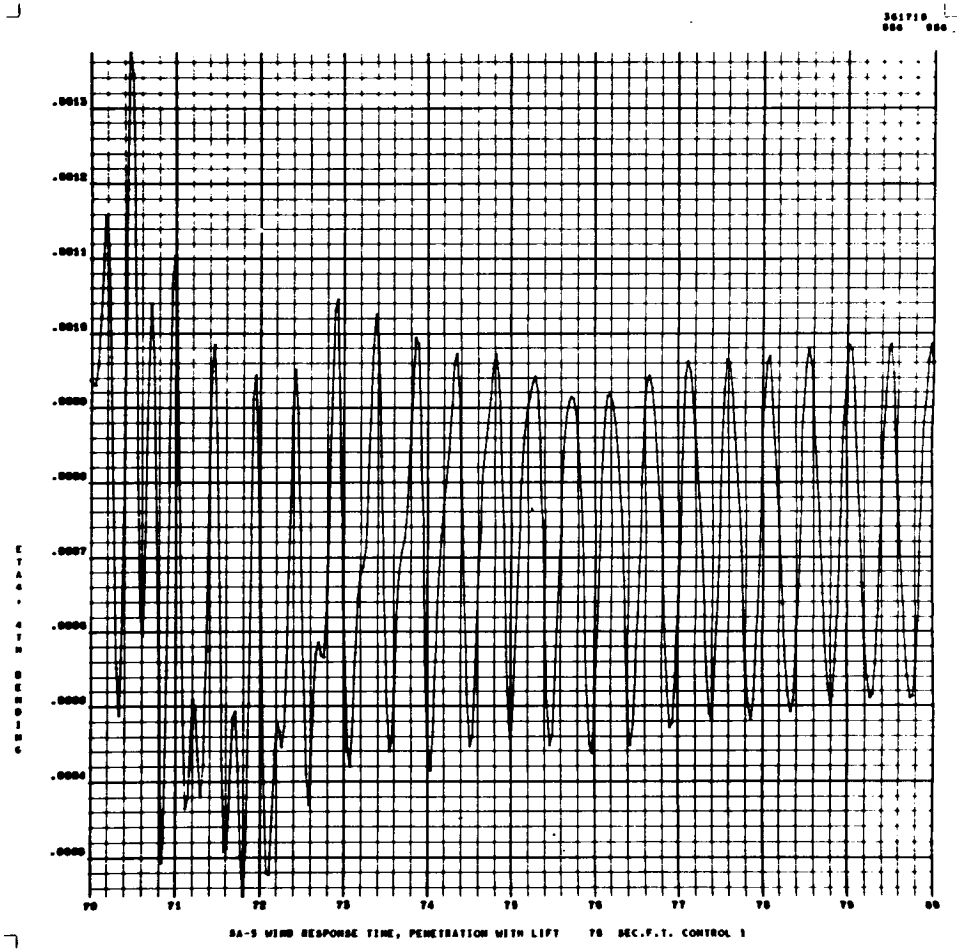

Fig. 40 - Sinusoidal Wind-Induced Response of Fourth Bending Considering Penetration With Lift Growth - Angle of Attack Control, 70-sec. Flight Time

SA-5 WIND RESPØNSE TIME, INSTANTANEØUS IMMERSIØN
70 SEC.F.T. CØNTRØL 1 BETAC, CØNTRØL DEFLECTIØN

70.14741	1.5202124E-02	MAX
70.30302	8.5648260E-03	MIN
70.52086	1.1292760E-02	MAX
70.76984	1.7195340E-03	MIN
70.92544	2.8749973E-03	MAX
71.04993	3.8491739E-04	CRØSS
71.14329	-2.8872986E-03	MIN
71.20553	-1.5390157E-03	CRØSS
71.36114	7.3450827E-03	MAX
71.48563	1.0149524E-03	CRØSS
71.64123	-5.3986718E-03	MIN
71.73460	-1.0785958E-03	CRØSS
71.85908	4.9505019E-03	MAX
71.98357	5.4414249E-05	CRØSS
72.10805	-4.2785308E-03	MIN
72.17029	-2.0464084E-03	CRØSS
72.32590	6.9454851E-03	MAX
72.48151	5.2386338E-06	CRØSS
72.54375	-1.7963147E-03	MIN
72.60599	-9.7500499E-04	CRØSS
72.79272	1.0204393E-02	MAX
73.04169	9.0771792E-04	MIN
73.29066	1.1904504E-02	MAX
73.50851	1.7525864E-03	MIN
73.75748	1.1882837E-02	MAX
73.97533	1.2858359E-03	MIN
74.22430	1.1743578E-02	MAX
74.44215	1.5219018E-03	MIN
74.69112	1.2052251E-02	MAX
74.94009	1.8277003E-03	MIN
75.15794	1.2108767E-02	MAX
75.40691	1.5173642E-03	MIN
75.65588	1.1593703E-02	MAX
75.87373	9.4974302E-04	MIN
76.12270	1.1258540E-02	MAX
76.34055	8.9892002E-04	MIN
76.58952	1.1403939E-02	MAX
76.83849	1.1581401E-03	MIN
77.05634	1.1564128E-02	MAX
77.30531	1.1318314E-03	MIN
77.52316	1.1393659E-02	MAX
77.77213	9.5412896E-04	MIN
78.02110	1.1316734E-02	MAX
78.23895	9.8507496E-04	MIN
78.48792	1.1467025E-02	MAX
78.73689	1.2177168E-03	MIN
78.95474	1.1617885E-02	MAX
79.20371	1.2143093E-03	MIN
79.42156	1.1567022E-02	MAX
79.67053	1.1175083E-03	MIN
79.91950	1.1437267E-02	MAX

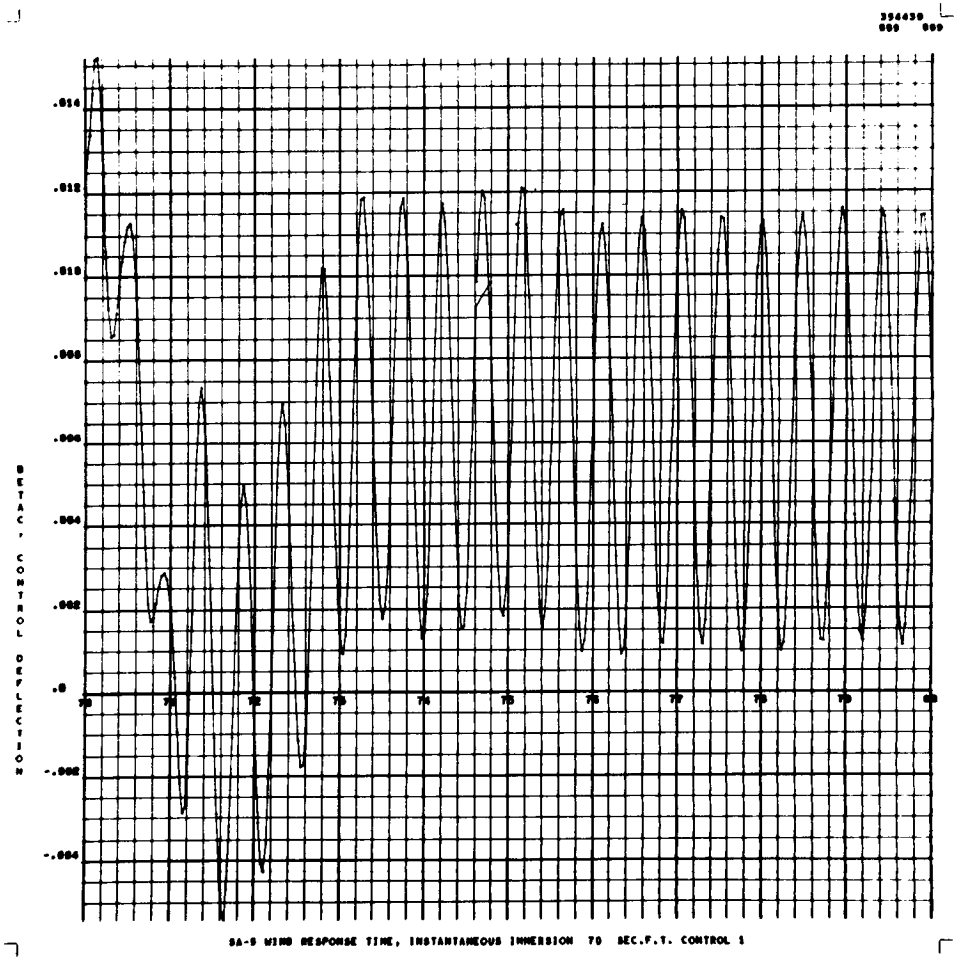

Fig. 41 - Sinusoidal Wind-Induced Response of Control Deflection Considering Instantaneous Immersion - Angle of Attack Control, 70-sec. Flight Time

SA-5 WIND RESPØNSE TIME, PURE PENETRATIØN

70 SEC.F.T. CØNTRØL 1	BETAC, CØNTRØL DEFLECTIØN	
70.14741	1.4010277E-02	MAX
70.36526	3.3765141E-03	MIN
70.58311	9.6641129E-03	MAX
70.70759	1.8625312E-03	CRØSS
70.86320	-4.2257892E-03	MIN
70.98768	-4.2386297E-04	CRØSS
71.04993	5.2542515E-04	CRØSS
71.04993	5.2542515E-04	MAX
71.23665	-7.0566985E-03	MIN
71.45450	-6.2859161E-05	CRØSS
71.48563	3.8235847E-04	MAX
71.51675	3.0844094E-04	CRØSS
71.73460	-9.6961379E-03	MIN
71.98357	-3.0507178E-04	MAX
72.20142	-8.4389499E-03	MIN
72.38814	-2.2746548E-04	CRØSS
72.45039	1.0629812E-03	MAX
72.51263	2.1212921E-04	CRØSS
72.66823	-5.8747229E-03	MIN
72.79272	-2.9351355E-04	CRØSS
72.91720	4.6874828E-03	MAX
73.04169	8.8062044E-04	CRØSS
73.13505	-2.9574080E-03	MIN
73.22842	-3.2335502E-04	CRØSS
73.38402	6.2306350E-03	MAX
73.53963	6.7798773E-04	CRØSS
73.63299	-2.2237262E-03	MIN
73.69524	-3.6802561E-04	CRØSS
73.85084	6.2974060E-03	MAX
74.00645	6.7455931E-04	CRØSS
74.09981	-2.5360432E-03	MIN
74.16206	-1.0332639E-03	CRØSS
74.31766	6.1563733E-03	MAX
74.47327	1.1521359E-03	CRØSS
74.56663	-2.1930016E-03	MIN
74.62888	-1.0541793E-03	CRØSS
74.81560	6.7045916E-03	MAX
74.97121	2.9478700E-04	CRØSS
75.06457	-1.6969644E-03	MIN
75.09570	-9.5034848E-04	CRØSS
75.28242	6.8642616E-03	MAX
75.43803	4.3032568E-04	CRØSS
75.53139	-2.0180843E-03	MIN
75.59364	-2.9256723E-04	CRØSS
75.74924	6.3885550E-03	MAX
75.90485	1.6604991E-04	CRØSS
75.99821	-2.5339538E-03	MIN
76.06046	-1.0659996E-03	CRØSS
76.21606	6.0149015E-03	MAX
76.37167	3.2398009E-04	CRØSS
76.46503	-2.5612020E-03	MIN
76.52728	-1.3004409E-03	CRØSS
76.71400	6.2028100E-03	MAX
76.83849	9.0573229E-04	CRØSS
76.93185	-2.2773492E-03	MIN
76.99409	-1.2783183E-03	CRØSS
77.18082	6.4225992E-03	MAX
77.30531	1.3656139E-03	CRØSS
77.39867	-2.2061365E-03	MIN

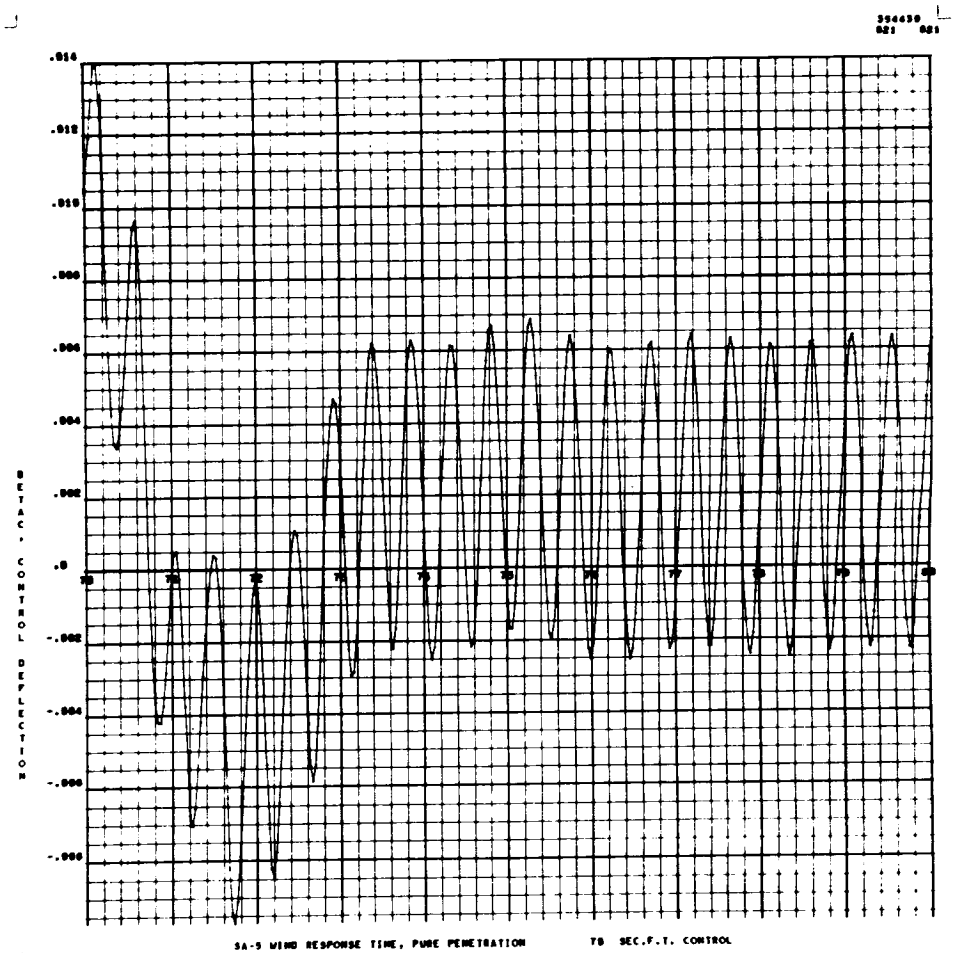

Fig. 42 - Sinusoidal Wind-Induced Response of Control Deflection Considering Pure Penetration - Angle of Attack Control, 70-sec. Flight Time

SA-5 WIND RESPØNSE TIME, PENETRATIØN WITH LIFT
70 SEC.F.T. CØNTRØL 1 BETAC, CØNTRØL DEFLECTIØN

70.14741	1.6034647E-02	MAX
70.36526	5.5705038E-03	MIN
70.58311	1.1647970E-02	MAX
70.76984	1.0198802E-05	CRØSS
70.86320	-1.8169741E-03	MIN
70.92544	-6.3799440E-04	CRØSS
71.04993	2.6686944E-03	MAX
71.11217	5.8949000E-04	CRØSS
71.23665	-4.4708817E-03	MIN
71.36114	-6.5827372E-04	CRØSS
71.51675	2.3577957E-03	MAX
71.67899	5.6779103E-04	CRØSS
71.73460	-7.0586813E-03	MIN
71.89020	-9.8984454E-04	CRØSS
71.98357	1.7056715E-03	MAX
72.04581	6.3772978E-04	CRØSS
72.20142	-5.7880442E-03	MIN
72.32590	-9.4279087E-04	CRØSS
72.48151	3.0100835E-03	MAX
72.57487	6.8751201E-06	CRØSS
72.66823	-3.2640406E-03	MIN
72.76160	-1.7579944E-04	CRØSS
72.94833	6.5386297E-03	MAX
73.10393	4.6247840E-04	CRØSS
73.16617	-3.7217273E-04	CRØSS
73.16617	-3.7217273E-04	MIN
73.38402	8.0237067E-03	MAX
73.63299	2.7401466E-04	MIN
73.85084	8.0962655E-03	MAX
74.09981	7.3598523E-06	MIN
74.34878	7.9962005E-03	MAX
74.56663	3.7805574E-04	MIN
74.81560	8.5545582E-03	MAX
75.06457	7.6392892E-04	MIN
75.28242	8.6949616E-03	MAX
75.53139	4.8768067E-04	MIN
75.74924	8.2067285E-03	MAX
75.99821	8.7213939E-06	MIN
76.24718	7.8201107E-03	MAX
76.46503	2.5049471E-06	MIN
76.71400	8.0813577E-03	MAX
76.93185	3.0060757E-04	MIN
77.18082	8.2670344E-03	MAX
77.42979	2.8548091E-04	MIN
77.64764	8.1139671E-03	MAX
77.89661	7.1177715E-05	MIN
78.11446	7.9189388E-03	MAX
78.36343	4.8993015E-05	MIN
78.61240	8.0746851E-03	MAX
78.83025	2.0953947E-04	MIN
79.07922	8.2134699E-03	MAX
79.29707	3.0229873E-04	MIN
79.54604	8.1627551E-03	MAX
79.79501	1.7204158E-04	MIN

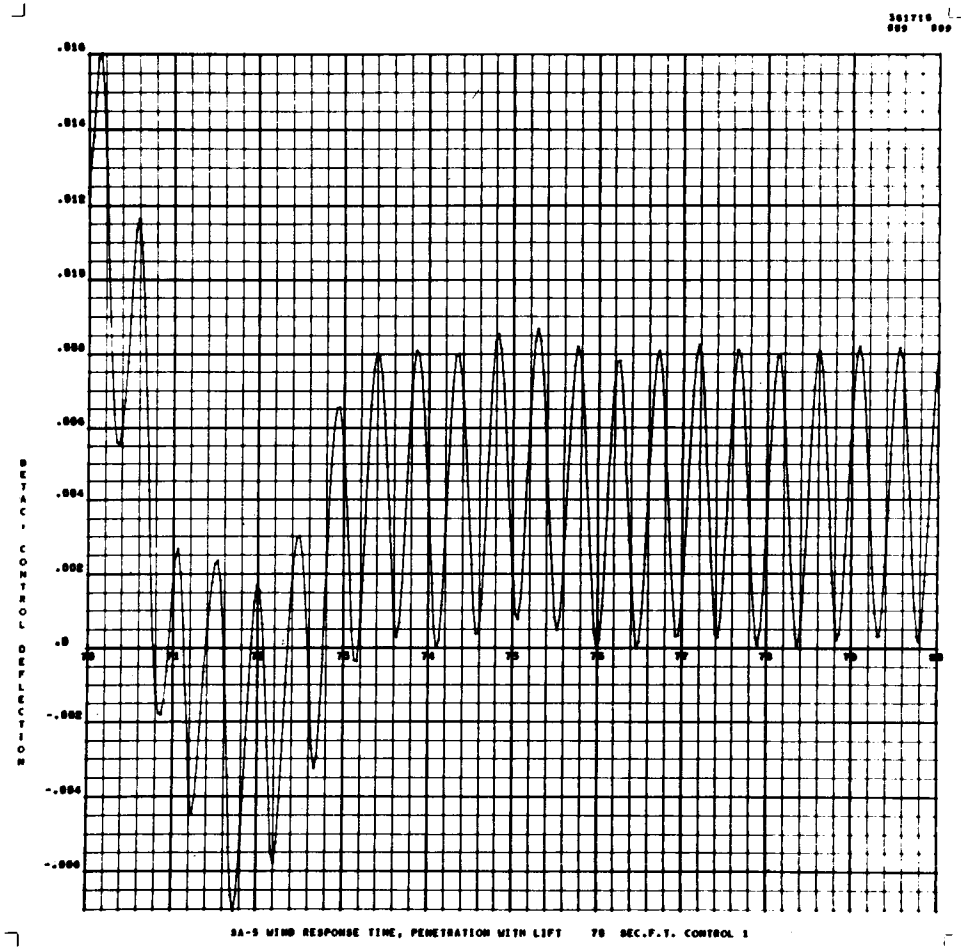

Fig. 43 - Sinusoidal Wind-Induced Response of Control Deflection Considering Penetration With Lift Growth - Angle of Attack Control, 70-sec. Flight Time

The vehicle's bending moment responses (reduced expression) to the Imbedded Gust Profile, shown in Fig. 44, are presented in Figs. 45 through 56 for the three station locations. These responses evolve from both the angle of attack (Control 1) and attitude (Control 2) control systems and the two types of aerodynamic representations used.

The numerics presented alongside the wind-induced responses pertain to an analysis of the responses curves. The analysis performed was the same as that used for the impulsive responses.

A discussion of the preceding figures and results obtained from figures of this type is given in the next section.

IV. RESULTS AND DISCUSSION OF RESPONSE INVESTIGATION

In this section the results of the two phases of the investigation are referenced and discussed. The results are presented separately for each phase because of the purpose and use of the wind-induced responses sought for each of the two phases. The interpretations of results which follow can be drawn only for the Saturn V configuration used and modes considered.

A. Phase I

In this phase, the responses to NASA's Sinusoidal Gust Criteria are compared to determine the effects and importance of penetration and growth of lift on vehicle responses. Only the angle of attack control system was considered in this phase of the investigation.

The estimation of the importance of the effects of penetration and growth of lift will be discussed in terms of two portions of the responses: the transient and steady-state. The steady-state portion is that region in which the oscillatory response is in tune with the driving frequency of the sinusoidal profile. In general, the maximum responses occurred within the transient portion. Consequently, this region will be discussed first.

1. Transient responses: In discussing the maximum responses to the Sinusoidal Gust Profile, it is convenient to first digress and reconsider the impulsive responses. In [1], it was suggested that the importance of penetration and lift growth would be apparent in the comparison of impulsive (and indicial) responses based on the three aerodynamic representations.

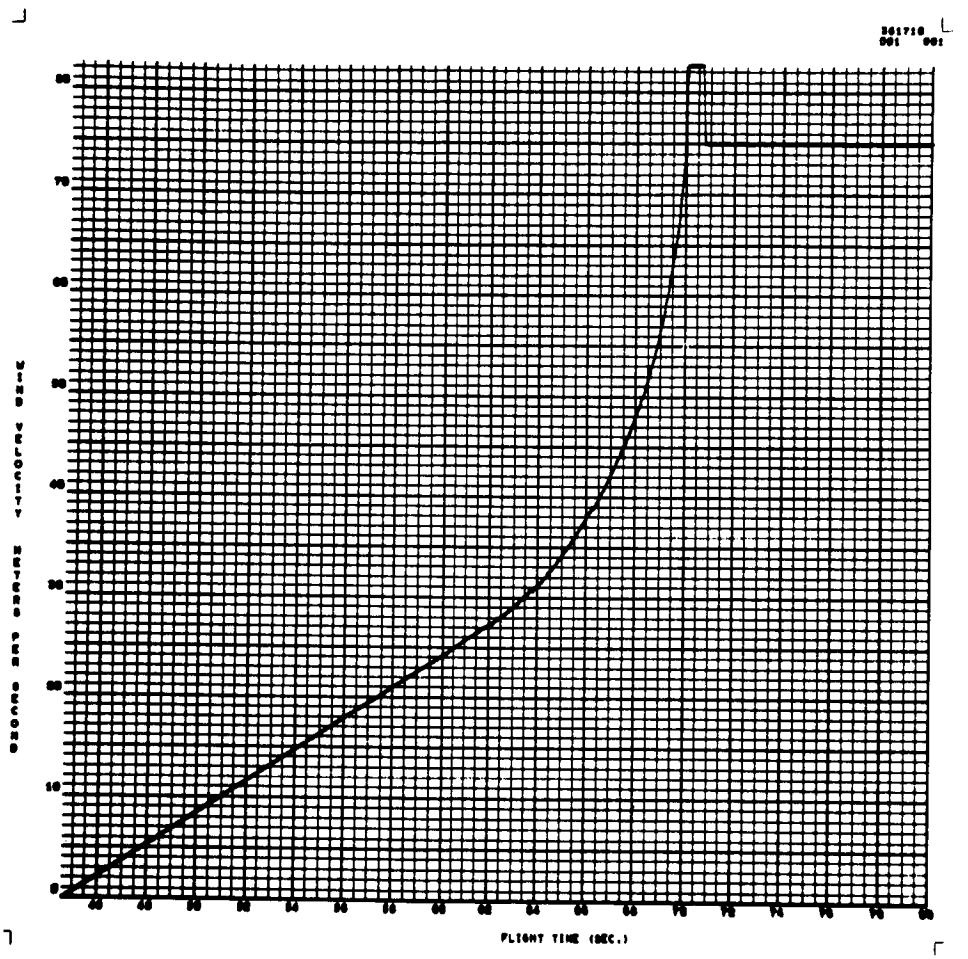

Fig. 44 - Imbedded Gust Profile

SA-5 WIND RESPØNSE TIME, PURE PENETRATIØN
REDUCED BENDING MØMENT TIMES 0.00001 ¶ KG
AT STATIØN 1 70 SEC.F.T. CØNTRØL 1

70.08516	-2.0094787E-01	MIN
70.11628	-1.9794219E-01	MAX
70.27188	-2.4417138E-01	MIN
70.33413	-2.4023203E-01	MAX
70.52085	-4.5547878E-01	MIN
70.70758	-9.8279577E-02	MAX
70.83207	-1.8328625E-01	MIN
70.95655	-9.6036671E-02	MAX
71.08104	-2.5292084E-01	MIN
71.17440	-6.6230368E-02	CRØSS
71.23654	2.3799923E-02	CRØSS
71.23654	2.3799923E-02	MAX
71.39225	-2.3149142E-01	MIN
71.51674	-1.5985555E-01	MAX
71.64122	-2.0443380E-01	MIN
71.92131	-1.0887539E-01	MAX
72.04580	-1.8492045E-01	MIN
72.20141	-1.1235797E-01	MAX
72.32589	-2.0235798E-01	MIN
72.48150	-1.3000523E-01	MAX
72.60598	-1.7152734E-01	MIN
72.73047	-1.5293011E-01	MAX
72.82383	-1.6408952E-01	MIN
72.88607	-1.6188927E-01	MAX
73.04158	-1.9743879E-01	MIN
73.16617	-1.6392836E-01	MAX
73.29065	-2.0676394E-01	MIN
73.44626	-1.6858167E-01	MAX
73.57074	-2.0046019E-01	MIN
73.69523	-1.7859620E-01	MAX
73.78859	-1.9180164E-01	MIN
73.91308	-1.7831181E-01	MAX
74.00644	-1.8938036E-01	MIN
74.13093	-1.6828148E-01	MAX
74.25541	-1.8780553E-01	MIN
74.41102	-1.6524759E-01	MAX
74.53550	-1.8670791E-01	MIN
74.65999	-1.7004227E-01	MAX
74.78447	-1.8512806E-01	MIN
74.87784	-1.7493191E-01	MAX
75.00232	-1.8776573E-01	MIN
75.12681	-1.7702922E-01	MAX
75.25129	-1.9167544E-01	MIN
75.37578	-1.7779658E-01	MAX
75.50026	-1.9153711E-01	MIN
75.62475	-1.7767101E-01	MAX
75.74923	-1.8784227E-01	MIN
75.87372	-1.7666846E-01	MAX
75.96708	-1.8441723E-01	MIN
76.09157	-1.7464597E-01	MAX
76.21605	-1.8287129E-01	MIN
76.34054	-1.7305937E-01	MAX
76.46502	-1.8255114E-01	MIN
76.58951	-1.7397427E-01	MAX
76.71399	-1.8329684E-01	MIN
76.83848	-1.7652911E-01	MAX
76.96296	-1.8469634E-01	MIN
77.08745	-1.7894528E-01	MAX
77.21193	-1.8593699E-01	MIN

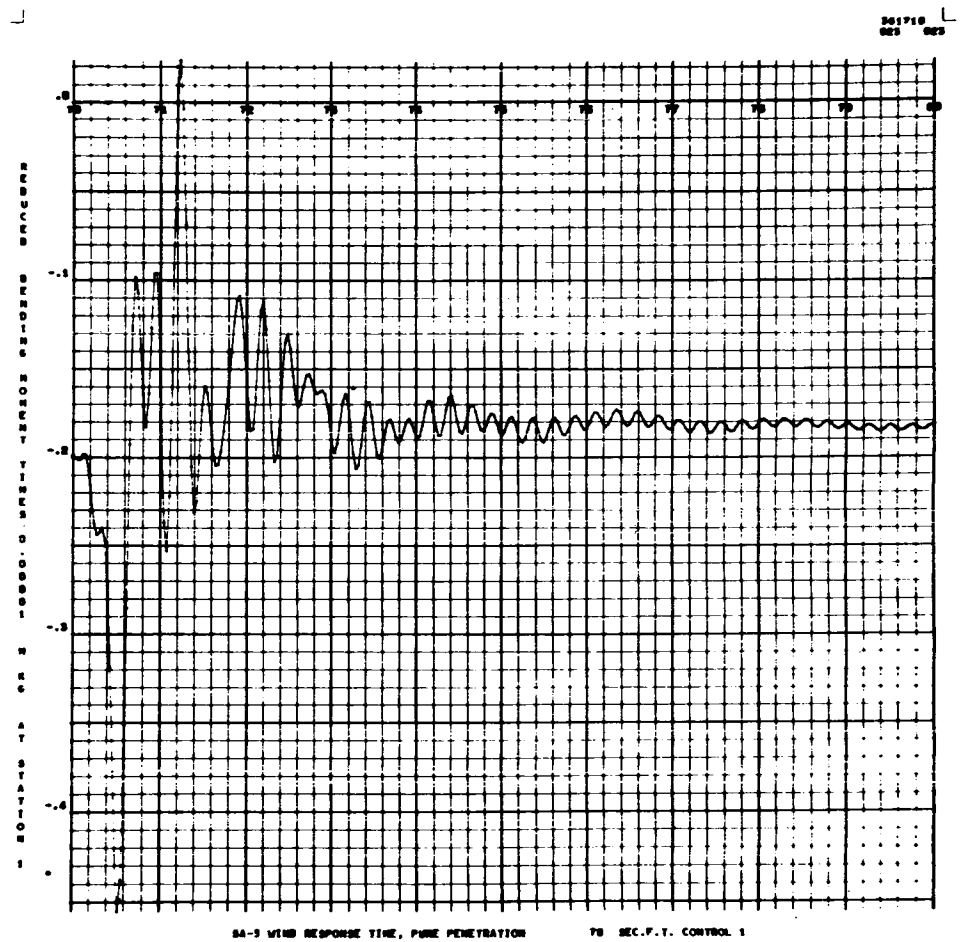

Fig. 45 - Bending Moment Response at Station 1 to Imbedded Gust Profile Considering Pure Penetration -- Angle of Attack Control, 70-sec. Flight Time

SA-5 WIND RESPØNSE TIME, PURE PENETRATIØN
REDUCED BENDING MØMENT TIMES 0.00001 M KG
AT STATIØN 1 70 SEC.F.T. CØNTRØL 2

70.11628	-2.3882651E-01	MIN
70.17852	-2.3774516E-01	MAX
70.70758	-3.4036466E-01	MIN
70.92543	-1.7825998E-01	MAX
71.04992	-2.4761719E-01	MIN
71.17440	-2.2897475E-01	MAX
71.26777	-2.4862573E-01	MIN
71.42337	-1.6376045E-01	MAX
71.61010	-2.8494116E-01	MIN
71.79683	-2.2772012E-01	MAX
71.89019	-2.3342925E-01	MIN
72.10804	-2.0756337E-01	MAX
72.26365	-2.3919399E-01	MIN
72.41925	-2.0867481E-01	MAX
72.54374	-2.3611831E-01	MIN
72.69935	-2.0579564E-01	MAX
72.82383	-2.1872355E-01	MIN
72.91720	-2.1551147E-01	MAX
73.01056	-2.1720690E-01	MIN
73.10392	-2.1634966E-01	MAX
73.22841	-2.2765602E-01	MIN
73.38401	-2.1397845E-01	MAX
73.50850	-2.2872942E-01	MIN
73.63299	-2.1522547E-01	MAX
73.75747	-2.2590924E-01	MIN
73.91308	-2.1911130E-01	MAX
74.00644	-2.2178407E-01	MIN
74.13093	-2.1727767E-01	MAX
74.22429	-2.2016422E-01	MIN
74.34877	-2.1196512E-01	MAX
74.47326	-2.1900243E-01	MIN
74.59774	-2.1038512E-01	MAX
74.72223	-2.1720461E-01	MIN
74.84671	-2.1125446E-01	MAX
74.97120	-2.1585504E-01	MIN
75.09569	-2.1240227E-01	MAX
75.22017	-2.1641055E-01	MIN
75.31353	-2.1273512E-01	MAX
75.43802	-2.1743572E-01	MIN
75.56250	-2.1253260E-01	MAX
75.68699	-2.1675725E-01	MIN
75.84260	-2.1175287E-01	MAX
75.93596	-2.1475902E-01	MIN
76.06045	-2.1046662E-01	MAX
76.18493	-2.1261655E-01	MIN
76.30942	-2.0854622E-01	MAX
76.43390	-2.1092046E-01	MIN
76.55839	-2.0702260E-01	MAX
76.68287	-2.0984413E-01	MIN
76.80736	-2.0654201E-01	MAX
76.93184	-2.0930745E-01	MIN
77.02521	-2.0675278E-01	MAX
77.14969	-2.0921766E-01	MIN
77.27418	-2.0686652E-01	MAX
77.39866	-2.0917628E-01	MIN
77.52315	-2.0661345E-01	MAX
77.64763	-2.0863891E-01	MIN
77.77212	-2.0586790E-01	MAX
77.89660	-2.0744892E-01	MIN

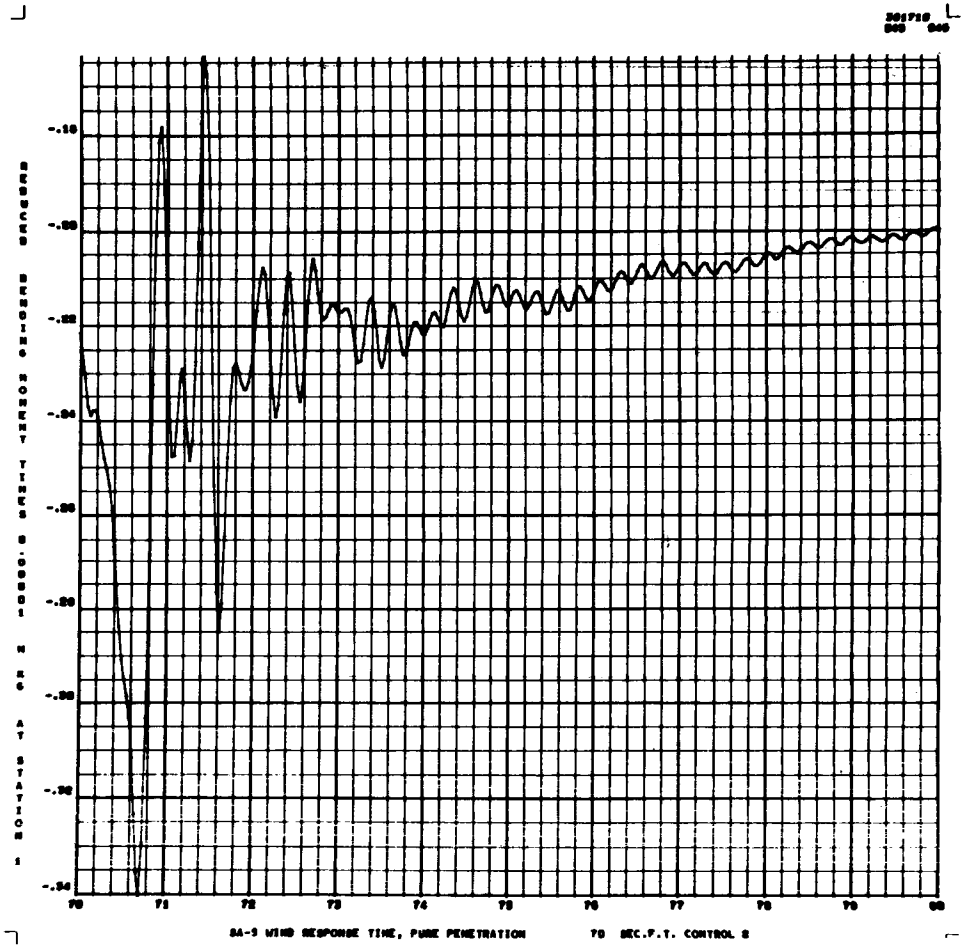

Fig. 46 - Bending Moment Response at Station 1 to Imbedded Gust Profile Considering Pure Penetration -- Attitude Control, 70 sec. Flight Time

SA-5 WIND RESPØNSE TIME, PURE PENETRATIØN
REDUCED BENDING MØMENT TIMES 0.00001 ¶ KG
AT STATIØN 2 70 SEC.F.T. CØNTRØL 1

70.20954	-2.3117983E	00	MIN
70.27188	-2.2768914E	00	MAX
70.42749	-3.2973577E	00	MIN
70.55198	-2.3367925E	00	MAX
70.67646	-2.7327592E	00	MIN
70.83207	-1.0579970E	00	MAX
70.95655	-1.9862389E	00	MIN
71.11216	-7.7558896E	-01	MAX
71.23664	-1.7516561E	00	MIN
71.36113	-8.5457361E	-01	MAX
71.48562	-2.0007755E	00	MIN
71.61010	-1.5181385E	00	MAX
71.73346	-1.7772011E	00	MIN
71.82795	-1.2990297E	00	MAX
71.95243	-1.6461655E	00	MIN
72.07692	-1.1260819E	00	MAX
72.20141	-1.8195533E	00	MIN
72.32589	-1.2205936E	00	MAX
72.45038	-1.8051084E	00	MIN
72.57486	-1.3159759E	00	MAX
72.69935	-1.7156950E	00	MIN
72.79271	-1.4519449E	00	MAX
72.94832	-1.8214208E	00	MIN
73.04168	-1.5466833E	00	MAX
73.16617	-1.9688822E	00	MIN
73.29065	-1.5914498E	00	MAX
73.41514	-1.9808179E	00	MIN
73.53962	-1.6350071E	00	MAX
73.66411	-1.9428800E	00	MIN
73.78859	-1.6595390E	00	MAX
73.91308	-1.8930131E	00	MIN
74.03756	-1.6252943E	00	MAX
74.13093	-1.8499243E	00	MIN
74.28653	-1.5922196E	00	MAX
74.37990	-1.8310442E	00	MIN
74.50438	-1.5992501E	00	MAX
74.62887	-1.8278090E	00	MIN
74.75335	-1.6330339E	00	MAX
74.87784	-1.8404889E	00	MIN
75.00232	-1.6665354E	00	MAX
75.12681	-1.8622437E	00	MIN
75.25129	-1.6891924E	00	MAX
75.37578	-1.8687458E	00	MIN
75.50026	-1.6958344E	00	MAX
75.62475	-1.8476455E	00	MIN
75.74923	-1.6897555E	00	MAX
75.84260	-1.8184389E	00	MIN
75.96708	-1.6741253E	00	MAX
76.09157	-1.7952376E	00	MIN
76.21605	-1.6593749E	00	MAX
76.34054	-1.7831233E	00	MIN
76.46502	-1.6605940E	00	MAX
76.58951	-1.7836987E	00	MIN
76.71399	-1.6783125E	00	MAX
76.83848	-1.7927991E	00	MIN
76.96296	-1.7023360E	00	MAX
77.08745	-1.8025286E	00	MIN
77.18081	-1.7187725E	00	MAX
77.30530	-1.8088187E	00	MIN

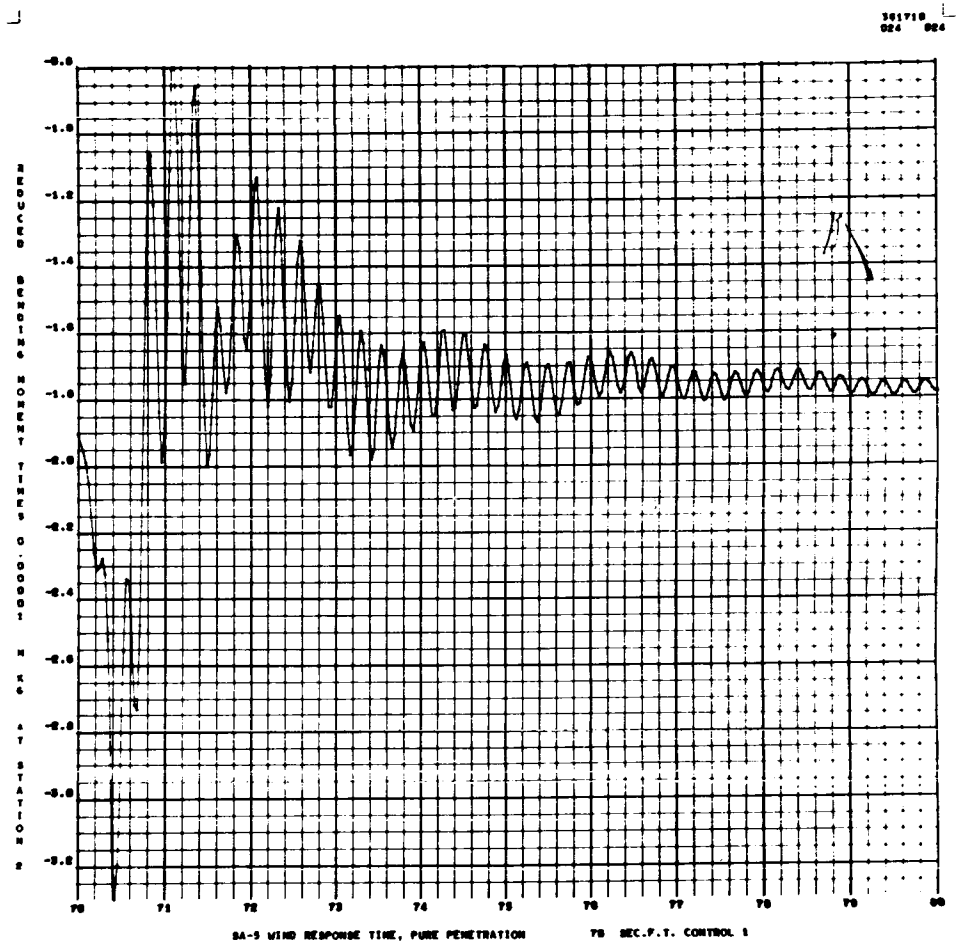

Fig. 47 - Bending Moment Response at Station 2 to Imbedded Gust Profile Considering Pure Penetration -- Angle of Attack Control, 70-sec. Flight Time

SA-5 WIND RESPØNSE TIME, PURE PENETRATIØN
REDUCED BENDING MØMENT TIMES 0.00001 M KG
AT STATIØN 2 70 SEC.F.T. CØNTRØL 2

70.61422	-2.9903162E 00	MIN
70.80095	-2.4370975E 00	MAX
70.86319	-2.4669942E 00	MIN
71.04992	-2.0487737E 00	MAX
71.17440	-2.4009077E 00	MIN
71.29889	-1.9610492E 00	MAX
71.45449	-2.3127299E 00	MIN
71.54786	-2.0896873E 00	MAX
71.70346	-2.4495802E 00	MIN
71.85907	-2.2214827E 00	MAX
71.89019	-2.2335388E 00	MIN
72.04580	-2.0941379E 00	MAX
72.13916	-2.2196687E 00	MIN
72.26365	-2.0449827E 00	MAX
72.41925	-2.2519334E 00	MIN
72.54374	-2.0239415E 00	MAX
72.66822	-2.1828932E 00	MIN
72.79271	-2.0172980E 00	MAX
72.91720	-2.1311064E 00	MIN
73.01056	-2.0539671E 00	MAX
73.13504	-2.1721180E 00	MIN
73.25953	-2.0686113E 00	MAX
73.38401	-2.2002164E 00	MIN
73.50850	-2.0662339E 00	MAX
73.63299	-2.1953431E 00	MIN
73.75747	-2.0795724E 00	MAX
73.88196	-2.1744382E 00	MIN
74.00644	-2.0803218E 00	MAX
74.09980	-2.1477885E 00	MIN
74.22429	-2.0530605E 00	MAX
74.34877	-2.1262514E 00	MIN
74.47326	-2.0283712E 00	MAX
74.59774	-2.1111001E 00	MIN
74.72223	-2.0238344E 00	MAX
74.84671	-2.1003245E 00	MIN
74.97120	-2.0302227E 00	MAX
75.09569	-2.0974710E 00	MIN
75.22017	-2.0392962E 00	MAX
75.31353	-2.0999481E 00	MIN
75.43802	-2.0417244E 00	MAX
75.56250	-2.0998973E 00	MIN
75.68699	-2.0370937E 00	MAX
75.81148	-2.0875589E 00	MIN
75.93596	-2.0260857E 00	MAX
76.06045	-2.0684751E 00	MIN
76.18493	-2.0111089E 00	MAX
76.30942	-2.0493506E 00	MIN
76.43390	-1.9971729E 00	MAX
76.55839	-2.0347815E 00	MIN
76.68287	-1.9896484E 00	MAX
76.77624	-2.0272939E 00	MIN
76.90072	-1.9878226E 00	MAX
77.02521	-2.0246394E 00	MIN
77.14969	-1.9884587E 00	MAX
77.27418	-2.0231877E 00	MIN
77.39866	-1.9880454E 00	MAX
77.52315	-2.0189606E 00	MIN
77.64763	-1.9837302E 00	MAX
77.77212	-2.0096761E 00	MIN

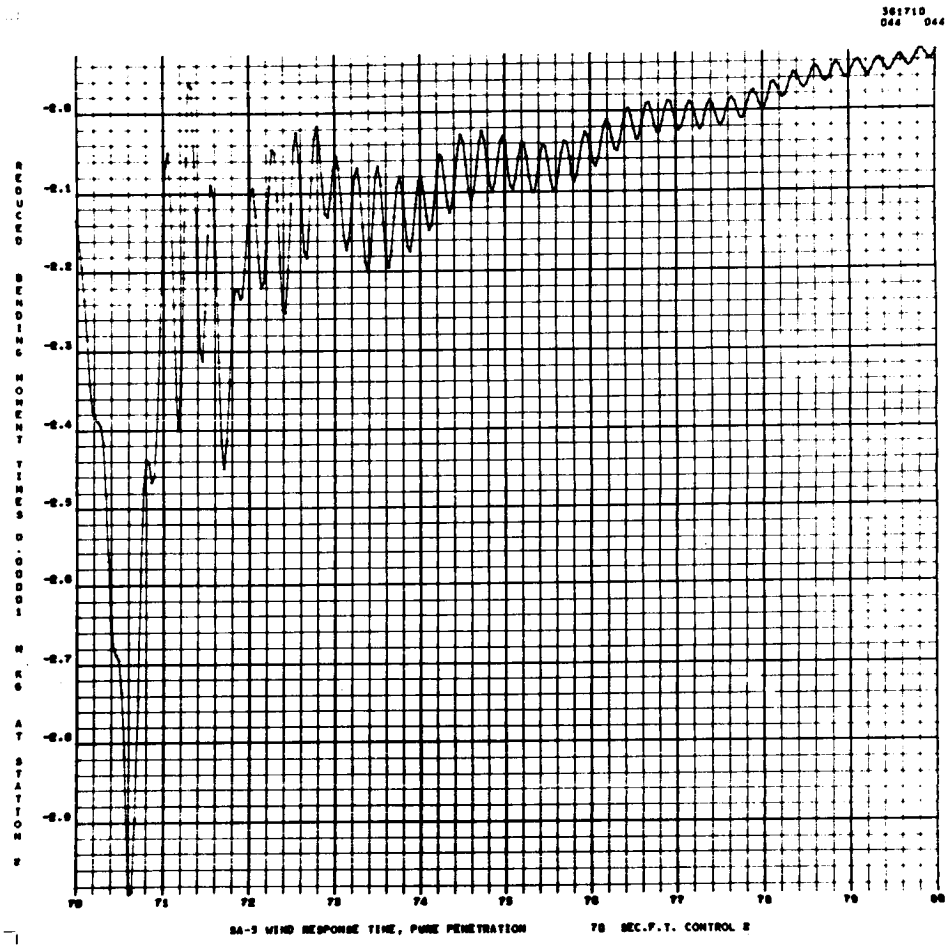

Fig. 48 - Bending Moment Response at Station 2 to Imbedded Gust Profile Considering Pure Penetration -- Attitude Control, 70-sec. Flight Time

SA-5 WIND RESPØNSE TIME, PURE PENETRATIØN
REDUCED BENDING MØMENT TIMES 0.00001 M KG
AT STATIØN 3 70 SEC.F.T. CØNTRØL 1

70.24076	-2.7571285E	01	MIN
70.33413	-2.3880256E	01	MAX
70.45851	-2.9426238E	01	MIN
70.58310	-2.2823951E	01	MAX
70.67646	-2.5308198E	01	MIN
71.11216	-1.0058421E	01	MAX
71.20552	-1.3773643E	01	MIN
71.33001	-1.0031935E	01	MAX
71.45449	-1.5969571E	01	MIN
71.57898	-9.5066404E	00	MAX
71.70346	-1.7254503E	01	MIN
71.82795	-1.1043788E	01	MAX
71.95243	-1.5577006E	01	MIN
72.07692	-1.1226591E	01	MAX
72.20141	-1.4712928E	01	MIN
72.32589	-1.1962063E	01	MAX
72.45038	-1.5904920E	01	MIN
72.54374	-1.2535751E	01	MAX
72.69935	-1.7293063E	01	MIN
72.79271	-1.3869354E	01	MAX
72.94832	-1.8315975E	01	MIN
73.04158	-1.5694641E	01	MAX
73.16617	-1.9087484E	01	MIN
73.29055	-1.6871398E	01	MAX
73.41514	-1.9695082E	01	MIN
73.53962	-1.6991493E	01	MAX
73.66411	-1.9674750E	01	MIN
73.78859	-1.5709351E	01	MAX
73.91308	-1.9131433E	01	MIN
74.03756	-1.6444340E	01	MAX
74.16205	-1.8418925E	01	MIN
74.28653	-1.6314425E	01	MAX
74.37990	-1.8126985E	01	MIN
74.50438	-1.6243827E	01	MAX
74.62887	-1.8259610E	01	MIN
74.75335	-1.6485396E	01	MAX
74.87784	-1.8524814E	01	MIN
75.00232	-1.6887504E	01	MAX
75.12681	-1.8685314E	01	MIN
75.25129	-1.7190196E	01	MAX
75.37578	-1.8647500E	01	MIN
75.50026	-1.7224836E	01	MAX
75.59363	-1.8444347E	01	MIN
75.71811	-1.7028221E	01	MAX
75.84260	-1.8141728E	01	MIN
75.96708	-1.6751010E	01	MAX
76.09157	-1.7829303E	01	MIN
76.21605	-1.6601746E	01	MAX
76.34054	-1.7666578E	01	MIN
76.46502	-1.6640568E	01	MAX
76.58951	-1.7700861E	01	MIN
76.71399	-1.6837826E	01	MAX
76.83848	-1.7853966E	01	MIN
76.93184	-1.7085484E	01	MAX
77.08745	-1.7993425E	01	MIN
77.18081	-1.7263882E	01	MAX
77.30530	-1.8070359E	01	MIN
77.42978	-1.7328837E	01	MAX
77.55427	-1.8030536E	01	MIN

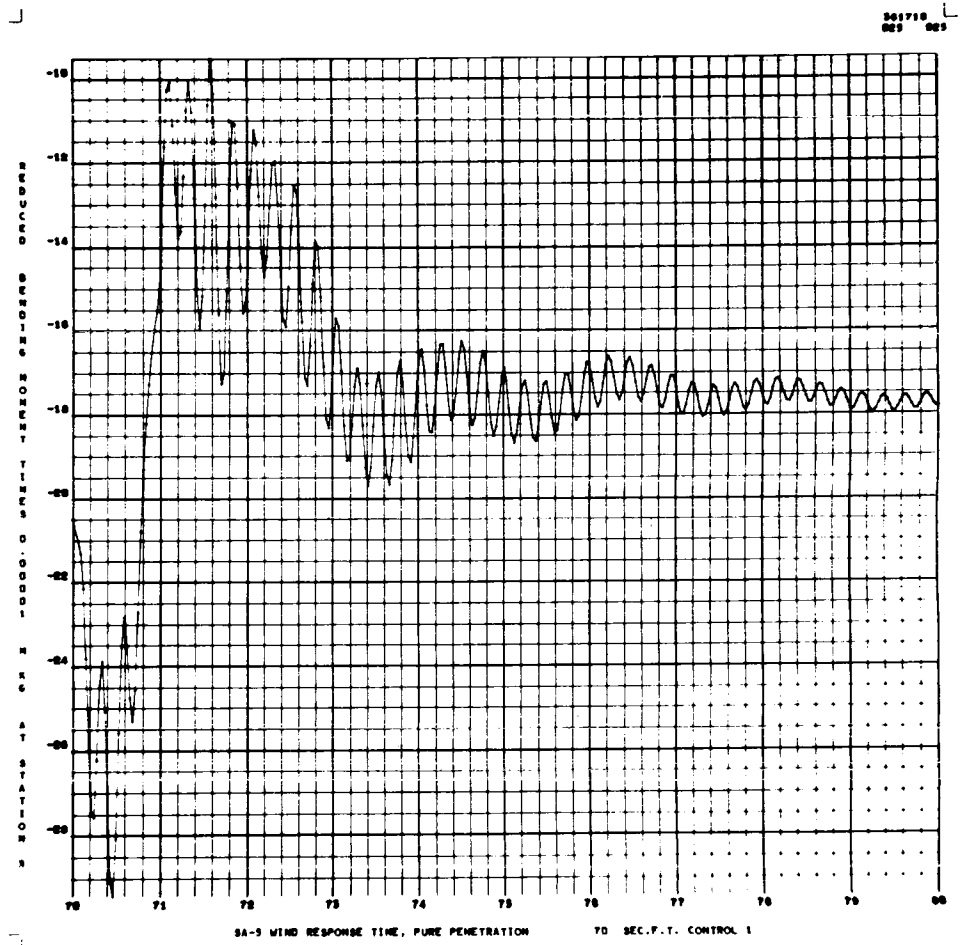

Fig. 49 - Bending Moment Response at Station 3 to Imbedded Gust Profile Considering Pure Penetration -- Angle of Attack Control, 70-sec. Flight Time

SA-5 WIND RESPONSE TIME, PURE PENETRATION
REDUCED BENDING MOMENT TIMES 0.00001 M KG
AT STATION 3 70 SEC.F.T. CONTROL 2

70.42749	-2.8044081E 01	MIN
70.52085	-2.6493731E 01	MAX
70.64534	-2.8507272E 01	MIN
70.80095	-2.6630114E 01	MAX
70.89431	-2.7352557E 01	MIN
71.11216	-2.2846210E 01	MAX
71.17440	-2.3152475E 01	MIN
71.29889	-2.1823210E 01	MAX
71.42337	-2.3394839E 01	MIN
71.54786	-2.2036407E 01	MAX
71.67234	-2.3682641E 01	MIN
71.79683	-2.1488134E 01	MAX
71.92131	-2.3896892E 01	MIN
72.07692	-2.1287222E 01	MAX
72.17028	-2.2386225E 01	MIN
72.29477	-2.0914089E 01	MAX
72.41925	-2.1715498E 01	MIN
72.51262	-2.0681231E 01	MAX
72.63710	-2.1734474E 01	MIN
72.76159	-2.0329256E 01	MAX
72.88607	-2.1780874E 01	MIN
73.01056	-2.0484876E 01	MAX
73.13504	-2.1875397E 01	MIN
73.25953	-2.0992760E 01	MAX
73.38401	-2.2044144E 01	MIN
73.50850	-2.1270877E 01	MAX
73.63299	-2.2103289E 01	MIN
73.75747	-2.1212703E 01	MAX
73.85083	-2.2034241E 01	MIN
74.00644	-2.1021992E 01	MAX
74.09980	-2.1756167E 01	MIN
74.25541	-2.0817412E 01	MAX
74.34877	-2.1411206E 01	MIN
74.47326	-2.0616076E 01	MAX
74.59774	-2.1209704E 01	MIN
74.72223	-2.0524643E 01	MAX
74.84671	-2.1183524E 01	MIN
74.97120	-2.0565269E 01	MAX
75.09569	-2.1226214E 01	MIN
75.22017	-2.0679238E 01	MAX
75.34466	-2.1242280E 01	MIN
75.43802	-2.0743319E 01	MAX
75.56250	-2.1220106E 01	MIN
75.68699	-2.0688123E 01	MAX
75.81148	-2.1097517E 01	MIN
75.93596	-2.0529931E 01	MAX
76.06045	-2.0891324E 01	MIN
76.18493	-2.0342007E 01	MAX
76.30942	-2.0669834E 01	MIN
76.43390	-2.0194200E 01	MAX
76.52727	-2.0509360E 01	MIN
76.68287	-2.0121513E 01	MAX
76.77624	-2.0440488E 01	MIN
76.90072	-2.0093600E 01	MAX
77.02521	-2.0428906E 01	MIN
77.14969	-2.0105497E 01	MAX
77.27418	-2.0420837E 01	MIN
77.39866	-2.0106229E 01	MAX
77.52315	-2.0370783E 01	MIN

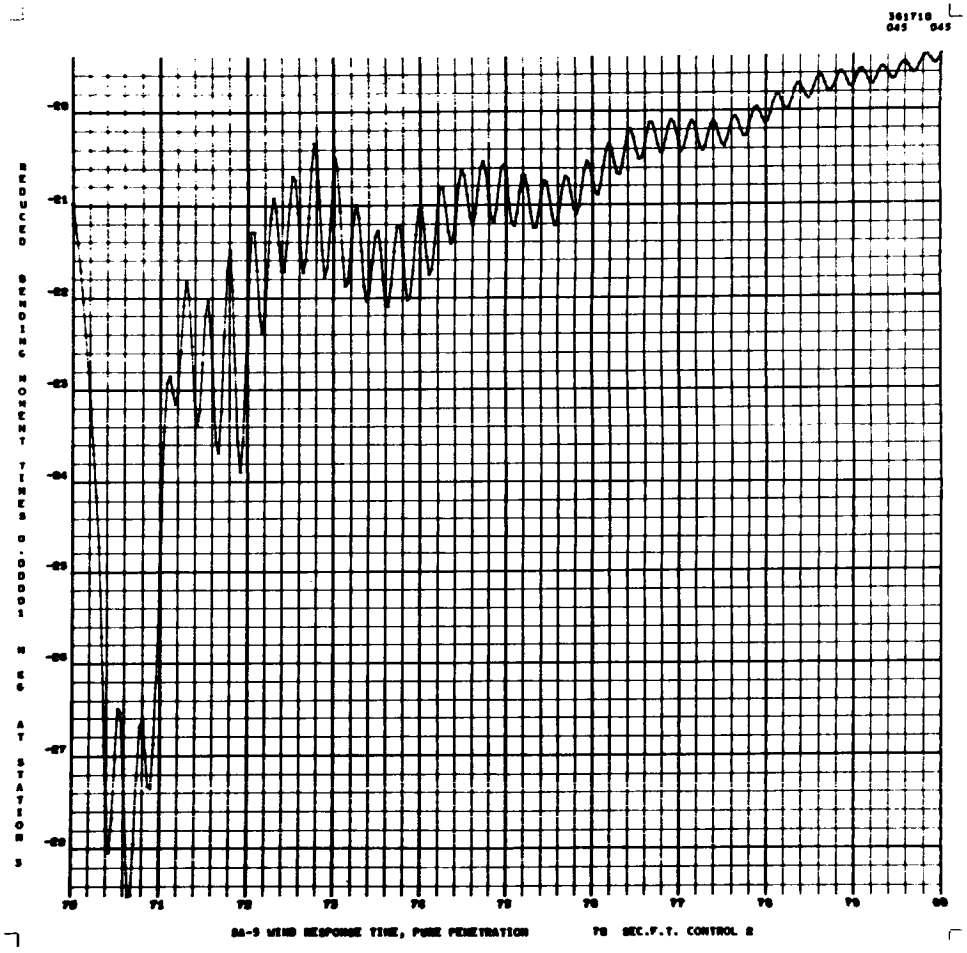

Fig. 50 - Bending Moment Response at Station 3 to Imbedded Gust Profile Considering Pure Penetration - Attitude Control, 70-sec. Flight Time

SA-5 WIND RESPØNSE TIME, INSTANTANEØUS IMMERSIØN
REDUCED BENDING MØMENT TIMES 0.00001 M KG
AT STATIØN 1 70 SEC.F.T. CØNTRØL 1

70.11628	-1.8639456E-01	MAX
70.48973	-5.1583122E-01	MIN
70.64534	-5.5117373E-02	CRØSS
70.70758	4.7413398E-02	MAX
70.73870	9.5169084E-03	CRØSS
70.86319	-2.1167029E-01	MIN
70.95655	-1.7667368E-01	MAX
71.04992	-2.5554808E-01	MIN
71.14328	-7.8540866E-02	CRØSS
71.23664	9.3110128E-02	MAX
71.26777	3.1258024E-02	CRØSS
71.39225	-3.4310630E-01	MIN
71.57898	-1.4378237E-01	MAX
71.70346	-1.9097182E-01	MIN
71.89019	-9.2125331E-02	MAX
72.04580	-2.1001599E-01	MIN
72.20141	-1.1073128E-01	MAX
72.32589	-2.1838038E-01	MIN
72.48150	-1.2310888E-01	MAX
72.63710	-1.7714566E-01	MIN
72.76159	-1.6432655E-01	MAX
73.01056	-2.0788112E-01	MIN
73.16617	-1.6462238E-01	MAX
73.29065	-2.1264646E-01	MIN
73.44626	-1.6870965E-01	MAX
73.57074	-2.0401893E-01	MIN
73.69523	-1.8275318E-01	MAX
73.78859	-1.8926536E-01	MIN
73.91308	-1.8254362E-01	MAX
74.00644	-1.8960678E-01	MIN
74.13093	-1.6855828E-01	MAX
74.25541	-1.9068392E-01	MIN
74.41102	-1.6773387E-01	MAX
74.53550	-1.9014098E-01	MIN
74.65999	-1.7431561E-01	MAX
74.78447	-1.8735168E-01	MIN
74.87784	-1.8043156E-01	MAX
75.00232	-1.8998868E-01	MIN
75.12681	-1.8126461E-01	MAX
75.25129	-1.9425696E-01	MIN
75.37578	-1.8045208E-01	MAX
75.50026	-1.9324309E-01	MIN
75.62475	-1.7985995E-01	MAX
75.74923	-1.8862827E-01	MIN
75.87372	-1.7912682E-01	MAX
75.96708	-1.8518859E-01	MIN
76.09157	-1.7712022E-01	MAX
76.21605	-1.8445184E-01	MIN
76.34054	-1.7577729E-01	MAX
76.46502	-1.8484191E-01	MIN
76.58951	-1.7724144E-01	MAX
76.71399	-1.8579418E-01	MIN
76.83848	-1.8007696E-01	MAX
76.96296	-1.8702844E-01	MIN
77.08745	-1.8220313E-01	MAX
77.21193	-1.8799291E-01	MIN
77.30530	-1.8273646E-01	MAX
77.42978	-1.8818088E-01	MIN
77.55427	-1.8235416E-01	MAX

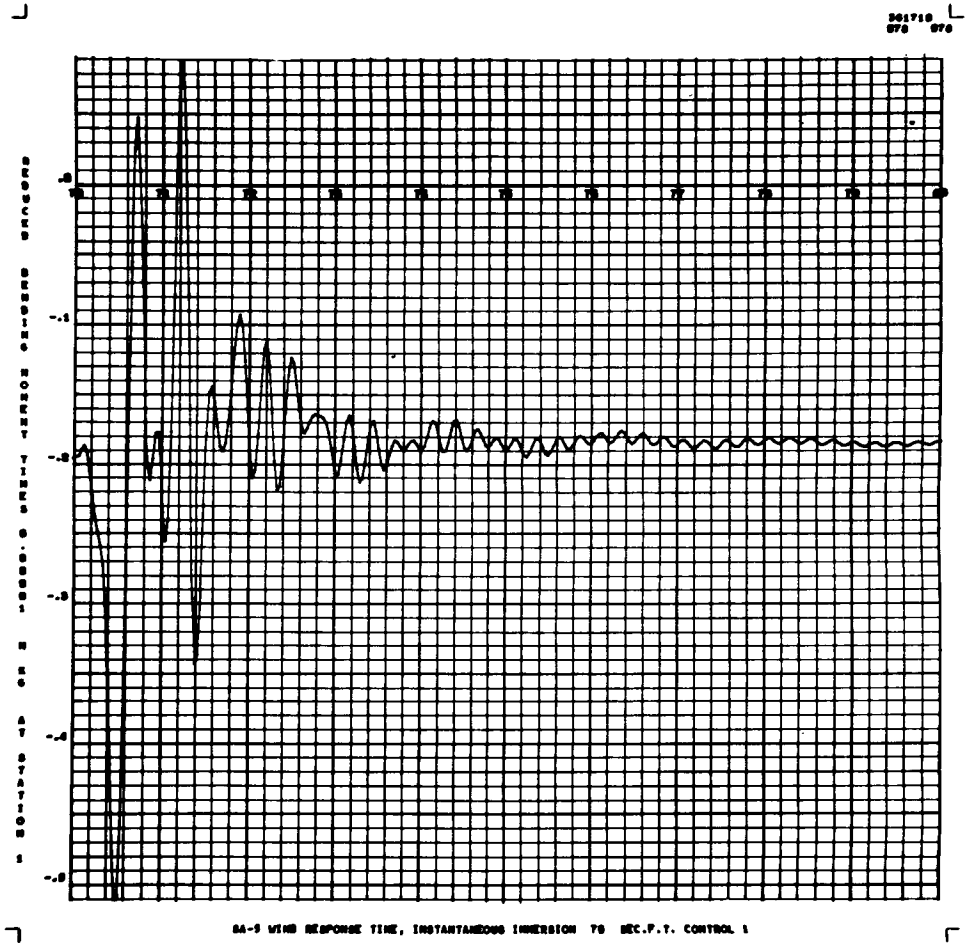

Fig. 51 - Bending Moment Response at Station 1 to Imbedded Gust Profile Considering Instantaneous Immersion -- Angle of Attack Control, 70-sec. Flight Time

SA-5 WIND RESPØNSE TIME, INSTANTANEØUS IMMERSIØN
REDUCED BENDING MØMENT TIMES C.CCCCI M KG
AT STATIØN 1 70 SEC.F.T. CØNTRØL 2

70.45861	-3.8349190E-01	MIN
70.67646	-1.8222984E-01	MAX
70.83207	-2.5131000E-01	MIN
70.86319	-2.5099447E-01	MAX
70.98767	-2.8305405E-01	MIN
71.17440	-1.3999160E-01	MAX
71.36113	-2.9407404E-01	MIN
71.54786	-2.3502130E-01	MAX
71.64122	-2.4691621E-01	MIN
71.85907	-2.0880422E-01	MAX
72.01468	-2.4668101E-01	MIN
72.13916	-2.1320696E-01	MAX
72.29477	-2.4822404E-01	MIN
72.45038	-2.1340819E-01	MAX
72.57486	-2.2609915E-01	MIN
72.79271	-2.1907351E-01	MAX
72.97944	-2.3259294E-01	MIN
73.10392	-2.1695213E-01	MAX
73.25953	-2.3165818E-01	MIN
73.38401	-2.1669990E-01	MAX
73.50850	-2.2773103E-01	MIN
73.66411	-2.2188317E-01	MAX
73.75747	-2.2364830E-01	MIN
73.85083	-2.2128382E-01	MAX
73.94420	-2.2369018E-01	MIN
74.09980	-2.1581503E-01	MAX
74.22429	-2.2268724E-01	MIN
74.34877	-2.1403329E-01	MAX
74.47326	-2.2075932E-01	MIN
74.59774	-2.1483961E-01	MAX
74.72223	-2.1837562E-01	MIN
74.84671	-2.1552904E-01	MAX
74.94008	-2.1830919E-01	MIN
75.06456	-2.1487956E-01	MAX
75.18905	-2.1931368E-01	MIN
75.31353	-2.1445672E-01	MAX
75.43802	-2.1873083E-01	MIN
75.56250	-2.1414003E-01	MAX
75.68699	-2.1695253E-01	MIN
75.81148	-2.1334996E-01	MAX
75.90484	-2.1514395E-01	MIN
76.06045	-2.1181667E-01	MAX
76.15381	-2.1387688E-01	MIN
76.30942	-2.1023429E-01	MAX
76.40278	-2.1262320E-01	MIN
76.52727	-2.0937269E-01	MAX
76.65175	-2.1164556E-01	MIN
76.77624	-2.0908258E-01	MAX
76.90072	-2.1110134E-01	MIN
77.02521	-2.0889819E-01	MAX
77.14969	-2.1079643E-01	MIN
77.27418	-2.0854810E-01	MAX
77.39866	-2.1029053E-01	MIN
77.52315	-2.0794218E-01	MAX
77.61651	-2.0942095E-01	MIN
77.77212	-2.0705958E-01	MAX
77.86548	-2.0820079E-01	MIN
78.02109	-2.0597904E-01	MAX
78.11445	-2.0691615E-01	MIN

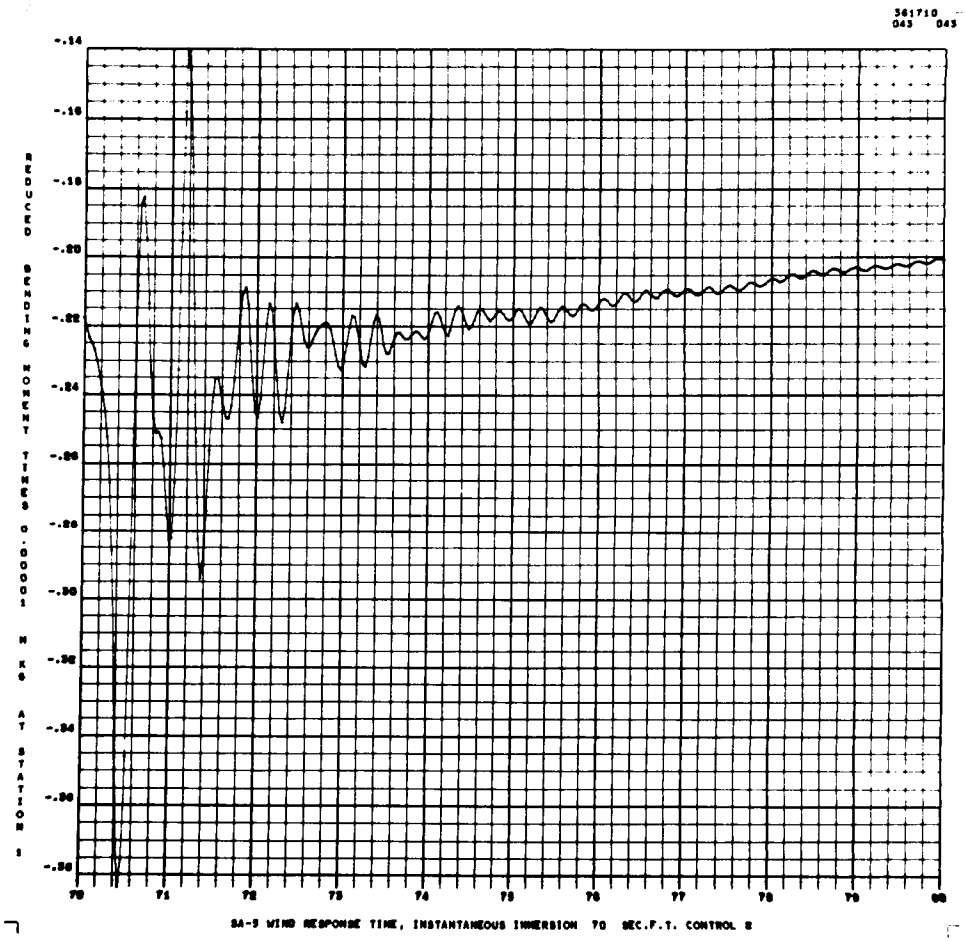

Fig. 52 - Bending Moment Responses at Station 1 to Imbedded Gust Profile Considering Instantaneous Immersion - Attitude Control, 70-sec. Flight Time

SA-5 WIND RESPØNSE TIME, INSTANTANEØUS IMMERSIØN
REDUCED BENDING MØMENT TIMES 0.00001 M KG
AT STATIØN 2 70 SEC.F.T. CØNTRØL 1

70.42749	-3.4879796E 00	MIN
70.58310	-2.1034118E 00	MAX
70.64534	-2.3526193E 00	MIN
70.80095	-8.4582333E-01	MAX
70.95655	-2.1182196E 00	MIN
71.11216	-6.6803829E-01	MAX
71.23664	-1.7369734E 00	MIN
71.36113	-9.8117191E-01	MAX
71.48562	-2.2267943E 00	MIN
71.64122	-1.5543639E 00	MAX
71.70346	-1.5563777E 00	MIN
71.82795	-1.2747088E 00	MAX
71.95243	-1.6170942E 00	MIN
72.04580	-1.1767079E 00	MAX
72.20141	-1.8948567E 00	MIN
72.32589	-1.2515813E 00	MAX
72.45038	-1.8073429E 00	MIN
72.57486	-1.3609325E 00	MAX
72.69935	-1.6995487E 00	MIN
72.79271	-1.5478912E 00	MAX
72.91720	-1.8533456E 00	MIN
73.04168	-1.6079222E 00	MAX
73.16617	-1.9879186E 00	MIN
73.29065	-1.6067462E 00	MAX
73.41514	-1.9738830E 00	MIN
73.53962	-1.6564011E 00	MAX
73.66411	-1.9171325E 00	MIN
73.78859	-1.6805429E 00	MAX
73.91308	-1.8559573E 00	MIN
74.03756	-1.6328745E 00	MAX
74.13093	-1.8304486E 00	MIN
74.25541	-1.5974995E 00	MAX
74.37990	-1.8247362E 00	MIN
74.50438	-1.6186441E 00	MAX
74.62887	-1.8229727E 00	MIN
74.75335	-1.6595852E 00	MAX
74.87784	-1.8353369E 00	MIN
75.00232	-1.6906099E 00	MAX
75.12681	-1.8576642E 00	MIN
75.25129	-1.7034128E 00	MAX
75.37578	-1.8598386E 00	MIN
75.50026	-1.7005389E 00	MAX
75.62475	-1.8327937E 00	MIN
75.74923	-1.6911967E 00	MAX
75.84260	-1.8011625E 00	MIN
75.96708	-1.6769164E 00	MAX
76.09157	-1.7815360E 00	MIN
76.21605	-1.6644996E 00	MAX
76.34054	-1.7755690E 00	MIN
76.46502	-1.6694620E 00	MAX
76.58951	-1.7807726E 00	MIN
76.71399	-1.6897576E 00	MAX
76.83848	-1.7909052E 00	MIN
76.96296	-1.7126989E 00	MAX
77.08745	-1.7988573E 00	MIN
77.18081	-1.7252604E 00	MAX
77.30530	-1.8026108E 00	MIN
77.42978	-1.7267258E 00	MAX
77.55427	-1.7972944E 00	MIN

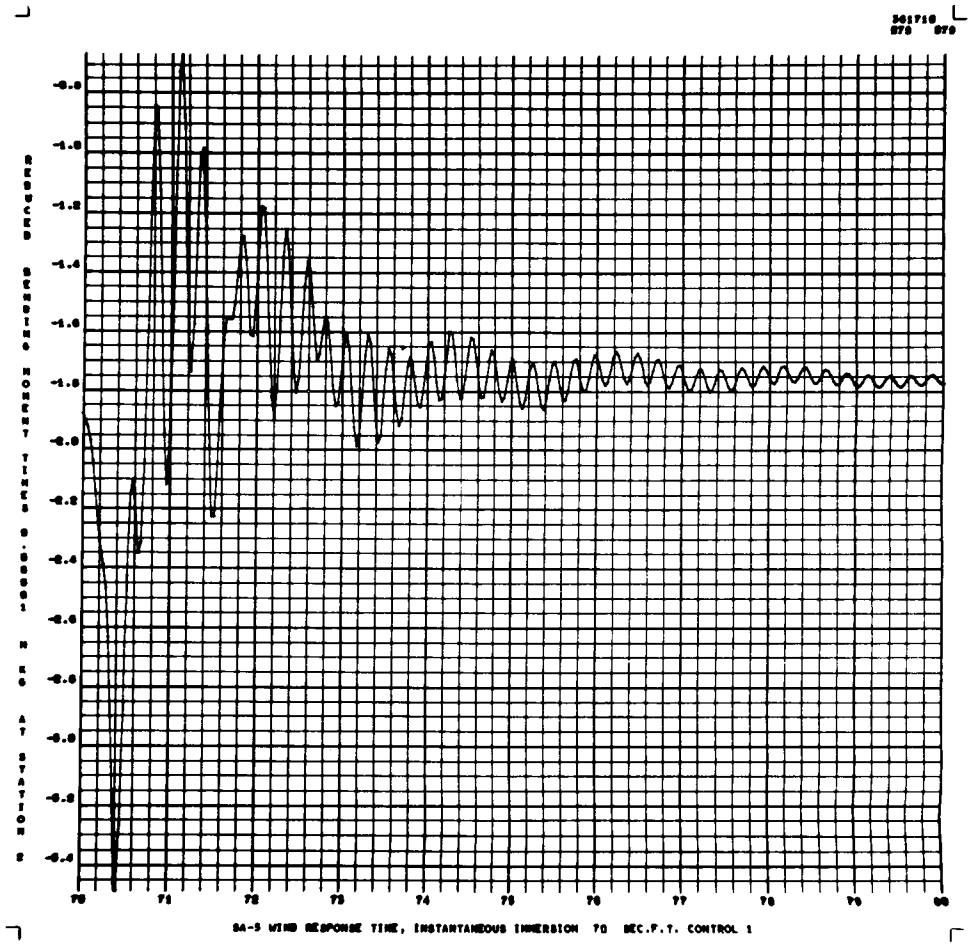

Fig. 53 - Bending Moment Responses at Station 2 to Imbedded Gust Profile Considering Instantaneous Immersion - Angle of Attack Control, 70-sec. Flight Time

SA-5 WIND RESPØNSE TIME, INSTANTANEØUS IMMERSIØN
REDUCED BENDING MØMENT TIMES 0.00001 M KG
AT STATIØN 2 70 SEC.F.T. CØNTRØL 2

70.39637	-2.9431611E 00	MIN
70.52085	-2.6013564E 00	MAX
70.61422	-2.6839399E 00	MIN
70.76983	-2.0954767E 00	MAX
70.92543	-2.5003312E 00	MIN
71.04992	-2.0158048E 00	MAX
71.17440	-2.3017416E 00	MIN
71.29889	-2.0384344E 00	MAX
71.45449	-2.4849847E 00	MIN
71.76571	-2.1529081E 00	MAX
71.89019	-2.2517056E 00	MIN
72.01468	-2.0756557E 00	MAX
72.13916	-2.3061240E 00	MIN
72.29477	-2.0906928E 00	MAX
72.38813	-2.2364959E 00	MIN
72.54374	-2.0734802E 00	MAX
72.63710	-2.1514173E 00	MIN
72.76159	-2.0904119E 00	MAX
72.88607	-2.1781537E 00	MIN
72.97944	-2.0900531E 00	MAX
73.10392	-2.2019485E 00	MIN
73.25953	-2.0745088E 00	MAX
73.38401	-2.1876295E 00	MIN
73.50850	-2.0841804E 00	MAX
73.63299	-2.1659890E 00	MIN
73.72635	-2.0932923E 00	MAX
73.85083	-2.1501057E 00	MIN
73.97532	-2.0681124E 00	MAX
74.09980	-2.1331838E 00	MIN
74.22429	-2.0443504E 00	MAX
74.34877	-2.1186841E 00	MIN
74.47326	-2.0386429E 00	MAX
74.59774	-2.1031111E 00	MIN
74.72223	-2.0411007E 00	MAX
74.81559	-2.0933073E 00	MIN
74.94008	-2.0413553E 00	MAX
75.06456	-2.0953010E 00	MIN
75.18905	-2.0398057E 00	MAX
75.31353	-2.0939474E 00	MIN
75.43802	-2.0364698E 00	MAX
75.56250	-2.0831836E 00	MIN
75.68699	-2.0296701E 00	MAX
75.81148	-2.0669634E 00	MIN
75.93596	-2.0189888E 00	MAX
76.02932	-2.0518159E 00	MIN
76.18493	-2.0066195E 00	MAX
76.27829	-2.0388449E 00	MIN
76.40278	-1.9956099E 00	MAX
76.52727	-2.0284214E 00	MIN
76.65175	-1.9898164E 00	MAX
76.77624	-2.0213929E 00	MIN
76.90072	-1.9874884E 00	MAX
77.02521	-2.0165300E 00	MIN
77.14969	-1.9854451E 00	MAX
77.27418	-2.0111920E 00	MIN
77.39866	-1.9815210E 00	MAX
77.49203	-2.0043893E 00	MIN
77.64763	-1.9748431E 00	MAX
77.74100	-1.9943370E 00	MIN

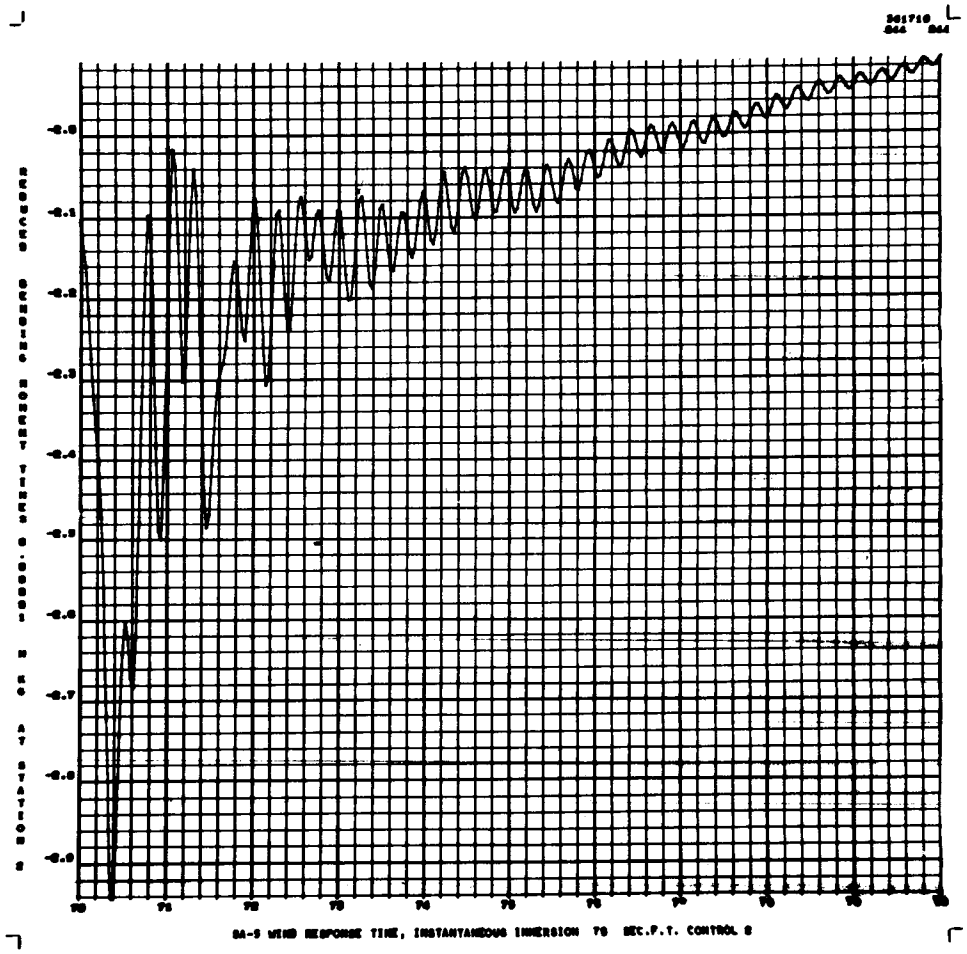

Fig. 54 - Bending Moment Response at Station 2 to Imbedded Gust Profile Considering Instantaneous Immersion - Attitude Control, 70-sec. Flight Time

SA-5 WIND RESPØNSE TIME, INSTANTANEØUS IMMERSIØN
REDUCED BENDING MØMENT TIMES 0.0CC01 M KG
AT STATIØN 3 70 SEC.F.T. CØNTRØL 1

70.20964	-3.0748539E 01	MIN
70.33413	-2.5278736E 01	MAX
70.45861	-2.9916635E 01	MIN
70.58310	-2.3379602E 01	MAX
70.57646	-2.4721602E 01	MIN
71.08104	-1.1414428E 01	MAX
71.20552	-1.5670576E 01	MIN
71.33001	-1.2710509E 01	MAX
71.45449	-1.7461732E 01	MIN
71.57898	-1.1193643E 01	MAX
71.70346	-1.9661595E 01	MIN
71.85907	-1.2324595E 01	MAX
71.98356	-1.6377414E 01	MIN
72.07692	-1.3315151E 01	MAX
72.20141	-1.6003530E 01	MIN
72.29477	-1.4249954E 01	MAX
72.41925	-1.7611075E 01	MIN
72.54374	-1.4486502E 01	MAX
72.69935	-1.9202415E 01	MIN
72.79271	-1.5907770E 01	MAX
72.94832	-2.0145427E 01	MIN
73.04168	-1.7883905E 01	MAX
73.16617	-2.0561507E 01	MIN
73.29065	-1.8766151E 01	MAX
73.41514	-2.0934680E 01	MIN
73.53962	-1.8496604E 01	MAX
73.66411	-2.0851967E 01	MIN
73.78859	-1.8054542E 01	MAX
73.91308	-2.0263413E 01	MIN
74.03756	-1.7824007E 01	MAX
74.16205	-1.9551092E 01	MIN
74.28653	-1.7813957E 01	MAX
74.37990	-1.9368358E 01	MIN
74.50438	-1.7816393E 01	MAX
74.62887	-1.9646389E 01	MIN
74.75335	-1.8084671E 01	MAX
74.87784	-1.9936081E 01	MIN
75.00232	-1.8464556E 01	MAX
75.12681	-2.0026287E 01	MIN
75.25129	-1.8699903E 01	MAX
75.37578	-1.9901507E 01	MIN
75.50026	-1.8639527E 01	MAX
75.59363	-1.9664761E 01	MIN
75.71811	-1.8379536E 01	MAX
75.84260	-1.9352727E 01	MIN
75.96708	-1.8115628E 01	MAX
76.09157	-1.9077101E 01	MIN
76.21605	-1.8026285E 01	MAX
76.34054	-1.8977212E 01	MIN
76.46502	-1.8121243E 01	MAX
76.58951	-1.9068111E 01	MIN
76.71399	-1.8338436E 01	MAX
76.83848	-1.9240551E 01	MIN
76.93184	-1.8565509E 01	MAX
77.08745	-1.9355809E 01	MIN
77.18081	-1.8704393E 01	MAX
77.30530	-1.9387841E 01	MIN
77.42978	-1.8720494E 01	MAX
77.55427	-1.9309718E 01	MIN

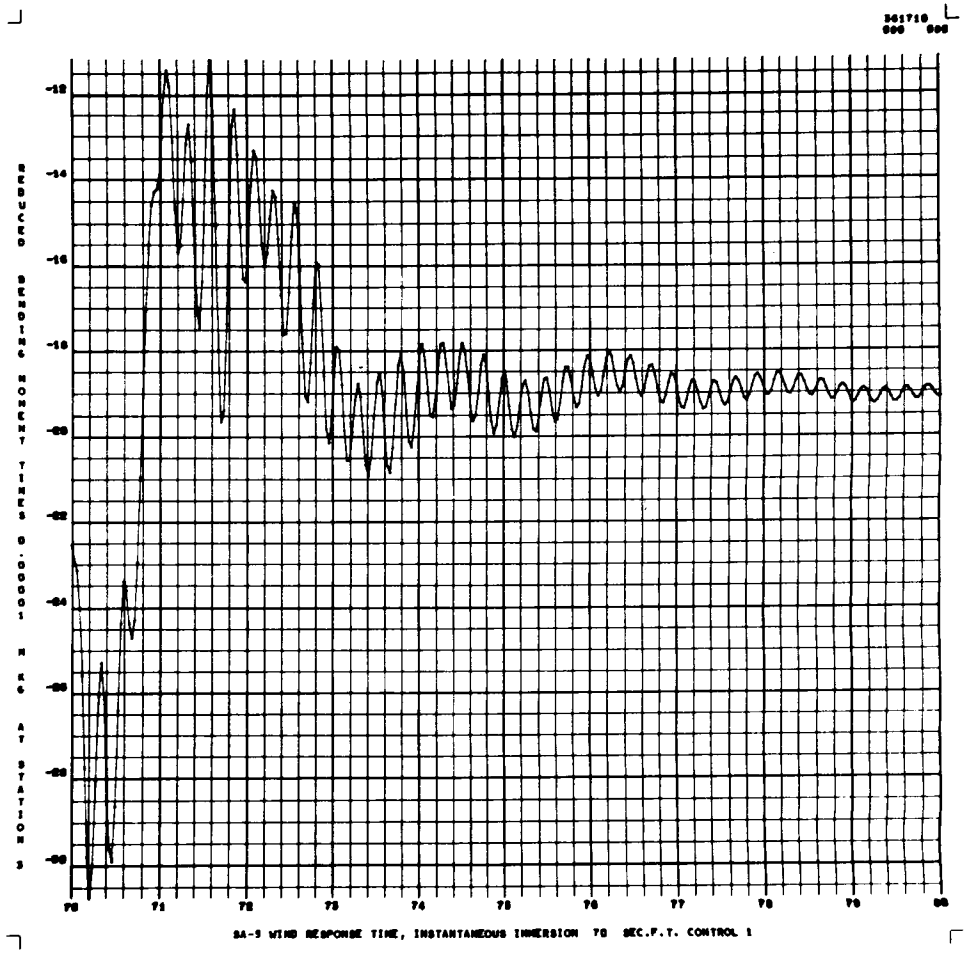

Fig. 55 - Bending Moment Response at Station 3 to Imbedded Gust Profile Considering Instantaneous Immersion - Angle of Attack Control, 70-sec. Flight Time

SA-5 WIND RESPØNSE TIME, INSTANTANEØUS IMMERSIØN
REDUCED BENDING MØMENT TIMES 0.00001 M KG
AT STATIØN 3 70 SEC.F.T. CØNTRØL 2

70.17852	-2.6601658E 01	MIN
70.27188	-2.5925858E 01	MAX
70.42749	-2.8526698E 01	MIN
70.52085	-2.7288475E 01	MAX
70.64534	-2.8127178E 01	MIN
71.04992	-2.3861275E 01	MAX
71.17440	-2.5119956E 01	MIN
71.26777	-2.4127867E 01	MAX
71.39225	-2.5473010E 01	MIN
71.51674	-2.3251422E 01	MAX
71.67234	-2.5962265E 01	MIN
71.79683	-2.3470490E 01	MAX
71.92131	-2.4445035E 01	MIN
72.04580	-2.3192128E 01	MAX
72.13916	-2.3762547E 01	MIN
72.26365	-2.2917762E 01	MAX
72.38813	-2.3781500E 01	MIN
72.51262	-2.2392502E 01	MAX
72.63710	-2.3669461E 01	MIN
72.76159	-2.2264484E 01	MAX
72.88607	-2.3447516E 01	MIN
73.01056	-2.2569113E 01	MAX
73.13504	-2.3382169E 01	MIN
73.22841	-2.2746877E 01	MAX
73.35289	-2.3414355E 01	MIN
73.47738	-2.2591081E 01	MAX
73.60186	-2.3388520E 01	MIN
73.72635	-2.2451470E 01	MAX
73.85083	-2.3179031E 01	MIN
73.97532	-2.2332545E 01	MAX
74.09980	-2.2875472E 01	MIN
74.22429	-2.2184748E 01	MAX
74.34877	-2.2659856E 01	MIN
74.47326	-2.2067478E 01	MAX
74.56662	-2.2591017E 01	MIN
74.69111	-2.2020607E 01	MAX
74.81559	-2.2569885E 01	MIN
74.94008	-2.2047049E 01	MAX
75.06456	-2.2548532E 01	MIN
75.18905	-2.2081534E 01	MAX
75.31353	-2.2509691E 01	MIN
75.43802	-2.2048954E 01	MAX
75.56250	-2.2418005E 01	MIN
75.68699	-2.1940549E 01	MAX
75.78035	-2.2265196E 01	MIN
75.93596	-2.1800801E 01	MAX
76.02932	-2.2093844E 01	MIN
76.18493	-2.1673573E 01	MAX
76.27829	-2.1938791E 01	MIN
76.40278	-2.1563649E 01	MAX
76.52727	-2.1834147E 01	MIN
76.65175	-2.1496572E 01	MAX
76.77624	-2.1774981E 01	MIN
76.90072	-2.1469887E 01	MAX
77.02521	-2.1730539E 01	MIN
77.14969	-2.1451772E 01	MAX
77.24306	-2.1671754E 01	MIN
77.39866	-2.1409017E 01	MAX
77.49203	-2.1596550E 01	MIN

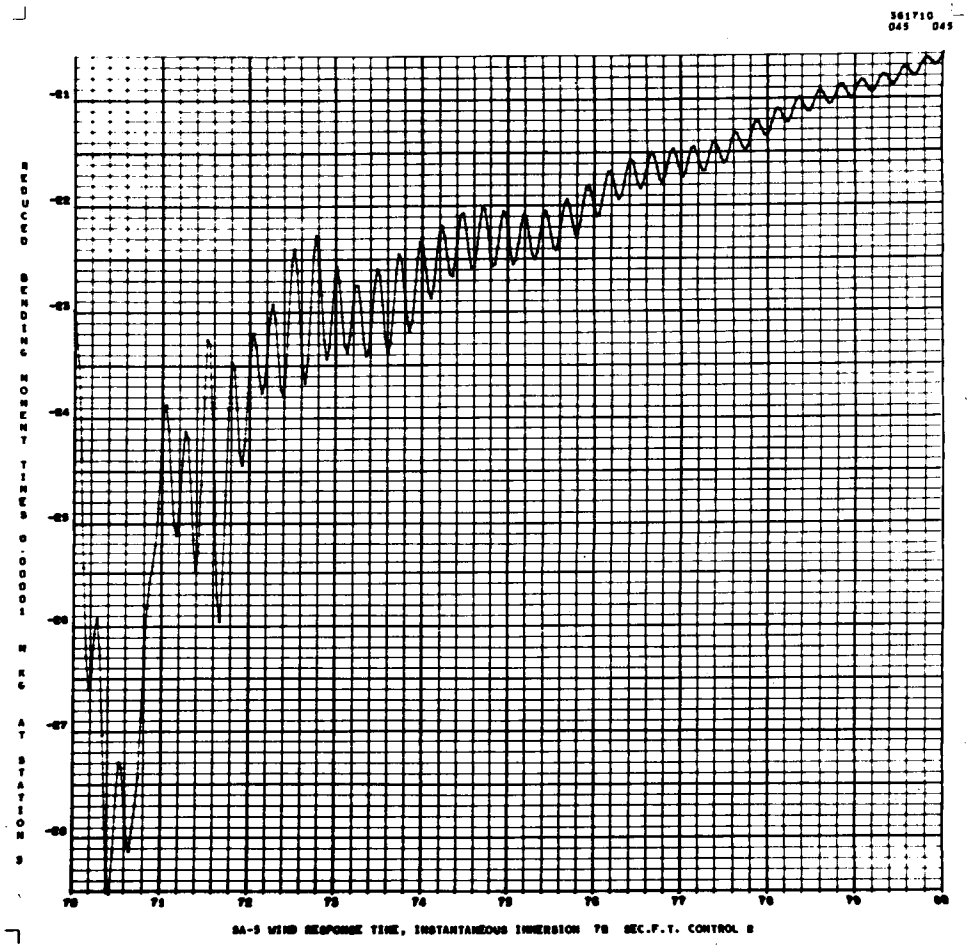

Fig. 56 - Bending Moment Response at Station 3 to Imbedded Gust Profile Considering Instantaneous Immersion - Attitude Control, 70-sec. Flight Time

The results presented here substantiate the fact that the differences and similarities observed in the impulsive responses can be used with sufficient success to predict the effects of penetration and lift growth.

The three aerodynamic representations yield basically similar responses to the impulsive wind. The most noticeable differences occur during the highly oscillatory response shortly after immersion in the gust.

The following refers to Figs. 13 - 27 which contain responses at 70 sec. using the angle of attack control. For the first three bending mode responses, pure penetration (PP) and penetration with lift growth (PWLG) representation yield moderately smaller oscillatory excursions than instantaneous immersion (II). These differences range from 15 to 23 percent of the excursion amplitude. For the fourth bending response PWLG yields slightly larger oscillatory excursions (9 to 13 percent of excursion amplitude) than II and PP. For control deflection, both PP and PWLG yield slightly larger oscillations (11 percent of excursion amplitude). The effects of penetration on rotation, local angle of attack,* and the two sloshing modes produce smaller oscillatory excursions than II (5 percent or less of excursion amplitude). The above differences for the three aerodynamic representations are generally less for the 80-sec. flight time condition.

The effects and importance of the aerodynamic representation upon responses will now be discussed in terms of the wind-induced responses. Samples of the 70-sec. wind-induced responses to the Sinusoidal Gust Criteria are shown in Figs. 29 through 43 for the three aerodynamic representations. These particular responses are driven by the second bending frequency. The general behavior** of these responses is very similar to those obtained for the other driving frequencies and flight time.

---

* The local angle of attack referred to is that at the top of the escape tower.

** All of the sinusoidal responses are bounded for the frequencies of excitation considered. When the system is driven at the fourth bending frequency, the maximum response values of second, third and fourth bending modes and control deflection occur near the end of the response record. The influence of fourth bending excitation on the system is extensive because of the extremely low damping of fourth bending (-0.3338 rad/sec and -0.1593 rad/sec for the 70- and 80-sec. flight time condition, respectively). Thus, the effect of fourth bending propagates throughout the system before it damps out. Consequently, the validity of the response values obtained from fourth bending frequency excitation is questioned for the 70- and expecially 80-sec. flight times because of the low fourth bending damping.

The same types of differences and similarities observed in the impulsive responses occur here also. Ratios of values of observed maximum responses to the Sinusoidal Gust Criteria are presented in Table II for the 70 and 80-sec. flight times. The penetration with lift growth results are used as a reference in forming the ratios since this representation is the most accurate. The maximum response values resulting from penetration with lift growth considerations are given in Table III.

It is seen in Table II that the maximum responses of bending and control deflection are the modes most significantly affected by the inclusion of penetration and lift growth effects. The amount of conservativeness and unconservativeness of instantaneous immersion on these modes depends upon the driving frequency. In general, instantaneous immersion is conservative for the first three bending modes and unconservative for the fourth bending mode and control deflection. The largest difference between instantaneous immersion and penetration with lift growth, occurs for that mode being driven by its natural frequency.

The difference between pure penetration and penetration with lift growth is seen to be larger for the higher bending modes and also the control deflection. Pure penetration is unconservative for third and fourth bending by 3.2 to 10.0 percent. For control deflection, pure penetration effects range from being unconservative by 14.6 percent to being conservative by 1.0 percent.

It is seen, also, from Table II that the differences in maximum responses for rotation, first and second sloshing and local angle of attack for the aerodynamic representations do not appear significant in an engineering sense. Rotation evaluated with instantaneous immersion considerations is unconservative (small compared to penetration with lift growth) by 0.01 to 3.0 percent; first sloshing with instantaneous immersion is conservative by 1.8 to 4.1 percent; second sloshing with instantaneous immersion is conservative by 1.3 to 4.1 percent; and local angle of attack with instantaneous immersion is unconservative by 0.1 to 0.5 percent.

It is felt that the significant differences between responses calculated with and without penetration can be directly attributed to the inclusion of third and fourth bending and the fins and engine shrouds into the analysis. This is substantiated by the fact that the response study in [1], in which third and fourth bending and fin-shroud effects were neglected, showed the instantaneous immersion representation to be conservative by less than 5 percent. This small difference was considered insignificant in an engineering sense.

The differences between responses calculated with and without penetration are seen, in general, to diminish with increasing flight time.

TABLE II

RATIOS OF OBSERVED MAXIMUM RESPONSES TO SINUSOIDAL GUST CRITERIA*

Flight Time	Driving Frequency	Ratio	Rotation ϕ	1st Bend η_1	2nd Bend η_2	3rd Bend η_3	4th Bend η_4	1st Slosh ξ_1	2nd Slosh ξ_2	Control β_C	Local Angle of Attack α_L
	ω_1 (λ = 305.8 m, A = 11.6 m/sec)	II/PWLG	0.9710	1.1260+	1.0400	1.0511	1.0303	1.0320	1.0250	0.9530	0.9987
		PP/PWLG	1.0303	0.9906+	0.9916	0.9881	0.9683	0.9911	0.9870	0.8735	0.9972
70	ω_2 (λ = 190.2 m, A = 8.6 m/sec)	II/PWLG	0.9705	1.0379	1.2447+	1.1778	0.9840	1.0379	1.0134	0.9481	0.9988
		PP/PWLG	1.0304**	0.9827	0.9981	0.9696	0.9429	0.9907	0.9846	0.8738	0.9972
	ω_3 (λ = 127.1 m, A = 6.5 m/sec)	II/PWLG	0.9699	1.0366	1.0377	1.2573+	1.1568+	1.0177	1.0166	1.0865	0.9988
		PP/PWLG	1.0304+	0.9821	0.9917	0.9016+	0.9005+	0.9875	0.9840	0.8730	0.9971
	ω_4 (λ = 97.8 m, A = 5.4 m/sec)	II/PWLG	0.9704	1.0355	0.9420**	0.8590**	0.8150**	1.0216	1.0207	0.8730+	0.9989
		PP/PWLG	1.0335**	0.9818	0.9611**	0.9299**	0.9165**	0.9876	0.9848	0.8541+	0.9972
--	ω_1 (λ = 399.5 m, A = 13.5 m/sec)	II/PWLG	0.9994	1.0597+	1.0522	1.0551	0.9744	1.0383	1.0360	0.9334	0.9953
		PP/PWLG	1.0009	1.0003+	0.9534	0.9653	1.0059	0.9771	0.9740	1.0050	1.0019
80	ω_2 (λ = 247.8 m, A = 10.2 m/sec)	II/PWLG	0.9992	1.0197	1.1705	1.1833	1.0002	1.0412	1.0260	0.9302	0.9954
		PP/PWLG	1.0008	0.9960	0.9770+	0.9948	1.0001	0.9769	0.9716	1.0042	1.0019
	ω_3 (λ = 163.1 m, A = 7.7 m/sec)	II/PWLG	0.9991	1.0193	1.0500	1.4131+	1.2606+	1.0403	1.0387	0.9686	0.9955
		PP/PWLG	1.0009	0.9958	0.9539	1.0436+	1.0183+	0.9754	0.9742	1.0103	1.0020
	ω_4 (λ = 124.1 m, A = 6.4 m/sec)	II/PWLG	0.9992	1.0188	1.0741**	1.0963**	1.0872**	1.0403	1.0410	1.0793**	0.9954
		PP/PWLG	1.0007	0.9957	0.9207**	0.9090**	0.9078**	0.9755	0.9738	0.9187**	1.0020

\+ Denotes the maximum response occurred between 75 and 79 or 85 and 89 sec.

* Some of the larger percent values presented are associated with maximum responses occurring near the end of the response record (80 or 90-sec. flight times). There might be some question about the validity of these maximum response values. It is suggested in 6 that the sinusoidal phase of the wind profile should extend only for a discrete number of cycles. If this recommendation were explicitly followed a number of maximum responses would be missed. The sinusoidal results given in this report are obtained by assuming the sinusoidal phase of the profile extends to the end of the flight time band.

** Denotes the maximum response occurred at the end of the flight time band.

TABLE III

MAXIMUM PENETRATION WITH LIFT GROWTH WIND-INDUCED RESPONSE VALUES RESULTING FROM SINUSOIDAL GUST CRITERIA

Flight Time (sec.)	Driving Frequency	Rotation ϕ (Deg.)	1st Bend η_1 (m)	2nd Bend η_2 (m)	3rd Bend η_3 (m)	4th Bend η_4 (m)	1st Slosh ξ_2 (m)	2nd Slosh ξ_2 (m)	Control βc (Deg.)	Local Angle of Attack α_L (Deg.)
70	ω_1	-3.5960	4.4418×10^{-2}	1.1934×10^{-2}	0.4756×10^{-2}	0.1150×10^{-2}	-1.8323×10^{-1}	-1.7130×10^{-1}	0.9169	9.1013
	ω_2	-3.5868	4.1279×10^{-2}	1.1739×10^{-2}	0.4984×10^{-2}	0.1374×10^{-2}	-1.7209×10^{-1}	-1.6287×10^{-1}	0.9188	8.9216
	ω_3	-3.5858	3.9819×10^{-2}	1.1470×10^{-2}	1.2031×10^{-2}	0.2971×10^{-2}	-1.7437×10^{-1}	-1.6368×10^{-1}	0.9026	8.7835
	ω_4	-3.5857	3.9129×10^{-2}	1.4474×10^{-2}	1.7868×10^{-2}	1.8743×10^{-2}	-1.7408×10^{-1}	-1.6216×10^{-1}	2.4796	8.7155
--										
80	ω_1	-2.7672	3.9181×10^{-2}	0.9722×10^{-2}	0.4151×10^{-2}	0.1305×10^{-2}	-1.6180×10^{-1}	-1.5204×10^{-1}	1.1822	7.1069
	ω_2	-2.7579	3.4213×10^{-2}	1.0715×10^{-2}	0.4415×10^{-2}	0.1475×10^{-2}	-1.4978×10^{-1}	-1.4242×10^{-1}	1.1828	6.9578
	ω_3	-2.7558	3.2864×10^{-2}	0.9301×10^{-2}	1.1517×10^{-2}	0.3654×10^{-2}	-1.5177×10^{-1}	-1.4372×10^{-1}	1.2406	6.8290
	ω_4	-2.7568	3.2169×10^{-2}	1.3882×10^{-2}	2.3305×10^{-2}	2.7110×10^{-2}	-1.5096×10^{-1}	-1.4174×10^{-1}	3.3933	6.7668

This would be expected since with higher speeds the penetration requires less time and thus approaches instantaneous immersion.

The import of penetration effects on the steady-state oscillatory portion of the wind-induced responses will now be discussed.

2. Steady-state responses: The comparisons of the steady sinusoidal responses from the three aerodynamic representations are made using two measures of the response. The measures are obtained from a single set of adjunct maximum and minimum values for each response. These values are differenced to obtain a local excursion* and averaged to obtain a local average response. The adjunct response values for each response are taken from a common response time for each flight time band (approximately 79 and 89 sec.). Ratios of local average response and local excursion were formed for each response using the penetration with lift growth results as a reference. These values are not reproduced here, but simply summarized in the following.

The results indicated that the local average responses (except control deflection) were insignificantly affected by the inclusion of penetration and lift growth effects. Responses, other than control deflection, computed from instantaneous immersion generally were conservative by not more than 5 percent. Instantaneous immersion for control deflection was conservative by about 50 percent.

The local excursion of the responses (except local angle of attack) was significantly affected by the aerodynamic representation. Instantaneous immersion results were generally conservative by between 20 and 50 percent when the system was driven by the first, second and third bending frequencies. However, when fourth bending frequency was impressed on the system, instantaneous immersion was unconservative by about 20 percent. The local excursion of the local angle of attack was not affected appreciably by the aerodynamic representations.

* In [1], a more formal analytical method was used to investigate the aerodynamic representation effect on responses to two actual wind profiles. Only general qualitative results, however, are sought from the steady-state sinusoidal responses in this present investigation.

In summary, the steady-state local average responses, except control deflection, were independent of the aerodynamic representation.* The excursions from the local average, except for local angle of attack, are primarily affected by penetration effects. The effects of penetration on the excursions were seen to diminish with increasing flight time.

B. Phase II

In this phase the wind-induced responses of both the generalized coordinates and bending moments were used in investigating the influence of methods of control on vehicle responses and load alleviation when gust penetration effects are considered. Responses to NASA's Imbedded Gust Criteria were compared for two aerodynamic considerations: instantaneous immersion (II) and pure penetration (PP). The pure penetration responses were used as the basis of comparison since they are the more accurate of the two sets. Two types of vehicle control systems were investigated: (1) angle of attack and (2) attitude. The angle of attack control will be denoted as type I control, the attitude control as type II. These are referred to as "Control 1" and "Control 2," respectively, in the response figures.

To supplement the understanding of the fin and engine shroud effects on the responses, supplementary computations were made for the 70-sec. flight time condition. The empennage effects were omitted in these additional calculations, but the influences of third and fourth bending modes were retained.

The response of the generalized coordinates to the Imbedded Gust Criteria will be discussed first, followed by the presentation of the bending moment responses.

1. Generalized coordinate responses: The responses of the generalized coordinates to the Imbedded Gust Criteria were computed, plotted and analyzed. The most pertinent results, which are the maximum response values, are given in Tables IV and V. The plots themselves are not reproduced here since no useful purpose would be served. Certain general trends were noted, however, which will be mentioned before proceeding to the tables of maximums.

---

* In [1], the local average responses to actual winds were suggested as being independent of aerodynamic representation if the corresponding impulsive responses exhibited a long, slow approach toward steady-state values. The local average values of the wind-induced responses, in this case, depend largely on this long tail and the history of wind inputs. It is believed that it is this same situation that governs the local average values of the steady state oscillations.

TABLE IV

MAXIMUM PURE PENETRATION WIND-INDUCED RESPONSES RESULTING FROM IMBEDDED GUST CRITERIA

Flight Time (sec.)	Type of Control	Rotation ϕ (Deg)	1st Bend η_1 (m)	2nd Bend η_2 (m)	3rd Bend η_3 (m)	4th Bend η_4 (m)	1st Slosh ξ_1 (m)	2nd Slosh ξ_2 (m)	Control β_C (Deg)	Local Angle of Attack, α_L Station 1 (Deg)	Station 2 (Deg)	Station 3 (Deg)
	I	-3.7809	4.6404×10^{-2}	1.2889×10^{-2}	5.8801×10^{-3}	2.0617×10^{-3}	-2.0730×10^{-1}	-1.9433×10^{-1}	1.0965	9.3592	9.3256	9.1598
	II	0.3715	4.7494×10^{-2}	1.3294×10^{-2}	5.5107×10^{-3}	1.5006×10^{-3}	-2.2145×10^{-1}	-2.1670×10^{-1}	0.4898	10.7603	10.7611	10.7724
70	I*	-2.0834	4.6701×10^{-2}	1.3330×10^{-2}	6.1533×10^{-3}	2.0498×10^{-3}	-1.9140×10^{-1}	-1.8838×10^{-1}	2.9596	9.9639	9.9424	9.8317
	II*	2.0852	4.7692×10^{-2}	1.4140×10^{-2}	6.0014×10^{-3}	1.4057×10^{-3}	-2.5316×10^{-1}	-2.2428×10^{-1}	3.2370	11.4238	11.4550	11.5417
--	I	-2.8040	3.7899×10^{-2}	1.0065×10^{-2}	4.8958×10^{-3}	2.0108×10^{-3}	-1.7638×10^{-1}	-1.6567×10^{-1}	1.4185	7.2508	7.2293	7.1210
80	II	0.7148	3.9142×10^{-2}	1.0093×10^{-2}	4.7645×10^{-3}	1.6019×10^{-3}	-1.9384×10^{-1}	-1.8673×10^{-1}	1.0741	8.7642	8.7726	8.7962

* Effects of fins and shrouds neglected.

TABLE V

RATIOS (II/PP) OF OBSERVED MAXIMUM RESPONSES TO IMBEDDED GUST CRITERIA

Flight Time	Type of Control	Rotation ϕ	1st Bend η_1	2nd Bend η_2	3rd Bend η_3	4th Bend η_4	1st Slosh ξ_1	2nd Slosh ξ_2	Control β_C	Local Angle of Attack, α_L		
										Station 1	Station 2	Station 3
	I	0.9422	1.0450	1.0779	1.0937	0.9982	1.0221	1.0254	1.0026	1.0031	1.0049	1.0157
	II	1.3274	0.9987	1.0237	0.9779	1.0287	0.9160	0.9537	1.6405	1.0001	1.0003	1.0003
7												
0	I*	0.9674	1.0492	1.0480	1.0541	1.0126	1.0555	1.0569	1.0378	1.0012	1.0025	1.0105
	II*	1.0222	1.0316	1.0177	0.9966	1.0180	1.0225	1.0201	1.0245	1.0005	0.9992	0.9971
--												
	I	0.9985	1.0201	1.1202	1.1854	1.0228	1.0551	1.0581	0.9118	0.9951	0.9966	1.0054
8												
0	II	0.9728	0.9901	1.0725	1.1436	0.9709	0.9647	0.9902	1.0300	0.9929	0.9925	0.9920

* Effects of fins and shrouds neglected.

All of the responses to the Imbedded Gust Criteria are bounded. Larger response excursions were noted for the type I control than for type II. This was particularly true in the vicinity of the imbedded gust. The excursion magnitudes of the type I responses, however, were seen to diminish as the steady-state responses were approached. The smaller type II control response excursions were expected since this control system does not contain the angle of attack feedback term.

Several observations regarding the effects of control type upon maximum responses can be drawn from Table IV. These values were obtained using pure penetration aerodynamic considerations. When the effects of fins and engine shrouds are included, the maximum responses of rotation, third and fourth bending and control deflection are smaller for the type II control. Using the type I control responses as the basis for comparisons (see Table IV and both flight times), the type II response for rotation (absolute value) is smaller by approximately 75 to 90 percent; third bending is smaller by about 3 to 6 percent; fourth bending is smaller by about 20 to 25 percent; and control deflection is smaller by about 24 to 55 percent. The remaining responses are generally larger for the type II control. First and second bending are, however, about the same for the two types of control. The sloshing displacements and local angle of attack values are approximately 6 to 24 percent larger for the type II control.

It is interesting to note that almost all the type II control responses are larger than the type I when the effects of fins and engine shrouds are neglected. The only exception is fourth bending which is about 30 percent smaller. Also, control deflections are 8 to 10 percent larger; while the local angle of attack values are about 15 to 18 percent larger.

It is difficult to draw quantitative conclusions from Table V about the effects of aerodynamic representation because of the lack of consistent trends between control types and flight times. Several qualitative observations, however, are possible.

a. Instantaneous immersion maximum responses are generally conservative (larger than pure penetration) for both types of control. The amount of conservativeness of instantaneous immersion is, in most instances, larger for the type I control responses than the type II control (with the exception of the 70-sec. rotation and control deflection values).

b. Those responses most significantly affected by instantaneous immersion are: rotation, second and third bending and control deflection.*

c. The local angle of attack at the three station locations is insignificantly affected by the inclusion of penetration effects.

There are a few entries in Table IV where instantaneous immersion is unconservative by between 5.8 to 8.8 percent: rotation (type I control, 70 sec.), first sloshing (type II control, 70 sec.), and control deflection (type I control, 80 sec.). The reason why rotation for the type II control at 70 sec. is significantly affected by instantaneous immersion (32.7 percent) might be explained by the fact that control deflection for these conditons is also affected (64.1 percent). These two coordinate responses are strongly related for the type II control. The conservativeness of instantaneous immersion for second and third bending might be explained in terms of the relationship of their respective natural wavelengths to the wavelength of the imbedded gust. The wavelength of second and third bending are approximately 190 m and 127 m, respectively; the half wavelength of the imbedded gust is 150 m. Thus there appears the possibility of the imbedded gust exciting these two bending modes, especially when instantaneous immersion is considered.

The 70-sec. type I control responses computed without the effects of fins and engine shrouds are mildly affected by the inclusion of penetration effects. The corresponding type II control responses are insignificantly affected. Thus, it appears the significant effects of instantaneous immersion, especially for the rotation, second and third bending and control deflection, are mainly due to the fin and engine shroud effects.

The effects of control type and aerodynamic representation upon maximum bending moment responses will now be discussed.

---

* The conservativeness of instantaneous immersion for second and third bending and control deflection can also be seen from the impulsive responses of these coordinates. The instantaneous immersion excursions are significantly larger than the pure penetration, particularly just after immersion into the gust.

2. Bending moment responses: Plots of the 70-sec. wind-induced bending moment responses to the Imbedded Gust Criteria are presented in Figs. 45 through 56 for the three vehicle station locations.* These responses were computed using the reduced bending moment expression (3). For each station location, the first figure evolves from the angle of attack control system (type I control noted as "Control 1"), while the second figure evolves from the attitude control system (type II control noted as "Control 2"). The pure penetration results are given first in Figs. 45 through 50. All bending moment figures shown contain the influence of the fins and engine shrouds.

All the bending moment plots have about the same general character. They exhibit a maximum response peak close to the time of application of the imbedded gust (see Fig. 59) and then a damped oscillatory response approaching steady-state conditions The high frequency oscillation during decay toward steady-state is due mainly to the fourth bending mode frequency of the system.

The estimation of the effects of control type and importance of penetration on the bending moment response will be discussed in terms of the maximum responses. The effects of the types of control upon the maximum bending moment can be seen from Table VI.** Larger maximum bending moment values*** result from the type I control than from the type II control.

---

* The three station locations, x_k , (measured aft from the top of the escape tower) are:
Station 1 - Located at the base of the command module (x_k = 12 m)
Station 2 - Located at the base of the instrument unit (x_k = 25 m), and
Station 3 - Located near the midpoint of the LOX tank of the S-1C stage (x_k = 76.2 m).

** The negative sign of the bending moment values in Table VI denotes it is a counterclockwise moment as viewed in Fig. 57 (see p. 86).

*** A small amount of numerical difficulty was encountered in the evaluation of the pure penetration $M_{GUST}(x_k,\tau)$ term (see III-24 and III-25). This was discovered in comparing the steady-state pure penetration $M_{GUST}(x_k,\tau)$ with the corresponding instantaneous immersion term. In this comparison, the two results should be numerically identical. However, the pure penetration term was 3 to 5 percent lower than the instantaneous immersion term. It was therefore possible to correct the PP maximum bending moment response when the maximum response occurred at a time of steady-state $M_{GUST}(x_k,\tau)$. All of the numbers in Tables VI and VII that are not marked with (**) have been corrected with the instantaneous immersion values of $M_{GUST}(x_k,\tau)$. The remaining numbers could not be corrected since the maximum bending moment values occurred when the PP $M_{GUST}(x_k,\tau)$ was not at its steady-state value. It is felt, however, that those (**) values are only slightly different than they should be.

TABLE VI

PURE PENETRATION MAXIMUM REDUCED BENDING MOMENT RESPONSES AND RATIOS (II/PP) OF MAXIMUM REDUCED BENDING MOMENT AT THREE STATION LOCATIONS

Flight Time (sec.)	Type of Control	Pure Penetration Maximum Reduced Bending Moment (kg - m)			Ratio of Maximum Reduced Bending Moment (II/PP)		
		Station 1	Station 2	Station 3	Station 1	Station 2	Station 3
70	I	-4.4691×10^4	-3.1742×10^5	-2.8765×10^6	1.1542	1.0989	1.0689
	II	-3.4036×10^4**	-2.8671×10^5	-2.7846×10^6	1.1267**	1.0265	1.0244
	I*	-4.6250×10^4	-3.3083×10^5	-2.9286×10^6	1.0263	1.0246	1.0371
	II*	-3.0206×10^4	-2.7035×10^5	-3.0309×10^6**	1.0633	1.0315	0.9991**
80	I	-3.8960×10^4	-2.7155×10^5	-2.3262×10^6	1.0992	1.0386	1.0308
	II	-2.7392×10^4**	-2.4866×10^5**	-2.4058×10^6**	1.1294**	0.9632**	0.9419**

* Effects of fins and shrouds neglected.
** Slightly inaccurate (see text).

TABLE VII

VALUES OF THE RATIO, R

Flight Time (sec.)	Type of Control	Aero Rep.	R Station 1	R Station 2	R Station 3
	I	II	1.1987	0.5201	0.2112
		PP	0.9685	0.4469	0.2092
	II	II	0.4567	0.1801	0.0545
7		PP	0.2907**	0.1628	0.0580
0					
	I*	II	0.9174	0.4105	0.1441
		PP	0.9055	0.4095	0.1425
	II*	II	0.1708	0.0512	0.0241
		PP	0.1041	0.0258	0.0215**
--					
	I	II	1.2767	0.5133	0.2287
		PP	1.0356	0.4622	0.1487
8					
0	II	II	0.4011	0.1502	0.0503
		PP	0.2745**	0.1163**	0.0477**

* Effects of fins and shrouds neglected.
** Slightly inaccurate (see text).

When fins and engine shrouds are included, these values range from about 30 to 60 percent at station 1 to about 3 to 8 percent for station 3, depending on the aerodynamic representation used. When the empennage effects are neglected the range is from about 50 percent at station 1 to less than 3 percent at station 3.

To investigate the effect of penetration on bending moment response, ratios (II/PP) of observed maximum bending moment responses to the Imbedded Gust Criteria were formed. These values are presented in Table VI. Results pertaining to calculations without fin and engine shroud effects, but including third and fourth bending mode influence are shown also.

From Table VI it can be seen that instantaneous immersion results are conservative. The amount of conservativeness is largest at station 1 (10 to 15.4 percent when fin and engine shrouds are included). The conservativeness of instantaneous immersion decreases with increasing distance from the top of the vehicle. At station 3, II effects are conservative by only 2.4 to 6.9 percent. Also, II effects are less conservative for the type II control than for type I control.

When the fins and engine shrouds are neglected instantaneous immersion and pure penetration influence upon maximum bending moment responses are approximately equal. For this case II is slightly more conservative for the type II control than the type I control.

Even though instantaneous immersion effects are largest at station 1, the magnitude of the maximum bending moment at station 1 is considerably less than that at station 3. The results indicate that a slight relaxation can be made upon the vehicle design requirements if the designs are based on instantaneous immersion aerodynamics.

A subsidiary analysis was performed to provide insight into the contributing factors of the conservativeness of instantaneous immersion for the maximum bending moment responses at station 1. The ratio* (R) of elastic body bending moment to rigid body bending moment was computed from the following {see (3)}:

$$R = \frac{\sum_{i=1}^{4} M'_{\ddot{\eta}_i}(x_k)\ddot{\eta}_i(t)}{M_{GUST}(x_k,t) + M'_{\alpha}(x_k)\alpha(t) + M'_{\beta_C}(x_k)\,\beta_C} \tag{5}$$

* This same ratio was used in [2] to investigate the effects of accelerometer control gain on vehicle bending dynamics.

Two salient results can be extracted from (5):

1. It permits an appraisal of the relative importance of the bending mode dynamics (or bending mode inertia effects) on the loads at the various vehicle stations for each type of control. (A ratio value of unity means that the bending dynamics contribute half of the load.)

2. It yields a quantitative estimation of penetration effects upon bending dynamics, provided penetration effects upon the rigid body moment are known.

Values of R for each station location and aerodynamic representation are presented in Table VII. These ratios were formed at the time of maximum bending moment response.

It can be seen that the bending mode dynamics for the type I control are a significant part of the maximum bending moment at station 1. This is also true to a lesser extent for the type II control responses. The influence of bending mode dynamics on the load at station 3 is considerably smaller than at station 1. Here again, the effects of bending mode dynamics are much less for the type II control than the type I. The ratio values at station 3 indicate that rigid body effects are the dominant part of the maximum bending moment at this station.

For each station location, the aerodynamic representations yield almost identical results for the rigid body moment. Instantaneous immersion results are conservative by, at most, about 6 percent. The largest difference between the R values for the two aerodynamic representations occurs at station 1. This indicates that penetration effects have a greater tendency to reduce the bending mode dynamics (and consequently, the total load) at those stations significantly affected by bending dynamics. This reduction in dynamic effects possibly occurs through cancellation from the higher bending modes.

V. SUPPLEMENTARY DISCUSSION OF BENDING MOMENT COMPUTATION

The values of the maximum bending moment responses given in this report account for the actual phasing effect of the various components which make up the reduced bending moment expression. To compute the bending moment trace over a long response time requires rather large blocks of computer time.* The computer time becomes exorbitant if the bending moment responses at numerous station locations are desired.

* An average of 0.75 hr. of IBM 7094 was required to compute a 10-sec. response trace of the three bending moment expressions for both aerodynamic representations.

A procedure was tested to determine if computer time could be reduced, without sacrificing numerical accuracy, by neglecting the phase between components of the bending moment expression. Sample calculations of the maximum bending moment were obtained for the 70 sec. type I and II control by summing the maximum value of each component. These calculations were made using the reduced bending moment expression see (3). The maximum bending moments computed by neglecting the phasing were generally less than the actual values. This was caused by one of the dominant bending mode terms being of opposite sign from the maximum bending moment value. Less error was noted for the type I control responses. Considerable improvement was achieved by reversing the sign of one of the dominant bending mode contributions. This, however, requires a judicious treatment of the bending mode terms. It is for this reason that the maximum bending moment cannot be accurately predicted by summing the maximum values of each component.

If only maximum bending moment responses to the Imbedded Gust Criteria are desired, a considerable saving in computer time can be achieved by computing in the near vicinity of the imbedded gust. The maximum values generally occur within 1 or possibly 2 sec. after the beginning of the imbedded gust.

VI. CONCLUSIONS AND RECOMMENDATIONS

The specific conclusions drawn from the results in each phase of the investigation and the recommendations which follow are based on, and should be restricted to, the Saturn V configuration and methods of control considered. The conclusions for each phase of the investigation are listed separately.

A. Phase I - Response to Sinusoidal Gust Criteria

1. The maximum responses of the bending modes and control deflection are most notably affected by the inclusion of penetration and lift growth effects. Instantaneous immersion theory leads to generally conservative (large) results for the first three bending modes and unconservative results for fourth bending mode and control deflection. The amount of conservativeness and unconservativeness of instantaneous immersion depends on the driving frequency of the sinusoidal gust.

2. The difference between the effects of pure penetration and penetration with lift growth is largest for the third and fourth bending modes and control deflection. For these modes, pure penetration effects are unconservative.

3. Rotation, first and second sloshing and local angle of attack at the vehicle nose are insignificantly affected by the inclusion of penetration or lift growth effects.

B. Phase II - Response to Imbedded Gust Criteria

1. The maximum responses of rotation, third and fourth bending and control deflection are smaller for an attitude controlled vehicle than for one using an angle of attack control.

2. Smaller maximum bending moment responses result from an attitude control system than from an angle of attack control system.

3. The maximum coordinate responses calculated with instantaneous immersion are generally conservative for both the angle of attack and attitude control systems. The amount of conservativeness of instantaneous immersion is, in most cases, larger for the angle of attack control responses. The effects of penetration on the imbedded gust responses are not as pronounced, however, as those obtained for the sinusoidal gust responses.

4. The maximum response of local angle of attack (at various station locations) is insignificantly affected by the inclusion of penetration effects.

5. Maximum bending moment responses computed with instantaneous immersion theory are conservative. The amount of conservativeness is largest near the top of the vehicle where bending mode dynamics are a significant part of the bending moment response.

The overall general conclusions are:

1. The cases in which penetration and/or lift growth plays an important role in maximum coordinate responses can be detected, with sufficient reliability, by comparisons of the impulsive responses using the various aerodynamic theories.

2. The inclusion of third and fourth bending and the effects of fins and engine shrouds into the analysis produced significant differences (in an engineering sense) between responses computed with and without penetration considerations. This is opposite from the results obtained in [1] wherein penetration effects were found to be insignificant when third and fourth bending and empennage effects were neglected.

It is recommended that:

1. Bending moment response to the Sinusoidal Gust Criteria be computed considering penetration effects. It was in the coordinate responses to the Sinusoidal Gust Criteria that penetration effects were the most significant. Because of the small amount of damping of the higher bending modes, the influence of bending dynamics lasts for a long period of time. This persistence of oscillation can add significantly to the bending moment if cyclic shears are present, particularly if their frequency content occurs near bending mode frequencies.

2. Penetration effects be included in a computation of maximum bending moments using power spectral techniques. The use of a continuous wind frequency spectrum would provide a clearer insight into the importance of penetration for the most probable wind frequencies.

3. Additional computations be performed to determine the relative merits of other control systems (i.e., accelerometer and guidance or platform accelerometer control) on load alleviation when gust penetration effects are considered. These additional results should then be compared with the present results to determine the optimum control system from the standpoint of load reduction.

4. Penetration effects should be considered in computation of maximum bending moments for vehicle stations where bending mode dynamics are a significant part of the total load. The present results indicate that a slight relaxation of structural design requirements can be made for these vehicle stations if the previous designs were based on instantaneous immersion aerodynamics.

BIBLIOGRAPHY

1. Blackburn, R. R., and A. D. St. John, "Effects and Importance of Penetration and Growth of Lift on Space Vehicle Response," NASA CR-326, November 1965.

2. Ryan, Robert S., and J. R. Scoggins, "The Use of Wind Shears in the Design of Aerospace Vehicles," paper presented at 23rd meeting of the Structures and Materials Panel, AGARD, ONERA, Paris, France, October 4-11, 1966.

3. Townsend, Don, "Saturn V Wind Response Studies," NASA MTP-AERO-63-63, September 1963.

4. Townsend, Don, "A Method for the Determination of Control Law Effect on Vehicle Bending Moment," NASA TMX-53077, July 1964.

5. Penny, Morris M., "Design Criteria: Saturn V LOR Vehicle Contribution of Four 75 Ft^2 Fins and Engine Shrouds to the Total Vehicle Normal Force Coefficients," Internal Memorandum, NASA, George C. Marshall Space Flight Center, 13 May 1964.

6. Garner, Doyle, "Control Theory Handbook," NASA TMX-53036, April 1964.

7. Rheinfurth, M. H., "Control-Feedback Stability Analysis," ABMA Report, DA-TR-2-60.

8. Bisplinghoff, R. L., H. Ashley, and R. L. Halfman, Aeroelasticity, Addison-Wesley Publishing Co., Inc., Reading, Mass. (1957).

APPENDIX I

EQUATIONS OF MOTION AND CONTROL FOR SATURN V

The equations of motion (see [1] and [7]) of a flexible space vehicle system in vertical flight are given in this Appendix. The equations for the two methods of control used in this report are also given. Nine generalized coordinates are considered in the investigation: lateral translation, y_o ; rotation, ϕ ; first four bending mode deflections, η_1 , η_2 , η_3 and η_4 ; two sloshing mode deflections,* ξ_1 and ξ_2 , and control deflection, β_C (see Fig. 57). Slender body theory is used to describe the generalized aerodynamic forces.

For simplicity, the following terms of the equations of motion (see [1] and [7]) are neglected on the basis of being small by comparison:

1. The rotation of the vehicle's cross sections during bending.

2. I_{corr} (this neglects the effects of propellant sloshing upon the total moment of inertia, I_{cg}).

3. Generalized forces due to the flowing propellants. (This eliminates the terms containing the time derivatives of the mass of the propellant.)

4. The compliance of the swivel engines (difference between the actual swivel engine angle, β_E , and the control deflection, β_C). This amounts to making the linkage connection between the two variables infinitely rigid.

5. The mass of the swivel engine and the mass moment of inertia of the swivel engine about its swivel point.

Incorporating the above assumptions into the equations of motion given in [1] and assuming that the vehicle and atmospheric parameters are

* The oscillating propellants are described by a mechanical analogy (see [1]). Only the motion of the liquid in the booster tanks is investigated. The first sloshing mode is associated with the farthest aft tank, while the second sloshing mode is associated with the adjacent tank.

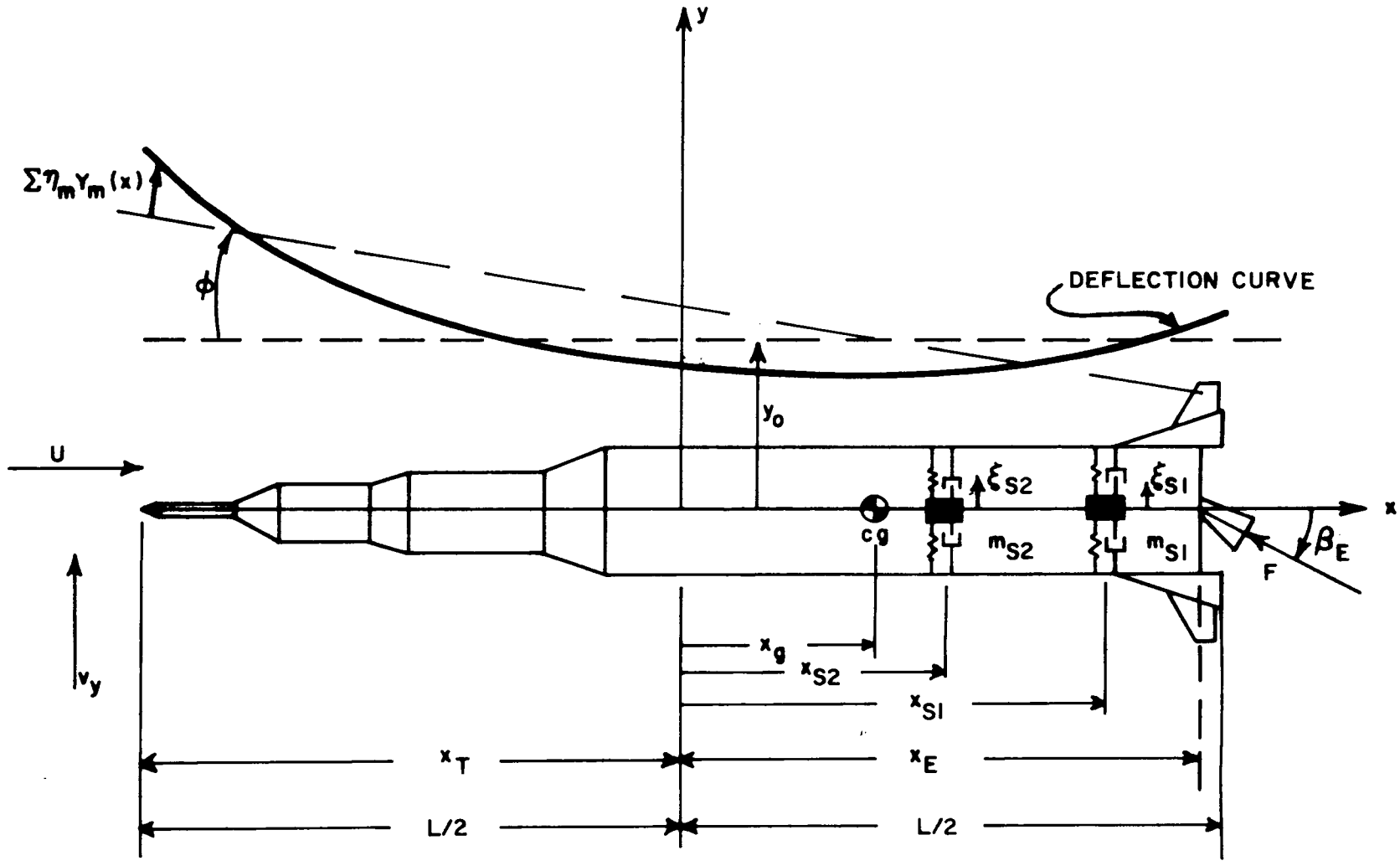

Fig. 57 - Saturn V Coordinate System

constant in predetermined time or altitude intervals, the equation of motion for translation* becomes

$$\left[m + \frac{QJ_o}{U^2}\right]\ddot{y}_o - \frac{QJ_1}{U^2}\ddot{\phi} + \sum_{i=1}^{4} \frac{QG_i}{U^2}\ddot{\eta}_i + m_{S1}\ddot{\xi}_1$$

$$+ m_{S2}\ddot{\xi}_2 + \frac{2QF_o}{U}\dot{y}_o - \frac{2Q}{U}\left[F_1+J_o\right]\dot{\phi} + \sum_{i=1}^{4} \frac{2Q}{U}\left\{D_i+H_i\right\}\dot{\eta}_i$$

$$- \left[F+2QF_o\right]\phi + \sum_{i=1}^{4} \left\{FY_i'(x_E) + QE_i\right\}\eta_i - \frac{4}{5}F\beta_C = N(t) \ , \qquad \text{(I-1)}$$

for rotation

$$- \frac{QJ_1}{U^2}\ddot{y}_o + \left[I_{cg} + \frac{QJ_2}{U^2}\right]\ddot{\phi} - \sum_{i=1}^{4} \frac{Q\bar{G}_i}{U^2}\ddot{\eta}_i$$

$$- m_{S1}(x_{S1}-x_g)\ddot{\xi}_1 - m_{S2}(x_{S2}-x_g)\ddot{\xi}_2 - \frac{2QF_1}{U}\dot{y}_o + \frac{2Q}{U}\left[J_1+F_2\right]\dot{\phi}$$

$$- \sum_{i=1}^{4} \frac{2Q}{U}\left\{\bar{D}_i+\bar{H}_i\right\}\dot{\eta}_i + 2QF_1\phi$$

$$- \sum_{i=1}^{4} \left\{F\left[(x_E-x_g)Y_i'(x_E) - Y_i(x_E)\right] - Q\bar{E}_i\right\}\dot{\eta}_i$$

$$- m_{S1}\overline{g\xi}_1 - m_{S2}\overline{g\xi}_2 + \frac{4}{5}(x_E-x_g)F\beta_C = M(t) \ , \qquad \text{(I-2)}$$

for m^{th} bending,

---

* The numerical constant, 4/5 , appearing in (I-1), (I-2), and (I-3) as a multiplier of β_C can be generalized to account for any percentage of the total number of engines which are swiveled.

$$\frac{QG_m}{U^2}\ddot{y}_o - \frac{Q\bar{G}_m}{U^2}\ddot{\phi} + T_m\ddot{\eta}_m + \sum_{i=1}^{4}\frac{QC_{mi}}{U^2}\ddot{\eta}_i$$

$$+ m_{S1}Y_m(x_{S1})\ddot{\xi}_1 + m_{S2}Y_m(x_{S2})\ddot{\xi}_2 + \frac{2QD_m}{U}\dot{y}_o$$

$$- \frac{2Q}{U}\left[\bar{D}_m + G_m\right]\dot{\phi} + T_m\omega_{Bm}g_{Bm}\dot{\eta}_m - \sum_{i=1}^{4}\frac{QB_{mi}}{U}\dot{\eta}_i$$

$$- 2QD_m\phi + T_m\omega_{Bm}^2\eta_m - \sum_{i=1}^{4}QA_{mi}\eta_i$$

$$+ m_{S1}\bar{g}Y_m'(x_{S1})\xi_1 + m_{S2}\bar{g}Y_m'(x_{S2})\xi_2$$

$$- \frac{4}{5}FY_m(x_E)\beta_C = Q\eta_m(t) \ , \qquad \text{(I-3)}$$

$$(m = 1,2,3,4)$$

for first sloshing,

$$\ddot{y}_o - (x_{S1}-x_g)\ddot{\phi} + \sum_{i=1}^{4}Y_i(x_{S1})\ddot{\eta}_i + \ddot{\xi}_i + \omega_{S1}g_{S1}\dot{\xi}_1 - \bar{g}\phi$$

$$+ \sum_{i=1}^{4}\bar{g}Y_i'(x_{S1})\eta_i + \omega_{S1}^2\xi_1 = 0 \ , \qquad \text{(I-4)}$$

and, for second sloshing,

$$\ddot{y}_o - (x_{S2}-x_g)\ddot{\phi} + \sum_{i=1}^{4}Y_i(x_{S2})\ddot{\eta}_i + \ddot{\xi}_2 + \omega_{S2}g_{S2}\dot{\xi}_2$$

$$- \bar{g}\phi + \sum_{i=1}^{4}\bar{g}Y_i'(x_{S2})\eta_i + \omega_{S2}^2\xi_2 = 0 \ . \qquad \text{(I-5)}$$

The terms $N(t)$, $M(t)$ and $Q_{\eta_i}(t)$ $(i=1,2,3,4)$ in the above equations are the generalized aerodynamic forces which are functions of the crossflow gust velocity, v_y .

The remaining equation of motion describes the control and actuator system of the vehicle. The two control systems considered in this report are special cases of a basic control system consisting of position gyro, rate gyro and alpha meter (see [1]). The position and rate gyros are both located at the engine gimbal station and the alpha meter is located at the top of the escape tower. The basic control system is given by a differential equation describing the relationship between the control deflection, β_C ; the indicated attitude, ϕ_i ; and the indicated angle of attack , α_i :

$$A_6\overset{VI}{\beta_C} + A_5\overset{V}{\beta_C} + A_4\overset{IV}{\beta_C} + A_3\dddot{\beta}_C + A_2\ddot{\beta}_C$$

$$+ A_1\dot{\beta}_C + A_o\beta_C = a_o\phi_i + a_1\dot{\phi}_i + b_o\alpha_i \quad , \tag{I-6}$$

where

$$\phi_i = \phi - \sum_{i=1}^{4} Y_i'(x_\phi)\eta_i \quad , \tag{I-7}$$

$$\alpha_i = -\frac{\dot{y}_o}{U} + \frac{(x_v-x_g)}{U}\dot{\phi} - \sum_{i=1}^{4}\frac{Y_i(x_v)}{U}\dot{\eta}_i + \phi$$

$$- \sum_{i=1}^{4} Y_i'(x_v)\eta_i + \alpha_w \tag{I-8}$$

and

$$\alpha_w = \frac{v_y}{U} \ . \tag{I-9}$$

The actuator coefficients, A_j , in (I-6) are time-independent and their numerical values are assumed to be independent of the control system. The gain values a_o , a_1 and b_o do, however, depend on time.

One of the control systems used in the numerical study is referred to as "angle of attack control." The system is obtained from (I-6) by gain stabilizing the bending mode influence* from the angle of attack sensor and gain stabilizing the third and fourth bending mode slopes sensed by the position and rate gyros:

$$\sum_{j=0}^{6} A_j \beta_C^{(j)} = a_o \phi_i + a_1 \dot{\phi}_i + b_o \alpha_i \ , \qquad \text{(I-10)}$$

where

$$\phi_i = \phi - \sum_{i=1}^{2} Y_i'(x_\phi)\eta_i \ ,$$

$$\alpha_i = -\frac{\dot{y}_o}{U} + \frac{(x_v - x_g)}{U}\dot{\phi} + \phi + \alpha_w$$

and

$$\alpha_w = \frac{v_y}{U} \ .$$

The second control system used in the numerical study is referred to as "attitude control." This system is also derived from (I-6) by gain stabilizing the angle of attack sensor ($b_o = 0$) and gain stabilizing the third and fourth bending mode slopes sensed by the position and rate gyros:

* The gain stabilization of the bending mode influence in (I-10) and (I-11) was necessary to (1) insure a stable vehicle system and (2) approximate the effect of filters present in an actual Saturn V control system.

$$\sum_{j=0}^{6} A_j \beta_C^{(j)} = \bar{a}_o \phi_i + a_1 \phi_i \qquad \text{(I-11)}$$

where

$$\phi_i = \phi - \sum_{i=1}^{2} Y_i'(x_\phi)\eta_i \quad .$$

The numerical value of $\bar{a}_o$ in (I-11) was set equal to the value of (a_o+b_o) from (I-6) in order to maintain a control frequency similar to that arising from (I-6) or (I-10).

The preceding equations of motion ((I-1) through (I-5) and (I-10)) describe the vehicle system defined as "angle of attack control" while ((I-1) through (I-5) and (I-11)) describe the system defined as "attitude control." The gust responses of each system of equations were evaluated in the numerical investigation.

APPENDIX II

AERODYNAMIC FORCE EXPRESSIONS RESULTING FROM UNIT STEP AND IMPULSE WIND PROFILE

The development of the indicial* and impulsive** transient, quasi-steady and steady aerodynamic force expressions for a Saturn V configuration without fins and engine shrouds was presented in [1]. Slender body theory was used in the formulation of the force expressions corresponding to rigid body and bending modes of vibration. Quadratic polynomials were used to curve fit segments of the mode shapes in evaluating the generalized forces associated with the bending modes.

The extension of the aerodynamic force expressions in [1] to include the effects of the fins and engine shrouds is presented in this Appendix. The technique used in [1] to describe the aerodynamic forces on a body of revolution does not apply directly to winged bodies. To obtain usable results for bodies with such empennages, the concept of an equivalent body of revolution is used.

This equivalent body concept, simply stated, is to replace the fin and engine shroud region of the vehicle with an artificial equivalent body of revolution. The latter is designed to have the same steady-state slope of the normal force coefficient as the original fin and engine shroud region. The hypothesis, then, is that the lift growth of the equivalent body of revolution approximates the lift growth of the body with empennages, to engineering accuracy.

To insure the most accurate representation possible within the framework of this technique, experimental data are used for the slope of the normal force coefficient of the fins and engine shrouds. The experimental data used are taken from wind tunnel tests [5] and account for the fin-shroud-body interference effect.

Once the equivalent body shape is defined, aerodynamics of bodies of revolution may be used. The wind induced aerodynamic forcing functions which are compared in this report and in [1] have both a geometric and an aerodynamic aspect.

---

* Response to a unit step wind profile.

** Response to a unit impulse wind profile.

In the geometric consideration two cases are used. In the simplest case (instantaneous immersion) all stations along the vehicle are assumed to be immersed in the same wind induced crossflow, namely the wind crossflow occurring at the nose. The more accurate geometric representation, called penetration, assigns to each station along the vehicle the wind crossflow which exists at the altitude occupied by the station. With penetration, the vehicle's nose enters a side gust first and in subsequent time successive stations along the vehicle length move into the crossflow.

Two aerodynamic aspects are considered: quasi-steady and transient. In the quasi-steady representation, the air forces at a vehicle station are those which would exist if the local crossflow persisted unchanged for an extended time. The transient representation is based on transient slender-body theory and includes the growth of lift with time.

Three types of wind induced forcing functions are assembled using combinations of the geometric and aerodynamic representations. The simplest type is called instantaneous immersion and uses the instantaneous immersion geometric representation with quasi-steady aerodynamics. A more accurate type, called pure penetration, uses penetration geometrics and quasi-steady aerodynamics. The most accurate forcing functions are called penetration with lift growth. These functions use the penetration geometrics with transient aerodynamics.* A summary is given in Table I of the geometric and aerodynamic combinations used to construct the three types of forcing functions.

The development of the equivalent body is now considered in detail. The basic configuration** of the Saturn V with simulated fins and engine shrouds is shown in Fig. 58. The nose spike on the front of the vehicle corresponds to the escape tower which is attached to the vehicle throughout the boost phase of flight. It is assumed that the aerodynamic contributions of the fins and engine shrouds can be approximated satisfactorily by two adjacent conic sections (see the aft end of the vehicle shown in Fig. 58).

The geometry of the above configuration is defined in Table VIII with conic characteristics defined by $\beta_n = \tan \alpha_n$ for $n = 0,1,2,3,4,5$.

---

* The crossflows induced by the vehicle motions are in all cases treated with quasi-steady aerodynamics. These crossflows are small in comparison to the wind induced crossflows and appear in the left hand side of the equations of motion.

** The vehicle is considered to be traveling in the negative x direction (see Fig. 58) with a constant velocity, U . At time zero, the nose encounters a side wind of magnitude $v_y(x,t)$ directed along the positive z axis.

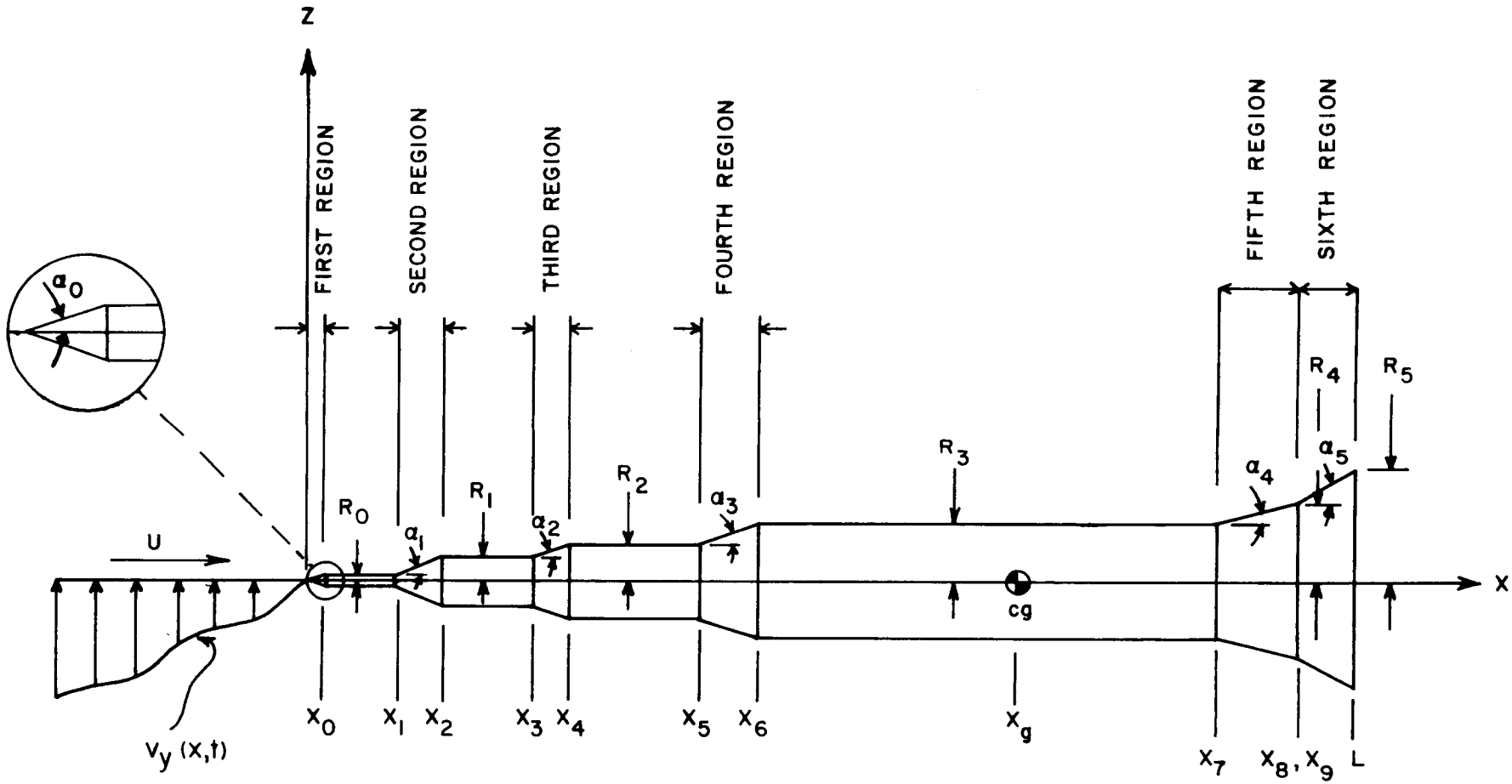

Fig. 58 - Saturn V Body Geometry

TABLE VIII

DEFINITION OF SATURN V BODY GEOMETRY

Body Radius $R(x)$	Area Derivative $S'(x)$	Region Applicable
$\beta_o x$	$2\pi\beta_o^2 x$	$0 \le x \le x_o$
R_o	0	$x_o \le x \le x_1$
$\beta_1(x-x_1) + R_o$	$2\pi\beta_1\left[\beta_1(x-x_1)+R_o\right]$	$x_1 \le x \le x_2$
R_1	0	$x_2 \le x \le x_3$
$\beta_2(x-x_3) + R_1$	$2\pi\beta_2\left[\beta_2(x-x_3)+R_1\right]$	$x_3 \le x \le x_4$
R_2	0	$x_4 \le x \le x_5$
$\beta_3(x-x_5) + R_2$	$2\pi\beta_3\left[\beta_3(x-x_5)+R_2\right]$	$x_5 \le x \le x_6$
R_3	0	$x_6 \le x \le x_7$
$\beta_4(x-x_7) + R_3$	$2\pi\beta_4\left[\beta_4(x-x_7)+R_3\right]$	$x_7 \le x \le x_8$
$\beta_5(x-x_9) + R_4$	$2\pi\beta_5\left[\beta_5(x-x_9)+R_4\right]$	$x_9 \le x \le L$

The last two rows in Table VIII correspond to the equivalent conical regions for the fins and engine shrouds. The upstream position of the first frustrum is located at the beginning of the engine shrouds, x_7 , while the other frustrum starts at the beginning of the fins, $x_9(=x_8)$.* It is convenient to consider the lead cone extending to the rear of the vehicle, L , with part of the frustrum located within the second cone. The cone angle, α_4 , is then selected to provide a steady state normal force equal to the force due to the shrouds alone. The second cone angle, α_5 , is chosen so that the second cone and the exposed fraction of the first cone provide the steady normal force due to the fin-shroud combination.

* The double numbering of the shroud and fin juncture was done for convenience in the computer program used to generate the generalized aerodynamic forces.

The method used to evaluate the two equivalent cone angles α_4 and α_5 (or slopes, β_4 and β_5), used to approximate the fin and engine shroud effect, will now be discussed. The steady-state slope of the normal force coefficient curve for the entire configuration can be obtained from the equation

$$C_{N_\alpha} = \frac{16}{D_o^2} \int_0^L R(x)R'(x)dx \tag{II-1}$$

where D_o is the reference diameter (= $2R_3$). In the same fashion, the steady-state slope of the normal force coefficient curve for the engine shrouds alone is given by

$$C_{N_{\alpha_E}} = \frac{16}{D_o^2} \int_{x_7}^L R(x)R'(x)dx \tag{II-2}$$

where, from Table VIII

$$R(x) = \beta_4(x-x_7) + R_3 \quad ,$$

$$R'(x) = \beta_4 \quad . \tag{II-3}$$

Substituting (II-3) into (II-2), integrating and solving for β_4 yields

$$\beta_4 = \frac{R_3}{(L-x_7)} \left[-1 + \sqrt{1 + \frac{C_{N_{\alpha_E}}}{2}} \right] \tag{II-4}$$

and, consequently, $\alpha_4 = \tan^{-1} \beta_4$.

Likewise, the steady-state slope of the normal force coefficient curve for the fins and engine shrouds combination is given by

$$C_{N_{\alpha_{FE}}} = \frac{16}{D_o^2} \int_{x_7}^{x_8} R(x)R'(x)dx + \frac{16}{D_o^2} \int_{x_9}^{L} R(x)R'(x)dx \quad . \qquad \text{(II-5)}$$

Again from Table VII

$$\left.\begin{aligned} R(x) &= \beta_4(x-x_7) + R_3 \\ R'(x) &= \beta_4 \end{aligned}\right\} x_7 \le x \le x_8 \quad , \qquad \text{(II-6)}$$

$$\left.\begin{aligned} R(x) &= \beta_5(x-x_9) + R_4 \\ R'(x) &= \beta_5 \end{aligned}\right\} x_9 \le x \le L \quad . \qquad \text{(II-7)}$$

Substituting (II-6) and (II-7) into (II-5), integrating and solving for β_5 yields upon simplification

$$\beta_5 = - \frac{\beta_4(x_8-x_7)}{L-x_9} + \frac{R_3}{L-x_9} \left[- 1 + \sqrt{1 + \frac{C_{N_{\alpha_{FE}}}}{2}} \right] \qquad \text{(II-8)}$$

and, consequently, $\alpha_5 = \tan^{-1} \beta_5$.

Numerical values for α_4 and α_5 were computed for 70 and 80 sec. flight times using experimental values of $C_{N_{\alpha_E}}$ and $C_{N_{\alpha_{FE}}}$ (see [3]) and are presented in Table IX.

TABLE IX

EQUIVALENT CONE ANGLES FOR SIMULATED FINS AND ENGINE SHROUDS

Flight Time (sec.)	Mach No.	$C_{N_{\alpha_E}}$ (Rad^{-1})	$C_{N_{\alpha_{FE}}}$ (Rad^{-1})	α_4	α_5
70	1.3448	1.14	2.67	9°5'	25°49'
80	1.7783	0.80	1.97	6°36'	20°53'

The center of pressure locations for the two equivalent conic sections were also computed for the two flight times. The resulting center of pressure locations were about 10 in. ahead of the theoretical predicted values given in [5]. This difference amounts to only a 0.9 per cent reduction in the fin-shroud moment arm measured with respect to the center of gravity of the vehicle. Thus, the conic section approximations are believed to be quite adequate for the response study.

The pertinent points regarding the aerodynamics used is now given. A complete description is given in [1] of the three types of forcing functions (instantaneous immersion, pure penetration, and penetration with lift growth) resulting from both a unit step and unit impulse wind profile. The results in that reference are for a Saturn V configuration without fins and engine shrouds. The incorporation of the aerodynamic contribution of the fins and engine shrouds into the three types of forcing functions requires a limited amount of repetition of the forcing function expressions given in [1]. For brevity, only those forcing functions resulting from a unit step wind profile will be presented.

The indicial aerodynamic forces corresponding to translational, rotational and bending coordinates for the case of penetration with lift growth are given by

$$N_s(\tau) = \frac{2q}{U} \int_0^{\left(\frac{U\tau}{L}\right)} S'(x) f_o \left\{ \frac{U\left(\tau - \frac{x}{U}\right)}{MR(x)} \right\} dx \ , \qquad \text{(II-9)}$$

$$M_s(\tau) = -\frac{2q}{U} \int_0^{\left(\frac{U\tau}{L}\right)} (x-x_g) S'(x) f_o \left\{ \frac{U\left(\tau - \frac{x}{U}\right)}{MR(x)} \right\} dx \ , \qquad \text{(II-10)}$$

and

$$Q\eta_m(\tau)_s = \frac{2q}{U} \int_0^{\left(\frac{U\tau}{L}\right)} Y_m(x) S'(x) f_o \left\{ \frac{U\left(\tau - \frac{x}{U}\right)}{MR(x)} \right\} dx \ ; \qquad \text{(II-11)}$$

while for the case of pure penetration,

$$N_s(\tau) = \frac{2q}{U} \int_0^{\left(\frac{U\tau}{L}\right)} S'(x) I\left(\tau - \frac{x}{U}\right) dx \quad , \tag{II-12}$$

$$M_s(\tau) = -\frac{2q}{U} \int_0^{\left(\frac{U\tau}{L}\right)} (x-x_g) S'(x) I\left(\tau - \frac{x}{U}\right) dx \quad , \tag{II-13}$$

and

$$Q\eta_m(\tau)_s = \frac{2q}{U} \int_0^{\left(\frac{U\tau}{L}\right)} Y_m(x) S'(x) I\left(\tau - \frac{x}{U}\right) dx \quad ; \tag{II-14}$$

and for the case of instantaneous immersion,

$$N_s(\tau) = \frac{2q}{U} I(\tau) \int_0^L S'(x) dx \quad , \tag{II-15}$$

$$M_s(\tau) = -\frac{2q}{U} I(\tau) \int_0^L (x-x_g) S'(x) dx \quad , \tag{II-16}$$

and

$$Q\eta_m(\tau)_s = \frac{2q}{U} I(\tau) \int_0^L Y_m(x) S'(x) dx \quad . \tag{II-17}$$

The notation used in (II-9) - (II-17) requires some remarks. The expression $\binom{U\tau}{L}$ means that the x integration is performed over $(0\ ,\ U\tau)$ or $(0,L)$ as the body has partially or totally penetrated the side wind profile $v_y\left(\tau - \frac{x}{U}\right)$. Here x_g is the distance from the nose to the center of gravity; and the sign of the moment equation is chosen so that positive $M(\tau)$ gives rise to a clockwise rotation of the vehicle as viewed in Fig. 57. The function, $f_o(\tau)$, together with its approximate mathematical form, which was used in the numerical investigation of this report is presented in [1]. The subscript s in the force expressions implies that these entities are due to a unit step wind profile.

The impulsive aerodynamic forces for the three types of forcing functions can be obtained from the first time derivative of the indicial forces given in (II-9) through (II-17).

The general expressions used in this report for the indicial and impulsive forcing functions for the three aerodynamic representations are given in Appendix II of [1]. These general expressions are written as functions of a set of coefficients dependent upon the vehicle geometry and free stream velocity (see Table VI of [1]). For instance, the indicial normal force (II-9) is written in general form as

$$N_s(\tau) = \sum_n F(a_n, b_n, c_n, \ldots, \ell_n) \qquad \text{(II-18)}$$

where $a_n, b_n, c_n, \ldots, \ell_n$ are various coefficients and n is the number of conical regions. The remaining generalized forcing functions are similar to the functional form of (II-18).

The incorporation of the fins and engine shrouds into the aerodynamic forcing functions necessitated expanding the number of frustrum regions from $n = 4$ to $n = 6$. This in turn increased the number of coefficients required for computation of the forcing functions. The addition of the empennages to the analysis, however, did not require extra coefficient forms. For completeness, the list of coefficients used in this report to evaluate the aerodynamic forcing functions is given in Table X. The elements in the fifth and sixth region rows correspond to the fin and engine shroud influence. The first four region rows are identical to those presented in [1].

TABLE X

COEFFICIENTS USED IN EVALUATING INDICIAL AND IMPULSIVE AERODYNAMIC FORCING FUNCTIONS

n	a_n	b_n	c_n	d_n	$\bar{d}_n$	e_n	$\bar{e}_n$	f_n	h_n	k_n	ℓ_n	Region
1	$\pi\beta_o^2U^2$	0	0	0	$\frac{x_o}{U}$	0	$\frac{MR_o}{U}$	$M\beta_o$	S_o	$\frac{2S_ox_o}{3}$	$\frac{S_ox_o^2}{2}$	First
2	$\pi\beta_1^2U^2$	$\frac{1}{U}\left(x_1 - \frac{R_o}{\beta_1}\right)$	S_o	$\frac{x_1}{U}$	$\frac{x_2}{U}$	$\frac{MR_o}{U}$	$\frac{MR_1}{U}$	$M\beta_1$	S_1-S_o	$\frac{2(S_1R_1-S_oR_o)}{3\beta_1}$	$\frac{S_1R_1^2-S_oR_o^2}{2\beta_1^2}$	Second
3	$\pi\beta_2^2U^2$	$\frac{1}{U}\left(x_3 - \frac{R_1}{\beta_2}\right)$	S_1	$\frac{x_3}{U}$	$\frac{x_4}{U}$	$\frac{MR_1}{U}$	$\frac{MR_2}{U}$	$M\beta_2$	S_2-S_1	$\frac{2(S_2R_2-S_1R_1)}{3\beta_2}$	$\frac{S_2R_2^2-S_1R_1^2}{2\beta_2^2}$	Third
4	$\pi\beta_3^2U^2$	$\frac{1}{U}\left(x_5 - \frac{R_2}{\beta_3}\right)$	S_2	$\frac{x_5}{U}$	$\frac{x_6}{U}$	$\frac{MR_2}{U}$	$\frac{MR_3}{U}$	$M\beta_3$	S_3-S_2	$\frac{2(S_3R_3-S_2R_2)}{3\beta_3}$	$\frac{S_3R_3^2-S_2R_2^2}{2\beta_3^2}$	Fourth
5	$\pi\beta_4^2U^2$	$\frac{1}{U}\left(x_7 - \frac{R_3}{\beta_4}\right)$	S_3	$\frac{x_7}{U}$	$\frac{x_8}{U}$	$\frac{MR_3}{U}$	$\frac{MR_4}{U}$	$M\beta_4$	S_4-S_3	$\frac{2(S_4R_4-S_3R_3)}{3\beta_4}$	$\frac{S_4R_4^2-S_3R_3^2}{2\beta_4^2}$	Fifth
6	$\pi\beta_5^2U^2$	$\frac{1}{U}\left(x_9 - \frac{R_4}{\beta_5}\right)$	S_4	$\frac{x_9}{U}$	$\frac{L}{U}$	$\frac{MR_4}{U}$	$\frac{MR_5}{U}$	$M\beta_5$	S_5-S_4	$\frac{2(S_5R_5-S_4R_4)}{3\beta_5}$	$\frac{S_5R_5^2-S_4R_4^2}{2\beta_5^2}$	Sixth

APPENDIX III

FORMULATION OF BENDING MOMENT EXPRESSIONS RESULTING FROM A UNIT IMPULSE AND ARBITRARY WIND PROFILE

The development of the expressions for the vehicle bending moment resulting from a unit impulse wind profile is presented in this Appendix. The expressions for the subsequent bending moment response to an arbitrary wind profile are also given. Two basic approaches for the calculation of the vehicle bending moments are described: (1) the summation of moments technique (see [4]) and (2) the mode displacement method (see [8]). Also, a reduced form of the summation of moments technique is presented. This latter form, referred to as the "reduced bending moment expression," is the basis upon which the bending moment response comparisons are made in this report. The effects of two aerodynamic representations, instantaneous immersion and pure penetration, are considered in the computation of the bending moment responses. The aerodynamic representations of the gust crossflow are both explicit and implicit in the summation of moments technique, while they are implicit in the mode displacement method.

The description of the summation of moments technique and subsequent development of the reduced bending moment expression will be given first.

The bending moment equation is derived by considering the forces and moments acting on a free-body segment of the vehicle, under the influence of unit impulse gust velocity. The bending moment expression is formulated for an arbitrary vehicle station, x_k , by considering the contributions of forces from x_k to the aft end of the vehicle. The effects of swivel engine inertia, sloshing and the time and spatial derivative of local angle of attack are neglected in the development. In this investigation the sign convention used is: positive translation upward, positive rotation clockwise and positive bending moment clockwise, as viewed in Fig. 57. The bending moment at the vehicle station, x_k , will be assumed to arise from three basic sources: areodynamic loading, thrust forces and inertia forces. Thus, the total bending moment is written as

$$M_{B_T}(x_k,\tau) = M_{B_{AERO}}(x_k,\tau) + M_{B_{THRUST}}(x_k,\tau) + M_{B_{INERTIA}}(x_k,\tau) \quad . \qquad \text{(III-1)}$$

The impulsive aerodynamic moment is given by

$$M_{B_{AERO}}(x_k,\tau) = - qS_o \int_{x_k}^{L} C'_{N_\alpha} \alpha(x,\tau)(x-x_k)dx \qquad \text{(III-2)}$$

where

$$\alpha(x,\tau) = \phi - \frac{\dot{y}_o}{U} + \frac{(x-x_{cg})}{U}\dot{\phi} - \sum_{i=1}^{4} \frac{Y_i(x)}{U}\dot{\eta}_i$$

$$- \sum_{i=1}^{4} Y'_i(x)\eta_i + \frac{\delta\left(\tau - \frac{x}{U}\right)}{U} \qquad \text{(III-3)}$$

and, according to slender body theory,

$$C'_{N_\alpha} = \frac{16}{D_o^2} R(x)R'(x) \quad . \qquad \text{(III-4)}$$

Rewriting $M_{B_{AERO}}(x_k,\tau)$ to account for gust penetration effects* yields

$$M_{B_{AERO}}(x_k,\tau) = M^{(1)}_{B_{AERO}}(x_k,\tau) + M^{(2)}_{B_{AERO}}(x_k,\tau) \quad . \qquad \text{(III-5)}$$

The first term of (III-5) is

$$M^{(1)}_{B_{AERO}}(x_k,\tau) = - qS_o \int_{x_k}^{L} C'_{N_\alpha} \bar{\alpha}(x,\tau)(x-x_k)dx \qquad \text{(III-6)}$$

---

* The bending moment equation arising from the summation of moments technique will be formulated first considering gust penetration effects. The equation will then be recast into the form resulting from instantaneous immersion considerations.

with

$$\bar{\alpha}(x,\tau) = \phi - \frac{\dot{y}_o}{U} + \frac{(x-x_g)}{U}\dot{\phi} - \sum_{i=1}^{4} \frac{Y_i(x)}{U}\dot{\eta}_i$$

$$- \sum_{i=1}^{4} Y_i'(x)\eta_i \quad . \qquad \text{(III-7)}$$

The second term of (III-5) is

$$M^{(2)}_{B_{AERO}}(x_k,\tau) = 0, \text{ for } x_k \geq U\tau$$

and

$$M^{(2)}_{B_{AERO}}(x_k,\tau) = - qS_o \int_{x_k}^{\left(\frac{U\tau}{L}\right)} C'_{N_\alpha}(x-x_k) \frac{\delta\left(\tau - \frac{x}{U}\right)}{U} dx \ , \qquad \text{(III-8)}$$

for $x_k \leq U\tau$.

The combined moment due to the thrust forces acting both perpendicular and parallel to the vehicle centerline at $x = x_k$ is given by

$$M_{B_{THRUST}}(x_k,\tau) = - \frac{4F}{5}(x_E-x_k)\beta_C + F(x_E-x_k)\sum_{i=1}^{4} \eta_i Y_i'(x_E)$$

$$- F\sum_{i=1}^{4} \eta_i \left[Y_i(x_E) - Y_i(x_k)\right] \quad . \qquad \text{(III-9)}$$

This moment expression is valid for a swivel engine controlled vehicle where the swiveled engines account for four-fifths of the total thrust force. In the development of the moment due to thrust, the terms containing cross products of the generalized coordinates are neglected on the basis of being small compared to those retained in (III-9).

The other moment to be considered is that arising from the inertial forces. These moments are due to accelerations perpendicular to the vehicle's trajectory:

$$\ddot{\tau} = \ddot{y}_o - (x-x_g)\ddot{\phi} + \sum_{i=1}^{4} \ddot{\eta}_i Y_i(x) \quad . \tag{III-10}$$

The moment due to the inertial forces is given by

$$M_{B_{INERTIAL}}(x_k,\tau) = \int_{x_k}^{L} m'(x)(x-x_k)\left[\ddot{y}_o - (x-x_g)\ddot{\phi} + \sum_{i=1}^{4} \ddot{\eta}_i Y_i(x)\right]dx \quad . \tag{III-11}$$

The terms, $\ddot{y}_o$ and $\ddot{\phi}$ are removed from (III-11) by using simplified forms of the translational and rotational equations of motion (see (I-1) and (I-2)). Rewriting (I-1) and (I-2) for the impulsive gust penetration case and retaining the dominant terms, the translational acceleration is given by

$$\ddot{y}_o = \frac{F}{m}\phi - \frac{F}{m}\sum_{i=1}^{4} \eta_i Y_i'(x_E) + \frac{4}{5}\frac{F}{m}\beta_C$$

$$+ \frac{qS_o}{m}\int_0^L C_{N_\alpha}'\bar{\alpha}(x,\tau)dx + \frac{qS_o'}{m}\int_0^{\left(\frac{U\tau}{L}\right)} C_{N_\alpha}' \frac{\delta\left(\tau - \frac{x}{U}\right)}{U}dx \tag{III-12}$$

and the rotational acceleration is given by

$$\ddot{\phi} = F\frac{(x_E-x_g)}{I_{cg}}\sum_{i=1}^{4} \eta_i Y_i'(x_E) - \frac{F}{I_{cg}}\sum_{i=1}^{4} \eta_i Y_i(x_E)$$

$$- \frac{4F}{5I_{cg}}(x_E-x_g)\beta_C - \frac{qS_o}{I_{cg}}\int_0^L C_{N_\alpha}'(x-x_g)\bar{\alpha}(x,\tau)dx$$

$$- \frac{qS_o}{I_{cg}}\int_0^{\left(\frac{U\tau}{L}\right)} C_{N_\alpha}'(x-x_g)\frac{\delta\left(\tau - \frac{x}{U}\right)}{U}dx \tag{III-13}$$

where $\bar{\alpha}(x,\tau)$ is given by (III-7) and the slope of the local normal force coefficient, C'_{N_α}, is given by (III-4).

Substituting (III-12) and (III-13) into (III-11); and (III-5), (III-9) and (III-11) into (III-1), the total impulsive bending moment response due to gust penetration is given by:

$$M_{B_T}(x_k,\tau) = M_{GUST}(x_k,\tau) + M'_{\phi}(x_k)\phi(\tau) + M'_{\alpha}(x_k)\alpha(\tau)$$

$$+ M'_{\beta_C}(x_k)\beta_C(\tau) + M'_{\dot{\phi}}(x_k)\dot{\phi}(\tau) + \sum_{i=1}^{4} M'_{\eta_i}(x_k)\eta_i(\tau)$$

$$+ \sum_{i=1}^{4} M'_{\dot{\eta}_i}(x_k)\dot{\eta}_i(\tau) + \sum_{i=1}^{4} M'_{\ddot{\eta}_i}(x_k)\ddot{\eta}_i(\tau) \qquad \text{(III-14)}$$

where

$$M_{GUST}(x_k,\tau) = -\frac{2q}{U}\int_{x_k}^{\left(\substack{U\tau\\L}\right)} S'(x)(x-x_k)\,\delta\left(\tau - \frac{x}{U}\right)dx$$

$$+ \frac{2q}{U}\int_{0}^{\left(\substack{U\tau\\L}\right)} S'(x)\,\delta\left(\tau - \frac{x}{U}\right)dx\left[I_m(x_k)\right]$$

$$+ \frac{2q}{U}\int_{0}^{\left(\substack{U\tau\\L}\right)} S'(x)(x-x_g)\,\delta\left(\tau - \frac{x}{U}\right)dx\left[I_I(x_k)\right] \quad , \qquad \text{(III-15)}$$

$$M'_{\phi}(x_k) = F\left[I_m(x_k)\right] \quad , \qquad \text{(III-16)}$$

$$M'_{\alpha}(x_k) = -2q\int_{x_k}^{L} S'(x)(x-x_k)dx + 2QF_o\left[I_m(x_k)\right]$$

$$+ 2QF_1\left[I_I(x_k)\right] \quad , \qquad \text{(III-17)}$$

$$M'_{\beta_C}(x\ ) = \frac{4F}{5}\left\{I_m(x_k) + (x_E-x_g)\left[I_I(x_k)\right] - (x_E-x_k)\right\} \quad , \qquad \text{(III-18)}$$

$$M'_{\dot{\phi}}(x_k) = -\frac{2q}{U}\int_{x_k}^{L} S'(x)(x-x_g)(x-x_k)dx + \frac{2QF_1}{U}\left[I_m(x_k)\right]$$

$$+ \frac{2QF_2}{U}\left[I_I(x_k)\right] \quad , \qquad \text{(III-19)}$$

$$M'_{\eta_i}(x_k) = F\left\{(x_E-x_k)Y'_i(x_E) - \left[Y_i(x_E) - Y_i(x_k)\right] - Y'_i(x_E)\left[I_m(x_k)\right]\right.$$

$$\left. + \left[Y_i(x_E) - (x_E-x_g)Y'_i(x_E)\right]\left[I_I(x_k)\right]\right\}$$

$$+ 2q\int_{x_k}^{L} S'(x)(x-x_k)Y'_i(x)dx - QE_i^*\left[I_m(x_k)\right]$$

$$+ Q\overline{E}_i^*\left[I_I(x_k)\right] \quad , \qquad \text{(III-20)}$$

$$M'_{\dot{\eta}_i}(x_k) = \frac{2q}{U}\int_{x_k}^{L} S'(x)(x-x_k)Y_i(x)dx - \frac{2Q}{U}D_i\left[I_m(x_k)\right]$$

$$- \frac{2Q}{U}\overline{D}_i\left[I_I(x_k)\right] \quad , \qquad \text{(III-21)}$$

$$M'_{\ddot{\eta}_i}(x_k) = I_i(x_k) \quad , \qquad \text{(III-22)}$$

and

$$\alpha(\tau) = \phi - \frac{\dot{y}}{U} \qquad \text{(III-23)}$$

also

$$I_m(x_k) = \frac{1}{m} \int_{x_k}^{L} m'(x)(x-x_k)dx \quad ,$$

$$I_I(x_k) = \frac{1}{I_{cg}} \int_{x_k}^{L} m'(x)(x-x_k)(x-x_g)dx \quad ,$$

$$I_i(x_k) = \int_{x_k}^{L} m'(x)(x-x_k)Y_i(x)dx \quad ,$$

$$F_k = \frac{1}{2S_3} \int_{0}^{L} S'(x)(x-x_g)^k dx \quad ,$$

$$D_i = \frac{1}{2S_3} \int_{0}^{L} S'(x)Y_i(x)dx \quad ,$$

$$\bar{D}_i = \frac{1}{2S_3} \int_{0}^{L} S'(x)(x-x_g)Y_i(x)dx \quad ,$$

$$E_i^* = \frac{1}{S_3} \int_{0}^{L} S'(x)Y_i'(x)dx \quad ,$$

and

$$\bar{E}_i^* = -\frac{1}{S_3} \int_{0}^{L} S'(x)(x-x_g)Y_i'(x)dx \quad .$$

The effects of gust penetration in (III-14) enter explicitly through the bending moment term associated with the angle of attack due to wind (III-15). This gust penetration term is dependent upon response time as well as station location. The limits of integration in (III-15) reflect the effects of gust penetration. The first integral does not contribute to the value of $M_{GUST}(x_k,\tau)$ until $U\tau \geq x_k$; while the latter two integrals become effective, the instant vehicle gust penetration begins.

The effects of gust penetration appear in (III-14) implicitly as well as through the $M_{GUST}(x_k,\tau)$ term. The other terms contain the weighted contributions of the generalized coordinates which are the impulsive gust responses determined from pure penetration aerodynamic considerations.

A comment on the numerical evaluation of $M_{GUST}(x_k,\tau)$ is warranted before concluding the discussion of the penetration effects upon the total bending moment expression. The computation of $M_{GUST}(x_k,\tau)$ is facilitated by recasting (III-15) in terms of the impulsive aerodynamic normal force, $N_i(\tau)$, and moment, $M_i(\tau)$, resulting from pure penetration considerations (see [1]). Thus, (III-15) becomes for $U\tau \leq x_k$

$$M_{GUST}(x_k,\tau) = N_i(\tau)\left[I_m(x_k)\right] - M_i(\tau)\left[I_I(x_k)\right] \qquad \text{(III-24)}$$

and for $U\tau \geq x_k$

$$M_{GUST}(x_k,\tau) = \left[(x_k-x_g) + I_m(x_k)\right] N_i(\tau) + \left[1 - I_I(x_k)\right] M_i(\tau) \qquad \text{(III-25)}$$

where $M_i(\tau)$ is taken about the center of gravity of the vehicle.

The total impulsive bending moment response resulting from instantaneous immersion aerodynamic considerations will now be presented. This bending moment expression is given by (III-14) with two minor differences. These differences correspond to the explicit and implicit effects of instantaneous immersion representation. The explicit difference is in the form that the $M_{GUST}(x_k,\tau)$ term takes. For instantaneous immersion, the integrals in (III-15) are independent of time and equal to their steady-state values. Thus,

$$M_{GUST}(x_k,\tau) = \left\{ - 2q \int_{x_k}^{L} S'(x)(x-x_k)dx + 2q \int_{0}^{L} S'(x)dx \left[I_m(x_k)\right] + 2q \int_{0}^{L} S'(x)(x-x_g)dx \left[I_I(x_k)\right] \right\} \frac{\delta(\tau)}{U} \quad . \qquad \text{(III-26)}$$

Comparing (III-26) with (III-17), it can be shown that for instantaneous immersion

$$M_{GUST}(x_k,\tau) = M'_\alpha(x_k)\,\frac{\delta(\tau)}{U} \quad . \qquad \text{(III-27)}$$

The second difference, which is implicit, is that the weighted generalized coordinate responses are determined from instantaneous immersion aerodynamic considerations. The weighting functions are given by (III-16) through (III-22) and are independent of the aerodynamic representation used. Therefore, the total impulsive bending moment response due to instantaneous immersion is described by (III-14), (III-27), (III-16) through (III-22) and the set of instantaneous immersion impulsive responses of the generalized coordinates.

A reduced form of the total bending moment expression, (III-14), will now be discussed. A numerical evaluation of (III-14) for both aerodynamic representations revealed that several component terms can be neglected on the basis of being small by comparison. These terms involve $\dot{\phi}$, η_i, $\dot{\eta}_i$ and the ϕ component given by (III-16).* Neglecting the effects of these terms results in an equation for the impulsive bending moment which is a function of the gust, α, β_C and $\ddot{\eta}_i$ terms. This equation is referred to as the "reduced bending moment expression." Referring to (III-14), the impulsive reduced bending moment equation is given by

$$M_{B_R}(x_k,\tau) = M_{GUST}(x_k,\tau) + M'_\alpha(x_k)\alpha(\tau) + M'_{\beta_C}(x_k)\beta_C(\tau)$$

$$+ \sum_{i=1}^{4} M'_{\ddot{\eta}_i}(x_k)\ddot{\eta}_i(\tau) \qquad \text{(III-28)}$$

* There is an additional ϕ component in the total bending moment expression which is contained in the rigid body angle of attack term (see (III-17) and (III-23)). This component is not small and must be retained in the reduction.

where

$$M'_{\alpha}(x_k) = -2q \int_{x_k}^{L} S'(x)(x-x_k)dx + 2QF_o \left[I_m(x_k)\right]$$

$$+ 2QF_1 \left[I_I(x_k)\right] \quad , \qquad \text{(III-29)}$$

$$M'_{\beta_C}(x_k) = \frac{4F}{5} \left\{ I_m(x_k) + (x_E - x_g)\left[I_I(x_k)\right] - (x_E - x_k) \right\} \quad , \qquad \text{(III-30)}$$

$$M'_{\ddot{\eta}_i}(x_k) = I_i(x_k) \quad , \qquad \text{(III-31)}$$

and

$$\alpha(\tau) = \phi - \frac{\dot{y}}{U} \quad . \qquad \text{(III-32)}$$

The $M_{GUST}(x_k,\tau)$ term in the reduced bending moment expression is the same as that given for the total bending moment: (III-24) and (III-25) for pure penetration considerations and (III-27) for instantaneous immersion.

Again, when computing the response of (III-28) for the two aerodynamic representations, the proper set of impulsive responses of the generalized coordinates must be used.

The third approach used to compute the impulsive bending moment responses will now be discussed. This approach utilizes the mode displacement method (see [4] and [5]). In this instance, the bending moment at any vehicle station location, x_k , is computed from elementary beam theory considerations:

$$M_{B_M}(x_k,\tau) = -\sum_{i=1}^{n} EIY_i''(x_k)\eta_i \quad . \qquad \text{(III-33)}$$

Rewriting this expression in terms of the integral in (III-22) yields,

$$M_{B_M}(x_k,\tau) = - \sum_{i=1}^{n} \omega_{Bi}^2 I_i(x_k)\eta_i \quad . \qquad \text{(III-34)}$$

For this method, the effects of aerodynamic representation enter implicity through the impulsive response of the generalized coordinates associated with bending, η_i .

The mode displacement bending moment expression, (III-34), is written as a sum of n-bending mode effects. The accuracy of this technique is limited because of the large number of bending modes necessary for convergence. In this report $n = 4$ was used in the numerical evaluation of (III-34).

The wind induced bending moment responses arising from the three moment expressions (total, reduced and mode displacement) were computed for both aerodynamic representations. These wind induced responses were formed using the Duhamel superposition integral [1]:

$$M_B(x_k,t) = \int_0^t M_{B_i}(x_k,t-\tau)v_y(\tau)d\tau \quad . \qquad \text{(III-35)}$$

$M_{B_i}(x_k,t-\tau)$ is the impulsive bending moment response given by (III-14), (III-28) or (III-34) and $M_B(x_k,t)$ is the bending moment response to the wind profile, $v_y(t)$. The "Imbedded Gust Criteria" (see Appendix IV) was the wind profile used in the bending moment computations presented in this report.

Several concluding comments about the wind-induced bending moment responses are necessary. The bending moment response comparisons given in this report are based on the reduced bending moment expression. Of the three equations, the reduced expression affords the greatest numerical reliability. Numerical difficulties were encountered in evaluating some of the weighting coefficients of the small terms in the total bending moment expression. (These terms were not present in the reduced expression.) In addition, convergence uncertainties existed in the mode displacement method since only four flexible modes were considered.

APPENDIX IV

SINUSOIDAL AND IMBEDDED GUST CRITERIA

A description is given in this Appendix of the two types of wind profiles used in the computation of the wind-induced responses (both generalized coordinates and bending moments). The first type of profile, the Sinusoidal Gust Criteria, was used in the investigation to determine the effects and importance of penetration and growth of lift on the vehicle responses. The second, the Imbedded Gust Criteria, was used in the investigation of methods of control on vehicle response when gust penetration effects are considered.

The method used to construct the Sinusoidal and Imbedded Gust Criteria profiles is discussed in [6]. Both types of profiles can be broken down into three main regions as shown in Fig. 59a. Regions I and II contain the wind build-up while Region III contains a specific type of gust.

The wind speed build-up to the quasi-steady state wind velocity is constructed similarly for both profiles. The wind speed in Region II is determined downward from H using 99 percent probability-of-occurrence wind shears. The quasi-steady-state wind velocity (in Region III) is the 95 percent probability-of-occurrence maximum wind velocity (75 meters/sec). Discrete values of the wind velocity in Region II are given as a function of altitude in [6] over a 5 km. altitude layer extending downward from H. The discrete wind data were curve fitted with successive quadratic polynomials to provide intermediate velocity data points for the wind integration.

It was necessary to extend the wind profiles below the 5-km. layer to insure a reliable analytic description of the steady-state wind responses at the onset of the gust region. This was done by assuming that the winds may be described in Region I by a linear function of altitude from zero altitude to the tangent point, h_t , on the wind build-up curve.

Two different types of gust are superimposed on the quasi-steady maximum wind velocity in Region III. One is sinusoidal (see Fig. 59b). The wavelengths, λ , and associated amplitudes, A , of these sinusoids are given in [6] in tabular form. For the response studies, the wavelengths considered are those corresponding to the natural coupled frequencies of the vehicle system in the maximum dynamic pressure region (70 and 80 sec. flight times).

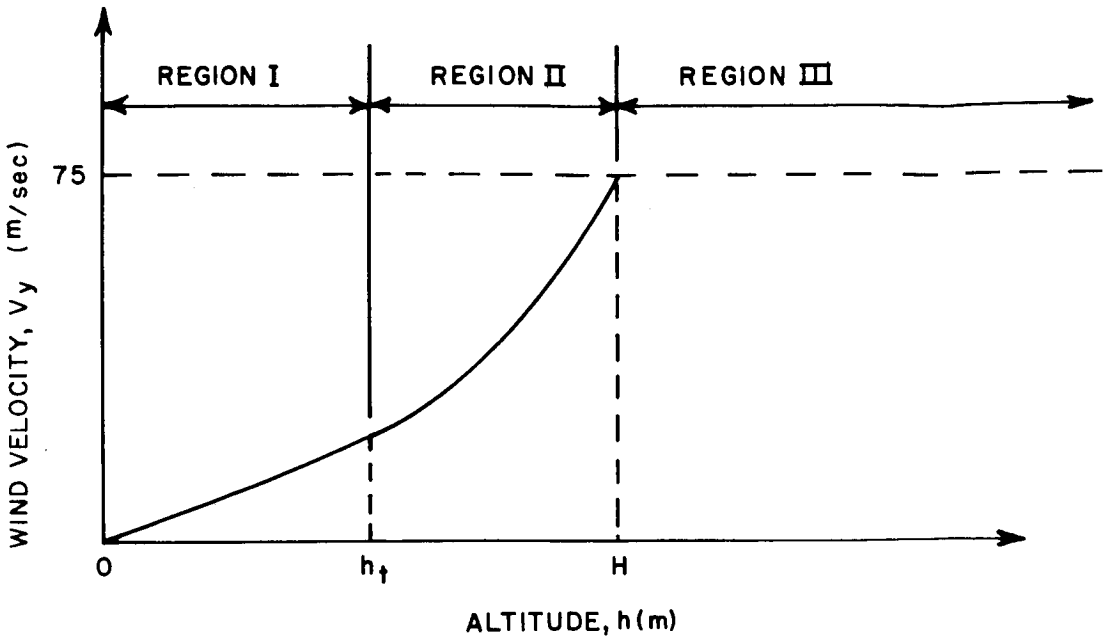

(a) PROFILE WIND BUILD-UP

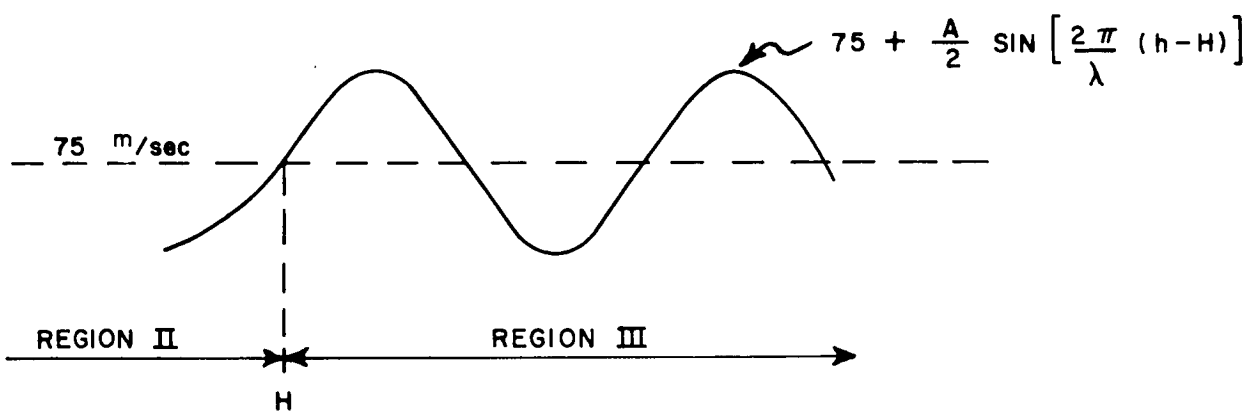

(b) SINUSOIDAL GUST

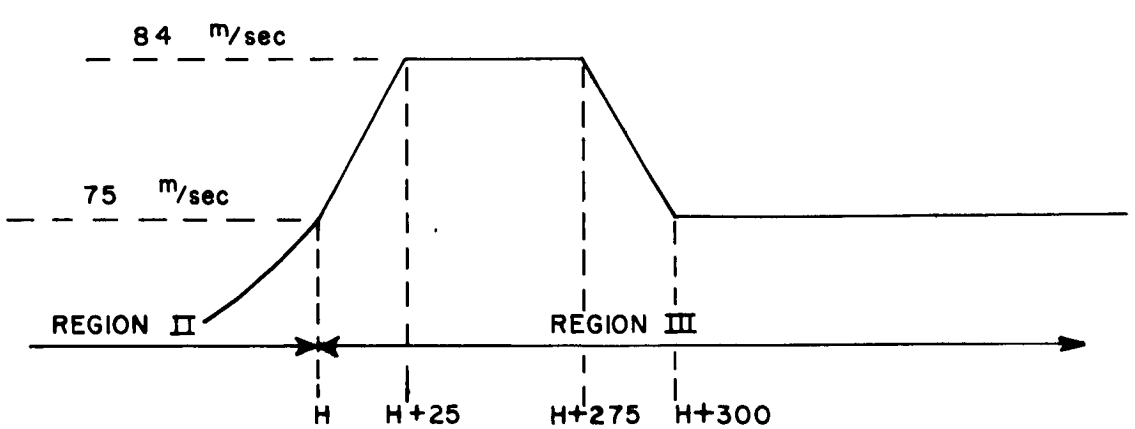

(c) IMBEDDED GUST

The second type of gust which is superimposed on the quasi-steady maximum wind is an imbedded gust of 9 meters/sec (see Fig. 59c). This "quasi-square wave gust" has a rise distance of 25 meters and a duration of 300 meters. The gust decreases at the same rate as the rise and then remains constant at 75 meters/sec. When the 9 meter/sec imbedded gust and the 99 percent shears are combined, both the gust and shears must be reduced by 15 percent to maintain a more likely probability level. In this instance, the imbedded gust produces a 82.65 meter/sec gust velocity. The quasi-steady-state maximum wind velocity remains at 75 meters/sec. (No reduction of gust and shears is required for the Sinusoidal Gust Criteria.)

Since the wind-induced responses are sought as a function of flight time (see Appendix III), the synthetic profiles were linearly transformed from altitude (as given in [6]) to flight time by use of a constant vehicle velocity. The vehicle velocity used was obtained from the set of frozen vehicle coefficients evaluated at the midpoint of a flight time band.* The 70 and 80 sec. flight time vehicle velocities were used in the profile transformation.

* This midpoint corresponds to the altitude, H , given in Fig. 59.

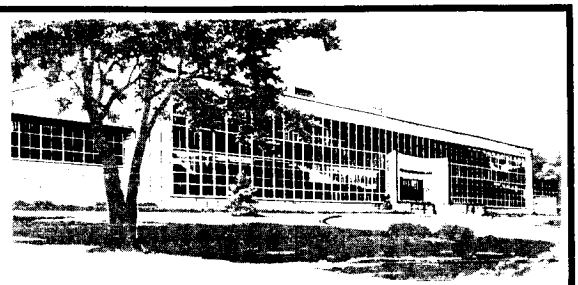

MIDWEST RESEARCH INSTITUTE/425 VOLKER BOULEVARD/KANSAS CITY, MISSOURI 64110